CRANFIELD UNIVERSITY

Paul Allen

Models for the Dynamic Simulation of Tank Track Components

Defence College of Management and Technology

CRANFIELD UNIVERSITY
ENGINEERING SYSTEMS DEPARTMENT

PhD THESIS
Academic Year 2005-2006

Paul Allen

MODELS FOR DYNAMIC SIMULATION OF TANK TRACK COMPONENTS

Supervisors
Dr Amer Hameed
Dr Hugh Goyder

Date of original submission
January 2006

Acknowledgements

The author acknowledges the excellent support and guidance he has received throughout this project from his supervisors, Dr Amer Hameed and Dr Hugh Goyder. They have both given many hours of their time to the project. Dr Hameed has been an outstanding supervisor, always supportive and encouraging. Dr Goyder has given specialist support and expert advice freely. The contributions made by both Dr Amer Hameed and Dr Hugh Goyder has been invaluable and I owe them many thanks.

I must acknowledge the support provided by Cranfield University, Engineering Systems Department (ESD) and the staff at the Defence College of Management and Technology (DCMT). The University and College have provided excellent facilities. Members of staff have been helpful and professional throughout their standard of work has also excellent. Particular departments at DCMT which have provided support for this project are the Engineering Dynamics Centre, Library Resources, Reprographics and the Mechanical Workshop.

I also wish to acknowledge the Engineering and Physical Sciences Research Council (EPSRC), QinetiQ Limited (QinetiQ)and Cranfield University DCMT, for providing financial support for this project and specifically, Dr Mark French of QinetiQ's Future Systems Technology division and Professor John Hetherington of DCMT, who have both been supportive throughout.

A final thanks to David Boast of AVON Materials Development Centre who has freely given advice and information which cleared much of the fog.

MODELS FOR THE DYNAMIC SIMULATION OF TANK TRACK COMPONENTS

ABSTRACT

This project has been sponsored by QinetiQ Limited (QinetiQ); whose aim it is to model the dynamics of a prototype high-speed military tracked vehicle. Specifically their objective is to describe the mechanism by which force inputs are transmitted from the ground to the vehicle's hull.

Many track running gear components are steel and can be modelled as simple lumped masses or as linear springs without internal damping. These present no difficulty to the modeller. However tracked vehicle running gear also has nonlinear components that require more detailed descriptions. Models for two rubber components, the road wheel tyre and track link bush, and a model for the suspensions rotary damper, are developed here. These three components all have highly nonlinear dynamic responses. Rubber component nonlinearities are caused by the materials nonlinear elastic and viscoelastic characteristics. Stiffness is amplitude dependent and the material exhibits a significant amount of internal damping, which is predominantly Coulombic in nature but also relaxes overtime. In this work, a novel method for measuring the elastic and viscoelastic response of Carbon Black Filled Natural Rubber components has been devised and a 'general purpose' mathematical model developed that describes the materials response and is suited to use in multibody dynamic analysis software.

The vehicle's suspension rotary damper model describes three viscous flow regimes (laminar, turbulent and pressure relief), as a continuous curved response that relates angular velocity to damping torque. Hysteresis due to the compression of entrapped gas, compliance of the dampers structure and compression of damper oil is described

by a single non-parametric equation. Friction is considered negligible and is omitted from the model.

All components are modelled using MSC.ADAMS™ multibody dynamic analysis software. The models are shown to be easily implemented and computationally robust. QinetiQ's requirement for 'practical' track running gear component models has been met.

Lists of contents

Index

Models for the Dynamic Simulation of Tank Track Components ----------b

Acknowledgements----------i

Abstract----------ii

List of Contents----------iv

List of tables ----------ix

List of Figures ----------x

List of abbreviations----------xvii

Nomenclature for Chapters 1 to 8 ----------xvii

Nomenclature for Chapters 9 to 13----------xviii

Chapter 1: **The background and objectives of this study** ----------1

1.0 Introduction ----------1

1.1 The Warrior APC---------- 3

Chapter 2: Literature review of high-speed tracked vehicle dynamic models ----5

2.0 Introduction ----------6

2.1 Robertson, B.----------6

2.2 Ma, Perkins, Scholar and Assanis et. al.,----------7

2.3 Ryu, Bae, Choi and Shabana----------8

2.4 Slattengren ----------9

Chapter 3: The characteristic behaviour of Carbon Black Filled Natural rubber-

----------11

3.0 Introduction ----------11

3.1 Frequency and temperature dependence----------11

3.2 Stress relaxation (Viscous flow)----------15

3.3 Characteristic hysteresis loop shape----------16

3.4 Summary----------17

Chapter 4: Literature review of models developed for Carbon Black Filled Natural Rubber----------18

4.0 Introduction ----------18

4.1 Descriptions for the Elastic stress component ----------19

4.2 Descriptions for the viscous stress component----------24

4.3 Summary ---------- 38

Chapter 5: Test rig design, experimental procedure and measurement for rubber components ----------40

5.0 Introduction----------40

5.1 Warrior APC track rubber components----------42

5.2 Test rigs design and experimental procedure ----------44

5.3 Measurement I: Low amplitude displacement with various preloads, 1Hz sinusoidal displacement----------47

5.4 Measurement II: Constant preload at various amplitudes,1Hz sinusoidal displacement----------56

5.5 Measurement III: Constant amplitude and constant preload at various frequencies----------58

5.6 Measurement IV: Stress relaxation: Force response to a stepped displacement over time----------60

5.7 Track bush torsional response at various radial loads----------62

5.8 Track bush torsional response to duel-sine displacement ----------63

Chapter 6: Development of a model for rubber components ----------64

6.0 Introduction----------64

6.1 The simplified Haupt and Sedlan model----------65

6.2 The time dependent viscoelastic element ----------67

6.3 Stress relaxation and the response to duel-sine motion----------75

6.4 Final model for carbon black filled natural rubber components----------83

6.5 Summary ---------- 86

Chapter 7: Comparison between measured and simulated rubber component response ----------87

7.0 Introduction----------87

7.1 Implementation of the final model in ADAMS software----------87

7.2 Comparison between measured and simulated response plots----------89

7.3 Summary----------96

Chapter 8 Summary of the rubber components investigation ----------97

8.0 Summary----------97

Chapter 9: The Warrior APC rotary damper ----------100

9.0 Introduction----------100

9.1 Design of the Warrior APC rotary damper ----------101

Chapter 10: Literature review of automotive suspension damper models ------107

10.0 Introduction----------107

10.1 Linear equivalent models ----------107

10.2 Restoring force maps----------109

10.3 Parametric or physical models ----------110

10.4 Spring and dashpot models ----------112

Chapter 11: Rotary damper test rig design and experimental procedure -------113

11.0 Test rig design and instrumentation ----------113

11.1 Data processing----------114

11.2 Test settings----------117

Chapter 12: Measured damper response and model development ----------118

12.0 Measured damper response----------118

12.1 Friction and laminar flow----------120

12.2 Laminar to turbulent flow transition----------121

12.3 Pressure relief valve characteristics (Blow-off)----------123

12.4 Hysteresis due to entrapped air, oil compression and chamber compliance ----------125

12.5 Model implementation----------128

12.6 Damper rotor inertia ----------129

Chapter 13: Comparison between measured and modelled rotary damper response ---------- 130

13.0 Introduction----------130

13.1 Measured and modelled results for the rotary damper----------131

13.2 Predicted response at high velocity----------133

Chapter 14: Rotary damper: Conclusion and Further work ----------135

14.0 Conclusion and further work ----------135

Chapter 15: Conclusion and further work ----------137

15.0 Overview----------137

15.1 Rubber component models ----------137

15.2 Suspension damper model ----------139

15.3 Further work----------139

References----------142

Appendix 1: Time independent force-displacement relationship for the Haupt and Sedlan viscoelastic element ----------1

Appendix 2: Response of the Haupt and Sedlan viscoelastic element to a stepped input ----------4

Appendix 3: Test rig frequency response for rubber component measurement ------6

Appendix 4a: The 'Four viscoelastic element' model

Values for the track bush torsional model ----------11

Appendix 4b: The final 'three viscoelastic-element' model

Values for the road wheel tyre model----------12

Values for the track bush torsional model----------13

Values for the track bush radial model ----------13

Appendix 5: Compression of damper oil, entrapped air and compliance of oil the chamber ----------14

Appendix 6: Torque-Angular velocity relationship for the Warrior APC rotary damper model (excluding hysteresis) ----------19

Appendix 7: Test rig design and instrumentation ----------22

List of tables

Table 4.1-1: *A Summary of recent Elastic Stress models developed for Carbon Black Filled Natural Rubber* ----------23

Table 10.3-1: *A summary of the various physical phenomena that are described in a selection of parametric models* ----------111

Table 11.2-1: *Rotary damper test settings* ----------117

Table A6-1: *Numeric data for the damper torque verses angular velocity response* ----------20

Table A7-1: *Data acquisition channel assignment for both random and sinusoidal drive signals*----------*23*

List of figures

Figure 1.0-1: *Qinetiq's prototype plastic tank, The Advanced Composite Armoured Vehicle Platform (ACAVP)* ----------2

Figure 1.1-1: *The Warrior Armoured Personnel carrier (APC)* ----------3

Figure 1.1-2: *Warrior APC running gear: Track, road wheels and support roller* --4

Figure 3.1-1: *Relationship between, In-phase modulus and Tan delta* ----------12

Figure 3.1-2: *Effect of temperature on in-phase modulus. Avon Rubber [2]* ---------13

Figure 3.1-3: *Tan delta over the temperature range -80 → +40°C showing different glass transition temperatures for various polymers Avon Rubber [2]* ----------13

Figure 3.1-4: *Frequency dependency of in-phase modulus for a variety of compounds at 20°C. Avon Rubber [2]* ----------14

Figure 3.1-5: *Frequency dependency of tan delta for a variety of compounds at 20°C. Avon Rubber [2]* ----------14

Figure 3.2-1: *Typical stress relaxation response for Carbon Black Filled Natural Rubber (CBFNR)-* ----------15

Figure 3.3-1: *Characteristic CBFNR hysteresis loops. Reproduced from Coveney and Johnson [8]* ----------16

Figure 3.3-2: *Typical response for CBFNR. Showing amplitude dependent stiffness (a) and amplitude independent loss angle (b). Reproduced from Coveney and Johnson [8]* ----------17

Figure 4.2.1-1: *Schematic representation of Berg's model* ----------24

Figure 4.2.2-1: *Schematic representation of the Triboelastic model* ----------26

Figure 4.2.3-1:*Schematic representation of the Rate Dependent Triboelastic (RT) model* ----------28

Figure 4.2.3-1: *Illustration showing the requirement for a linear viscous relationship at low velocity to prevent rapid changes in the force vector* ----------29

Figure 4.2.4-1: *Schematic representation of the Bergstrom and Boyce model* -------30

Figure 4.2.5-1: *Schematic representation of the Miehe and Keck model* ----------31

Figure 4.2.7-1: *A one-dimensional and simplified schematic representation of the Haupt and Sedlan model (with a single viscoelastic element only)*----34

Figure 4.2.7-2: *A one-dimensional schematic representation of the Haupt and Sedlan strain-history dependent viscosity model (with a single viscoelastic element only)* ----------37

Figure 5.1-1: *Warrior APC rubber track components; (A) A single Track link (B) Track bush sections removed from the track link casting (C) Road wheel tyres* ----------42

Figure 5.2-1: *(A) Measurement of track bush torsional characteristics by rotation about the track bush axis (B) Measurement of Track bush radial force and displacement (C) Measurement of road wheel tyre radial force and compression* ----------44

Figure 5.3.1-1: *Track bush torsional elastic-force response* ----------50

Figure 5.3.1-2: *Track bush radial elastic-force response* ----------50

Figure 5.3.1-3: *Road wheel tyre elastic-force response* ----------51

Figure 5.3.2-1: *Track bush torsional geometric factor* ----------53

Figure 5.3.2-2: *Track bush radial geometric factor* ----------53

Figure 5.3.2-3: *Road wheel tyre radial geometric factor* ----------54

Figure 5.4-1: *Track bush torsional force-displacement response* ----------56

Figure 5.4-2: *Track bush radial force-displacement response* ----------57

Figure 5.4-3: *Road wheel tyre radial force-displacement response* ----------57

Figure 5.5-1: *Road wheel tyre force-displacement response at several Frequencies* ----------58

Figure 5.5-2: *Track bush radial force-displacement response at several Frequencies* ----------59

Figure 5.6-1: *Track bush torsional stress relaxation* ----------60

Figure 5.6-2: *Road wheel tyre stress relaxation* ----------61

Figure 5.7-1: *Track bush torsional response at varying radial loads* ----------62

Figure 5.8-1: *Track bush torsional response to duel-sine displacement* ----------63

Figure 6.1-1: S*chematic representation of the simplified Haupt and Sedlan carbon black filled natural rubber component model* ----------66

Figure 6.2-1: *Rising and falling exponential curves produced by Equation 4.2-10* ----------68

Figure 6.2-2: *Track bush torsional viscoelastic force. Modelled using a single viscoelastic Element (Equations 4.2-10)* ----------69

Figure 6.2-3: *Track bush torsional viscoelastic force. Modelled using two parallel viscoelastic elements (Equations 4.2-10)* --------- ----------70

Figure *6.2-4:* *Track bush radial viscoelastic force. Modelled using two parallel viscoelastic elements (Equation 4.2-10)* ----------72

Figure 6.2-5: *Road wheel tyre viscoelastic force. Modelled using two parallel viscoelastic elements (Equation 4.2-10)* ----------72

Figure 6.2-6: *Quarter model of the tyre contact showing von Mises strain. Tyre compression is 8mm. Produced using ANSYS FEA software* ----------74

Figure 6.3-1: *Measured track bush torsional response to duel-sine displacement – 76*

Figure 6.3-2: *Simulation of track bush torsional response to duel-sine displacement produced by ADAMS simulation of the simplified Haupt and Sedlan* ----------77

Figure 6.3-3: *Four-element model: Two non-linear viscoelastic elements each with a nested rapidly decaying non-linear stiffening viscoelastic element* ---79

Figure 6.3-4: *Simulated track bush torsional response to duel-sine displacement produced by ADAMS simulation of the four-element viscoelastic model* ----------80

Figure 6.3-5: *Measured and simulated track bush torsional stress relaxation produced by ADAMS simulation of the four-element viscoelastic Model* ----------81

Figure 6.4-1: *Final model containing three non-linear viscoelastic elements* -------83

Figure 6.4-2: *Simulated track bush torsional response to duel-sine displacement. Produced by ADAMS simulation of the final three-viscoelastic element model* ----------84

Figure 6.4-3: *Measure and simulated track bush torsion stress relaxation, produced by ADAMS simulation of the final three viscoelastic element model -85*

Figure 7.1-1: *Implementation of the 'final model' in ADAMS software so that* $x_B \approx x_A$ ----------87

Figure 7.2-1: *Simulated Track bush radial force-displacement* ----------89

Figure 7.2-2: *Simulated track bush torsional force-displacement response* ----------90

Figure 7.2-3: *Simulated road wheel tyre radial force-displacement response* -------91

Figure 7.2-4: *Simulated road wheel tyre displacement-force response* ----------92

Figure 7.2-5: *Simulated road wheel tyre force-displacement response at several frequencies* ----------93

Figure 7.2-6: *Measure and simulated road wheel tyre stress relaxation* ----------94

Figure 7.2-7: *Measure and simulated track bush torsion stress relaxation* ----------94

Figure 7.2-8: *Simulated track bush torsional response to duel-sine displacement* –95

Figure 9.0-1: *Warrior Armoured Personnel Carrier running gear (Horstman Defence Systems Ltd)* ---------- 101

Figure 9.1-1: *Section through rotary damper* ----------102

Figure 9.1-2: *Sectioned view of the rotary damper* ----------102

Figure 9.1-3: *Design specification showing the allowable range of damper Torque* ---------- 104

Figure 9.1-4: *Characteristic graph of torque verses angular velocity, produced by Horstman Defense Systems Ltd* ----------105

Figure 10.4-1: *A physical damper model represented by non-linear dashpot and nonlinear spring in series* ----------112

Figure 11.0-1: *Schematic drawing of the rotary damper test rig* ----------113

Figure 11.1.2-1: *Comparison between normalised hydraulic ram and rotary damper motion* ----------115

Figure 11.1.3-1: *Schematic drawing of rotary damper test rig mechanism* ----------116

Figure 12.0-1: *Torque verses angular displacement (Work diagram)* ----------118

Figure 12.0-2: *Torque verses angular velocity (Characteristic diagram)* ----------119

Figure 12.1-1: *Torque angular velocity for the low frequency (0.1Hz) test* ----------120

Figure 12.2-1: *Torque angular velocity for the mid-range frequencies up to 0.5Hz* ----------122

Figure 12.2-2: *Laminar and turbulent flow regions of the viscous force* ----------123

Figure 12.3-1: *Data supplied by Horstman Defense Systems Ltd* ----------124

Figure 12.3-2: Rotary damper torque-angular velocity response without hysteresis ----------125

Figure 12.4-1: *Schematic diagram illustrating the compression and expansion of entrapped gas* ----------126

Figure 12.5-1: *The rotary damper, modelled by a non-linear dashpot and non-linear spring in series* ----------128

Figure 13.1-1: *Modelled torque verses angular displacement (Work diagram)* ----131

Figure 13.1-2: *Modelled torque verses angular velocity (Characteristic diagram)* ----------132

Figure 13.2-1: *Modelled torque verses angular displacement in response to high frequency sinusoidal motion* ----------133

Figure 13.2-2: *Modelled torque verses angular velocity in response to high frequency sinusoidal motion* ----------134

Figure A1-1: *The viscoelastic Sedlan and Haupt element*----------1

Figure A2-1: *Response to stepped displacement*----------4

Figure A3-1a: *Road wheel tyre test rig* ----------8

Figure A3-1b: *Road wheel tyre test rig FRF*----------8

Figure A3-2a: *Track bush radial force test rig* ----------9

Figure A3-2b: *Track bush radial force test rig FRF* ----------9

Figure A3-3a: *Track bush torsional response test rig*----------10

Figure A3-3b: *Track bush torsional response test rig FRF* ----------10

Figure A4a-1: *Four viscoelastic element model* ---------- 11

Figure A4b-1: *Three viscoelastic element model* ----------12

Figure A5-1: *Schematic representation of the damper showing how entapped air is compressed and expanded as oil flows from one chamber into the other* ----------14

Figure A5-2: *Response described by Equation A5-15 for C_1 =1 and C_2 =2* ---------18

Figure A6-1: *The rotary damper viscous force-velocity response implemented in ADAMS software as a splined curve* ----------21

Figure A7-1 *Test rig control and instrumentation set up for random drive signal*

Figure A7-2 *Test rig for the measurement of Track Bush Radial Response*

Figure A7-3 *Test rig for the measurement of the Track Bush Torsional Response*

Figure A7-4 *Test rig for the measurement of the Road Wheel Tyre Response*

Figure A7-5 *Test rig for the measurement of the rotary damper's Response*

List of abbreviations

ACAVP	Advanced Composite Armoured Vehicle Platform
APC	Armoured Personnel Carrier
CBFNR	Carbon Black Filled Natural Rubber
LVDT	Linear Variable Displacement Transducer
Tan Delta	Tangent of phase angle between stress and strain

Nomenclature for Chapters 1 to 8

A, B, C, P, Q	Constants (Units vary depending on function)
c	Damping Coefficient. Units for this parameter vary depending on the material model. The units are most often either (Ns/m) or (N), however a power term may be require such as $(Ns/m)^n$ where n is the fractional power term.
E	Youngs Modulus (MPa)
F	Force (N)
k	Elastic stiffness (N/m)
t	Time (s)
x	Displacement (m)
$\dot{x}$	Velocity (m/s)
β	Constants (No units)
γ	Strain
ε	Strain
$\dot{\varepsilon}$	Strain rate
η	Coefficient of viscosity (Ns/m)
λ	Ratio of deformed length to original length

ξ	Constant (m/s)
σ	Stress (MPa)
τ	Time constant (s)

Subscripts

e	Elastic
0	Absolute displacement of rubber component
K, N	Integer
v	Viscoelastic

Superscripts

n	Power term

Nomenclature for Chapters 9 to 14

A	Amplitude of linear displacement (m)
B, C, D	Constants (NoUnits)
C_1, C_2	Constants (Units Vary depending on usage)
c	Damping Coefficient (Ns/m)
F	Force (N)
I	Inertia ($kg.m^2$)
k	Elastic stiffness (N/m)
m	Mass (kg)
P	Pressure (N/m^2)
R	Gas Constant (J/kg.K)
r	Radius arm length (m)
T	Torque (Nm)
t	Time (s)

V	Volume (m^3)
x	Displacement (m)
$\dot{x}$	Velocity (m/s)
$\ddot{x}$	Acceleration (m/s^2)
θ	Rotary damper Angle (Rads)
Θ	Amplitude of rotary motion (Rads)
ϕ	Drive signal phase angle (Rads)
ω	Frequency (Hz)

Subscripts

d	Dashpot
eq	Equivalent lineatized value
gb	Gas bubble
gs	Gas in solution
gt	Total quantity of gas
oil	Damper oil
s	Spring

Chapter 1

The background and objectives of this study

1.0 Introduction

The objective of the work presented here is to develop models for Warrior Armoured Personnel Carrier (APC) running gear components for use in multibody dynamic simulations.

There are two driving motivations for this work. Firstly; there is a requirement for reduced vehicle weight to optimise the transport of armoured fighting vehicles by air to regions of conflict. Secondly; there is a requirement to reduced noise and vibration for the comfort of personnel within the vehicle. To these ends Qinetiq Limited is investigating the practicality of replacing the Warrior's aluminium hull with a composite material. A prototype plastic tank has been built: the Advanced Composite Armoured Vehicle Platform (ACAVP, Fig. 1.0-1). The hull is constructed from moulded E-Glass fibre composite but the vehicle runs on standard Warrior APC tracks. Qinetiq has initiated a study of running gear dynamics so that the transmission of ground inputs to the hull can be modelled. The work presented here is part of this study, it aims to measure the dynamic response and validate models for individual components of the Warrior's track running gear.

Models for three track running gear components are developed: these are the 'road wheel tyre' the 'suspensions rotary damper' and the 'track link bush'. Models for the 'road wheel tyre' and the 'track link bush' are developed jointly in Chapters 3-8, since both are made from carbon black filled natural rubber (CBFNR). In chapters 9-14 a model for the Warrior's suspension rotary damper is developed. In each case measurements show that these components have significantly nonlinear dynamic

response and it is important that these nonlinearities are described in the component models if the full vehicle simulation is to be accurate. However it is also important (for computational efficiency) that component models are no more detailed than is necessary.

Fig. 1.0-1: *Qinetiq's prototype plastic tank, The Advanced Composite Armoured Vehicle Platform (ACAVP)*

With regard to implementation in the simulation software: component models should be robust and should be compatible with the software's algorithm. In the work presented here models have been developed and tested using MSC.ADAMS™ 2003 software. This type of implicit algorithm finds the solution to initial value problems by incrementing forward in time, making initial estimates of position, velocity, force and acceleration then correcting these values by repeated iterations until the systems equations of motion and geometric constraints equate to within a given accuracy. If the algorithm fails to find a solution within a given number of iterations the time increment is automatically reduced and another attempt made. However, the time

increment is also given a minimum value: so it is possible under certain circumstances for the simulation to fail to find a solution. The Newton-Raphson Predictor-Corrector algorithm is complex and is not discussed within the scope of this work; but detailed descriptions can be found in the following references [41, 42, 43, 44]. The significant point to appreciate when developing component models for use in this type of software is that the algorithm is susceptible to discontinuities, multiple or ill-defined solutions and sudden step changes, all of which may cause a simulation to fail [41, 44]. It is important therefore that component descriptions are ‘smooth’, continuous and unambiguous. This point is restated throughout this report when discussing how component models have been derived.

1.1 The Warrior APC

Fig. 1.1-1: *The Warrior Armoured Personnel carrier (APC)*

The Warrior Armoured Personnel Carrier (APC) is primarily designed as an armoured troop carrier although variations for, recovery, reconnaissance, command post, etc. are built. The Warrior is designed to have the speed and performance to keep up with

Challenger 2 main battle tanks, and the firepower and armour to support infantry in an assault.

The Warrior runs on single pin rubber bushed track, driven by sprockets at the front of the vehicle. A single roller supports the tracks top span. The twelve road wheels have torsion bar suspension with rotary dampers at the 1st, 2nd and 6th wheel stations. Road wheels, idler wheel and support roller all have moulded rubber tyres.

Fig. 1.1-2: *Warrior APC running gear: Track, road wheels and support roller*

As stated above; three components from the Warriors running gear are modelled in this study. These are the track link bush, the road wheel tyre and the suspensions rotary damper. These have been chosen because they have significant nonlinear stiffness and damping characteristics and it is important that these nonlinearities are described if a simulation of the complete vehicle is to be accurate. The suspensions torsion bar is simply a linear elastic element with very little internal damping and so does not require detailed study.

In summary the objectives of this work are:

1. Develop models for the Warrior APC track running gear components for use in multibody dynamic simulation software.
2. Validate the models by comparing them with the measured response of individual track components.
3. Describe significant nonlinear behaviour, but produce models that are no more detailed then necessary for full tracked vehicle running gear simulation.
4. Develop models that are, robust, computationally efficient and compatible with the software's algorithm. Models that do not produce discontinuities, multiple or ill-defined solutions or sudden stepped changes.

Chapter 2

Literature review of high-speed tracked vehicle dynamic models

2.0 Introduction

In this chapter a number of models developed for tank tracks and full tracked vehicle simulation are reviewed. In each case discussion focuses on how the stiffness and damping characteristics of the running gears nonlinear components (suspension damper, track bush and tyres) are described.

2.1 Robertson, B.

Robertson, B. (1980) [1] built a full-scale tank track test rig (Scorpion) and developed analytical models in an attempt to predict the transverse vibration of the tracks top span. This work was done prior to the development of automatic dynamic analysis software and high-specification personnel computers. The four models developed were based on, a string with axial velocity, an elastic beam and a viscoelastic beam with internal hysteretic damping and/or viscous damping. This work illustrates the limitations of the analytical approach and why it is only now using numerical multi-body dynamic analysis software that progress is being made. Robertson's analytical formula did not predict the resonant frequencies that he measured. The mechanical system Robertson attempted to model was too complex to be described by the track top span resonance alone. It was found that resonant frequencies occurred at multiples of drive sprocket and track revolution speed. Resonance of the track span was not detected by measurement. The dynamics of the system were a complex interaction between track, test rig structure and drive system that could not be predicted by an analytical track description alone. With regard to component descriptions for the

analytical model: the track was described as a continuous string or beam; Robertson was aware that the internal damping of the rubber track bush was ‘hysteretic’ or ‘Coulombic’ in nature not viscous (that is; frequency independent not frequency dependent. See section 3.1) but could not show that this type of damping best described the frequency response when stationary track was excited by swept sinusoidal motion. Robertson therefore concluded that viscous damping best described the frequency response he measured.

2.2 Ma, Perkins, Scholar and Assanis et. al.,

Ma, Perkins, Scholar and Assanis et. al., [4, 38, 39] develop a two-dimensional full vehicle model of the M1A1 tank. Here a hybrid model is used where the track span is described as a continuous uniform elastic rod connected kinematically to discrete models for sprocket, wheels and rollers. The objective is to model track vibration and track interaction with other components but reduce the large number of bodies in the model, thereby reducing the computational effort required.

Track response is linearized in the spans between wheels and rollers by assuming small deformation. Track force-displacement and force-velocity response is therefore described by parallel ‘linear stiffness’ and ‘linear viscous damping’ respectively. Detailed measurements of and descriptions for components such as tyres, track bushes, track footpads and suspension dampers are not included in this work because it is the vehicles general overall interaction between engine, track, terrain and hull; and the development of an efficient modelling algorithm that is of interest. Modelling inertial interactions and improved computational efficiency by the development of a hybrid model are the primary objectives. This approach developed by Ma, Perkins, Scholar and Assanis et. al., [4, 38, 39] is successful in achieving its objective; track

vibration, track-terrain and track-discrete body interactions are described and over limited frequency and amplitude range this may produce accurate predictions but more comparison with experimental data is required to validate this approach.

2.3 Ryu, Bae, Choi and Shabana

Ryu, Bae, Choi and Shabana [40] (2000) develop a three-dimensional multibody high-speed military tracked vehicle model with compliant track. That is; the joint between each track link is described by stiffness and damping values. This lumped mass model has 189 bodies and 954 degrees of freedom.

The suspensions torsion bar and Hydro-pneumatic unit are modelled as linear and non-linear spring elements respectively but suspension damping is not described. Contact stiffness between road wheel and track link and between adjacent track links are described 'for the sake of simplicity' by a splined curve based on static tests. Contact force damping is described as a linear viscous force where the 'effective damping coefficient' is determined from measurements of the amplitude of hystersis.

This contact force model [40] is further developed by Ryu, Huh, Bae and Choi [5] (2003) for a three-dimensional non-linear multi-body dynamic (MBD) simulation of a military high-speed tracked vehicle for the particular purpose of studying the feasibility and possible advantages of using an active track tensioner. This lumped mass model has 191 ridged bodies and 956 degrees of freedom. In this model the predominantly frequency independence characteristic of carbon black filled natural rubber is appreciated and rubber components hysteresis are modelled using 'Bergs' method [6] (see section 4.2.1). However the hydro-pneumatic suspension unit and torsion bar descriptions are unchanged from the earlier work [40] being described by a splined curve only; suspension damping is not included. This is a more accurate

description of running gear components than the previous model [40] but Berg's method of describing rubber hysteresis requires the storage of force and displacement values at turning points and how this was implemented is not described in detail.

2.4 Slattengren

Slattengren [41] (2000): '*This paper describes the features and use of the commercial multibody simulation program ADAMS (Automatic Dynamic Analysis of Mechanical Systems) in the simulation of tracked vehicle applications.*'

A tracked system created by the ADAMS add-on 'Tracked Vehicle Toolkit' (ATV) can be modified/extended in anyway ADAMS allows. Parameters for each building element in the tracked system are user defined. The building elements being: hull, track, road surface, road wheel, suspension and idler/track tensioner. The user also defines the description for compliance between elements such as track links and at points of contact such as tyres. Compliance is described by a parallel spring and damper (Kelvin) element, which may be either linear or nonlinear. Once all the vehicle's elements have been defined they are automatically assembled by the software to produce the full tracked vehicle model.

Slattengren's paper [41] is written as a guide to using the ATV software and offers advice for running successful simulations. As a general rule Slattengren states that, 'e*xperience has clearly shown that it is extremely hard to get successful simulations out from guessed data. The better the data is, the better the simulation will run*'. This comment emphasises the importance of using measured data for each component description. But Slattengren also discusses special considerations concerning the description of, damping, contact and friction, emphasising that modelling the contact force and friction presented particular difficulty. '*In order to be able to simulate the*

type of complex systems which are not only dominated by contact phenomenon and friction, but also show very large penetration due to the large masses and forces in the system, certain special functions were developed. The most important changes compared to the standard ADAMS functions are without question the impact and friction formulations'.

Chapter 3

The characteristic behaviour of Carbon Black Filled Natural Rubber

3.0 Introduction

All rubber components of the Warrior APC track running gear are made from Carbon Black Filled Natural Rubber (CBFNR). The benefits of using CBFNR in this application are that it reduces impact forces, increases track-life, damps noise and vibration and allows the track to run at higher speeds then is possible with metal-to-metal contact. Specifically CBFNR is chosen for its durability and low heat build up [2]. It is a material commonly used for high dynamic load applications such as truck or aircraft tyres, engine mountings and machine isolation.

In this chapter the characteristic dynamic behaviour of CBFNR is discussed. Models proposed by various researchers for describing this materials response are reviewed and their suitability for use in the simulation of Warrior Armoured Personnel Carrier (APC) running gear components assessed.

3.1 Frequency and temperature dependence

The first consideration when modelling an elastomeric component for dynamic simulations is the materials variation in stiffness (material modulus) and damping (phase or loss angle) over the relevant temperature and frequency operating range. Precise data for the rubber compounds used in Warrior APC track components, (40 and 60 parts per hundred rubber by weight (pphr)) are not available but similar highly filled natural rubber compounds are used in 'Truck Tread'. Data for truck tread (AVON rubber [2]) are presented in Figs. 3.1-2, 3.1-3, 3.1-4 and 3.1-5, which show 'In-phase modulus' and 'Tan delta' verses temperature and frequency. Where Tan

delta is the tangent of the phase angle (δ) between stress and strain when measured in response to sinusoidal motion and in-phase modulus is the in-phase component of the measured modulus, i.e. the dynamic modulus multiplied by the cosine of delta (Figure 3.1-1).

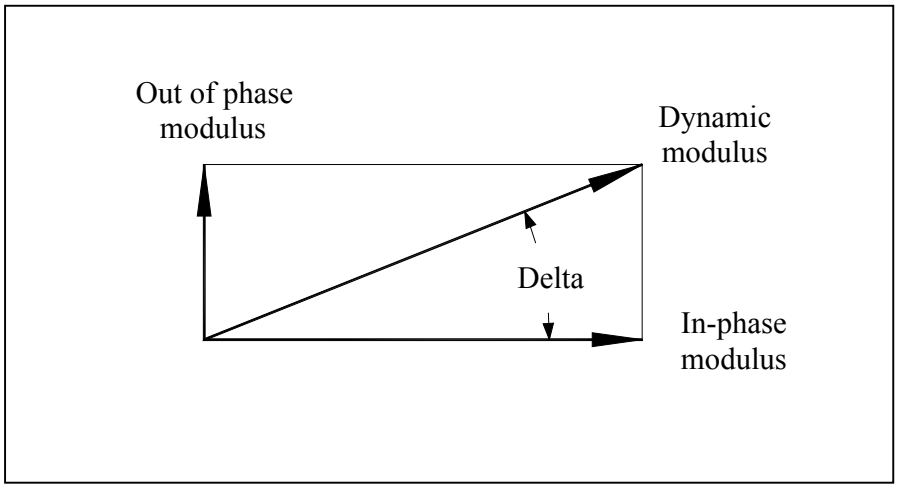

Fig. 3.1-1: *Relationship between, In-phase modulus and Tan delta*

Figures 3.1-3 and 3.1-5 show that for Truck Tread, Tan delta does not vary significantly over the temperature range 0º-20ºC and the frequency range 1-100Hz. Assuming that strain amplitude has been kept constant over this range; the predominantly frequency independent loss angle of Figure 3.1-5 suggests that a suitable damping model maybe a frictional or Coulombic description.

By contrast; the value of Tan Delta for unfilled Polyurethane Acoustic Absorber in Figure 3.1-5 shows significant frequency dependence suggesting a velocity depended (or viscous) damping model.

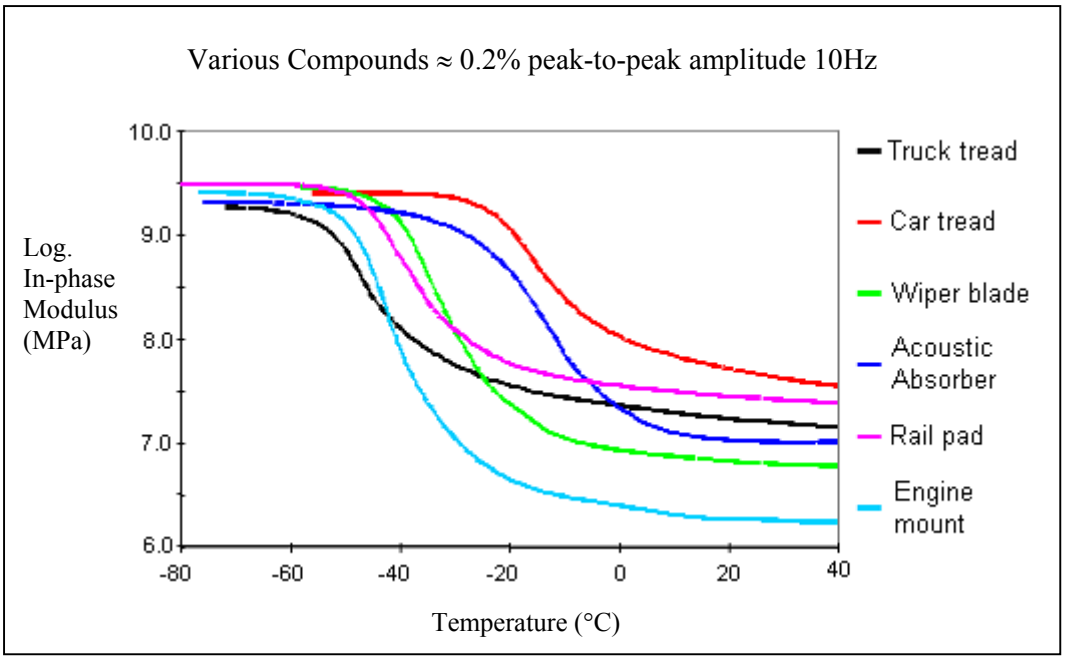

Fig. 3.1-2*: Effect of temperature on in-phase modulus. Avon Rubber [2]*

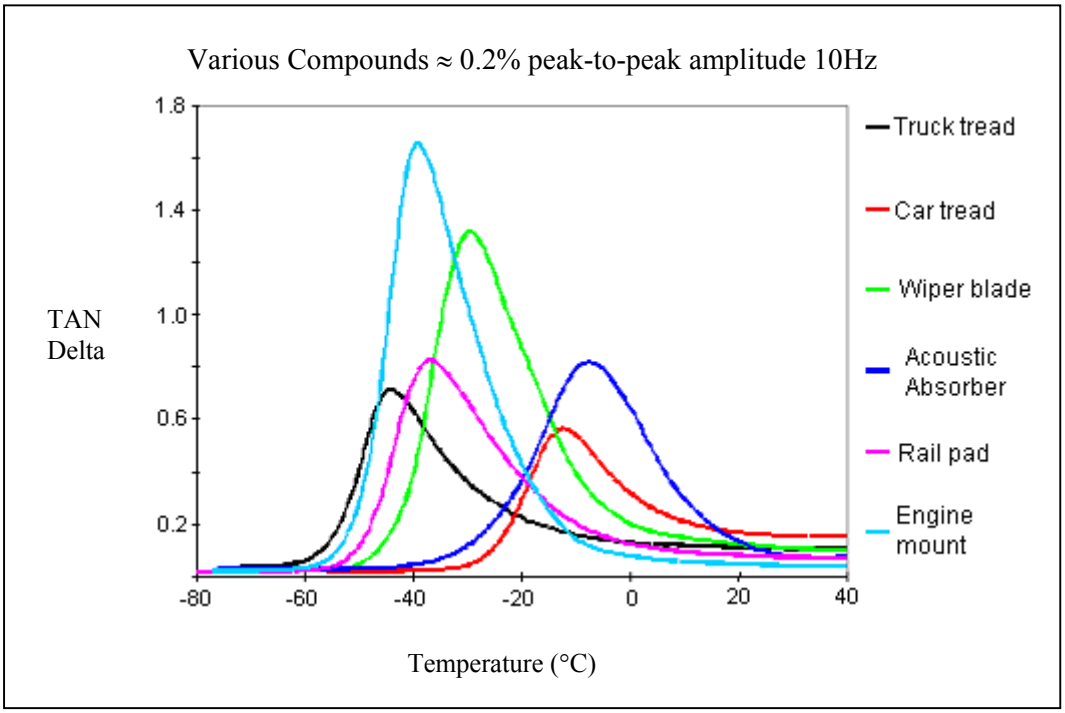

Fig. 3.1-3: *Tan delta over the temperature range -80 → +40°C showing different glass transition temperatures for various polymers. Avon Rubber [2]*

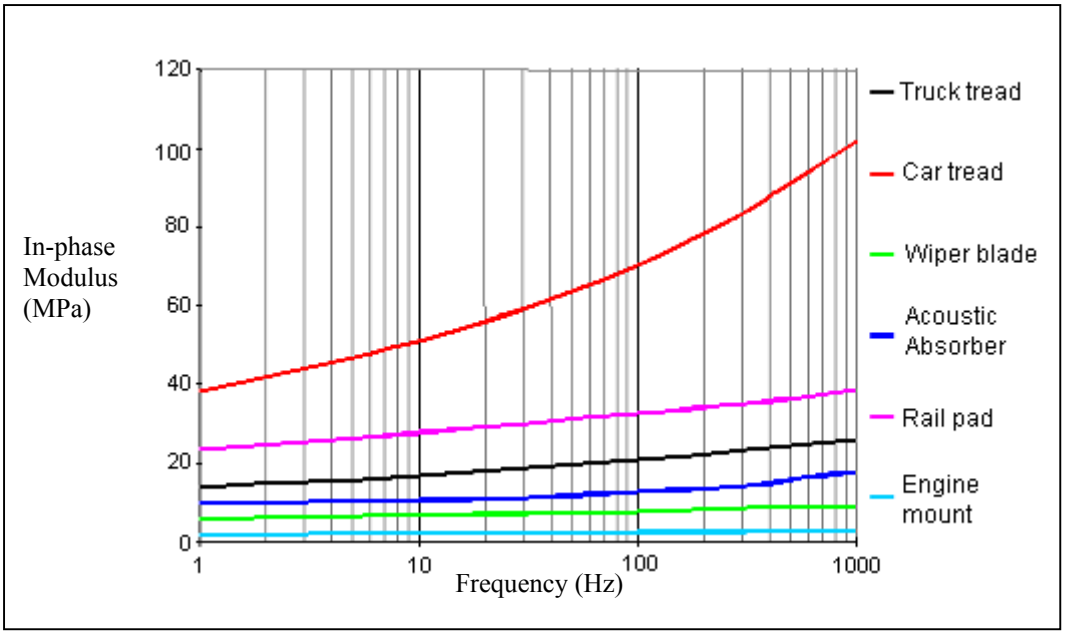

Fig. 3.1-4: *Frequency dependency of in-phase modulus for a variety of compounds at 20°C. Avon Rubber [2]*

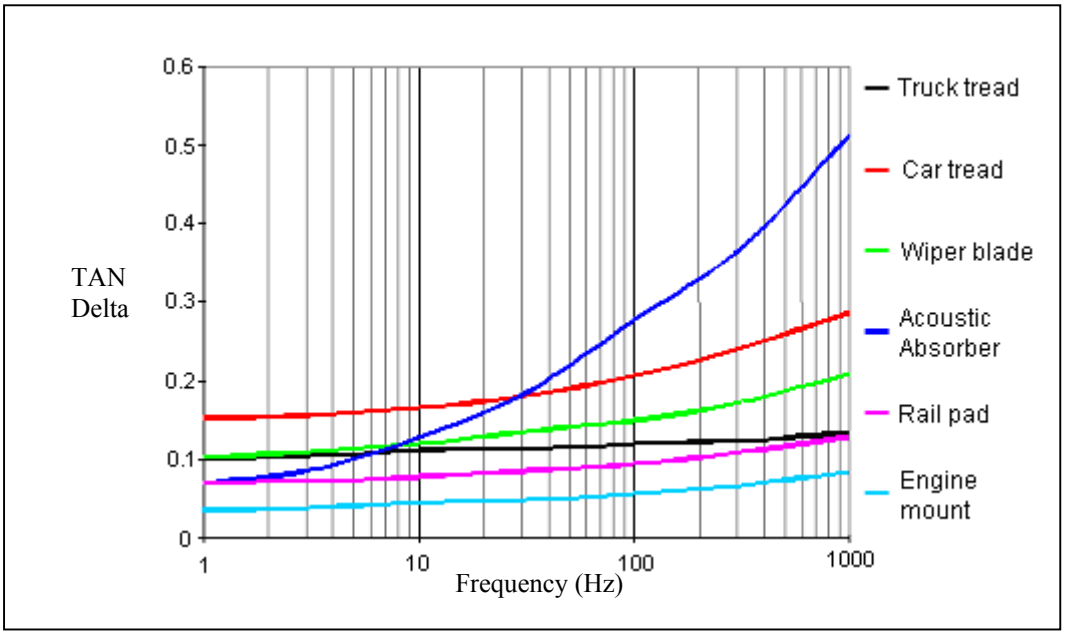

Fig. 3.1-5: *Frequency dependency of tan delta for a variety of compounds at 20°C. Avon Rubber [2]*

Figure 3.1-2 shows the in-phase modulus of Truck Tread varying between ≈32MPa and ≈20MPa in the range 0°C to 20°C and figure 3.1-4 shows in-phase modulus varying between ≈14MPa and ≈20MPa in the range 1Hz to 100Hz. These variations in modulus are approximately 50% and maybe significant enough to be included in a

model of CBFNR. However as a first approximation frequency and temperature effects over these ranges could be excluded for the sake of simplicity.

3.2 Stress relaxation (Viscous flow)

As mentioned in Section 3.1; the predominately frequency independent Truck Tread plot (Fig. 3.1-5) leads us to conclude that a Frictional or Coulombic description would approximate the damping force characteristic of CBFNR. However, when the material is subjected to a stepped strain history the initial stress response reduces rapidly at first then continues to decay slowly over time (Fig. 3.2-1). Measurements have shown that the material has almost total stress relaxation at infinite time [19]. This 'stress relaxation' is assumed to be equivalent to the viscous force component (out-of-phase stress) and the stress at infinity equivalent to the elastic force component (in-phase stress). However, relaxation (or viscous flow) is not described in a purely frictional model and so presents a problem to the 'modeller', to produce a predominately frequency independent damping force that also has stress relaxation.

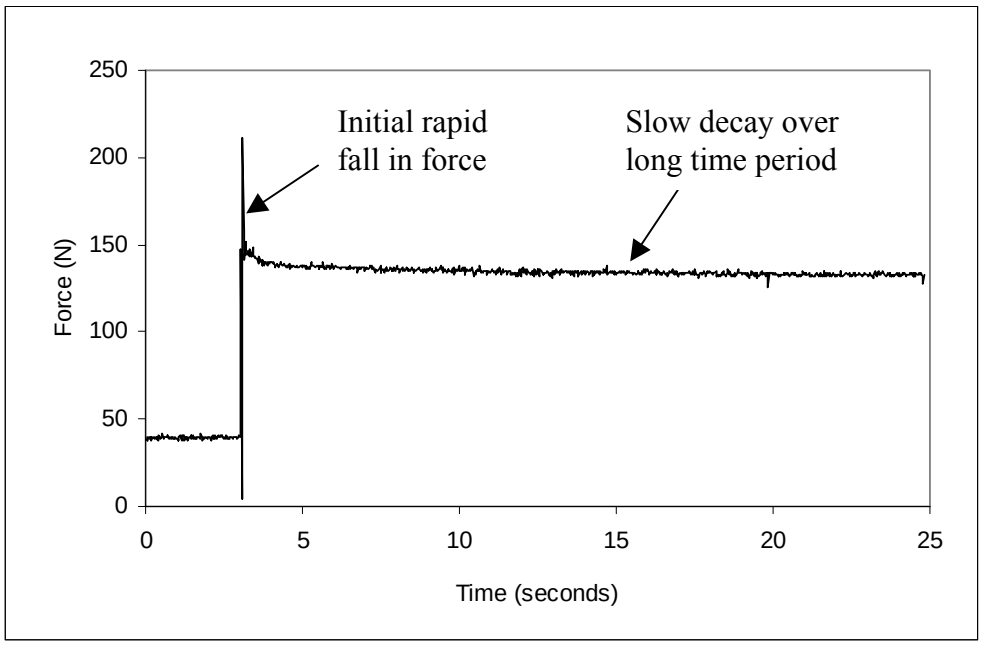

Fig. 3.2-1: *Typical stress relaxation response for Carbon Black Filled Natural Rubber (CBFNR)*

3.3 Characteristic hysteresis loop shape

A further characteristic of CBFNR is that the response to steady state cyclic displacement in the time domain produces hysteresis loops that are not elliptical, but have an asymmetric shape. This characteristic is independent of frequency. The rate of change of stress after a turning point is initially high but reduces to a lower level as the strain amplitude increases. This characteristic response has been reported many times by different researcher for both CBFNR material tests [7, 8] and CBFNR component tests [6, 11]. The stress-strain plots of Fig 3.3-1 shows the typical asymmetric hysteresis loop shape developing as amplitude increases.

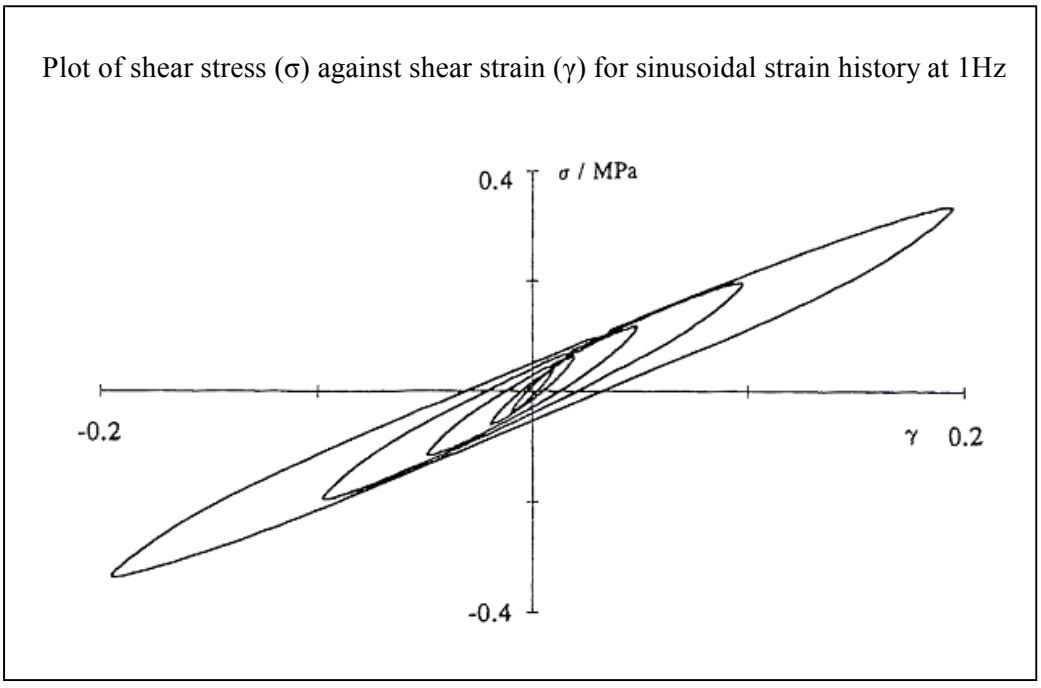

Fig 3.3-1: *Characteristic CBFNR hysteresis loops. Reproduced from Coveney and Johnson [8]*

This characteristic hysteresis loop shape results in amplitude-dependent stiffness (since the major axis changes with amplitude) while maintaining an almost constant, amplitude independent, loss angle (Fig 3.3-2).

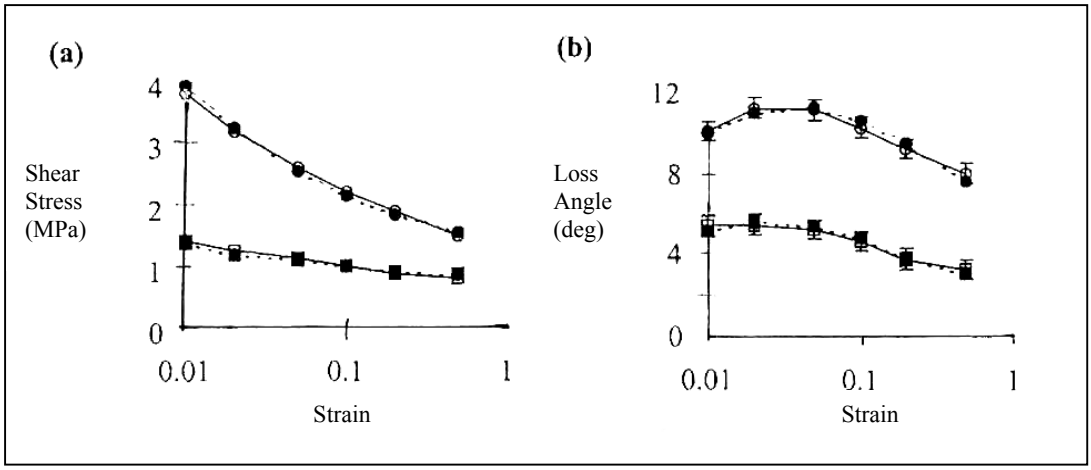

Fig 3.3-2: *Typical response for CBFNR. Showing amplitude dependent stiffness (a) and amplitude independent loss angle (b). Reproduced from Coveney and Johnson [8]*

3.4 Summary

To describe the dynamic behaviour of CBFNR a model should have the following four traits:

1. Two independent components: one representing the in-phase elastic force, the other representing out-of-phase damping force.
2. Predominately frequency independent hysteresis (Coulomic type damping).
3. The characteristic asymmetric hysteresis loop shape; resulting in amplitude dependent stiffness.
4. Viscous damping that produces a rapid initial stress relaxation followed by slow decay over a long time period.

Chapter 4

Literature review of models developed for Carbon Black Filled Natural Rubber

4.0 Introduction

In this chapter various models that have been developed in recent years for modelling the dynamic response of Carbon Black filled Natural Rubber (CBFNR) are discussed. Beginning with the simplest ‘time independent models’ then describing the more complicated ‘power’ and ‘exponential function’ models. All of the models discussed describe total stress as the sum of an elastic (in-phase) stress and a damping (out-of-phase stress) where each element responds independently of the other. Because the two elements respond independently, discussion of each is presented in separate subsections. In Section 4.1 the various types of elastic force description are compared. In Section 4.2 the various types of damping force description are compared. Some models have a third element, which is described as a, ‘plasto-elastic stress’ ‘weak equilibrium hysteresis stress’ or a ‘friction force’. However, this element could also be interpreted as a second ‘parallel’ damping element with very high viscosity and a resulting long relaxation time and so will be included in discussion on the damping component (section 4.2).

4.1 Descriptions for the Elastic stress component

Elastic stress (as described in Section 3.1) is the in-phase component of the materials force response. This elastic component is also referred to as the ‘equilibrium stress’ by some researchers because it is the component of the force that remains at infinite time when the viscous damping component has totally relaxed.

Here in Section 4.1 the functions used to describe the elastic stress in six different CBFNR models are discussed. These models are: Berg [6], Triboelastic [8, 9, 12], Bergstrom and Boyce [13, 14], Miehe and Keck [16], Lion [18], Haupt and Sedlan [19]. The functions are not all dissimilar, so it is possible to group these models together by the type of elastic function used. However it is also interesting to group the models by the method used to determine the parameters that define their respective functions. This is because determining parameters from experimental data requires significant data processing techniques. Also, if a precise measurement of the elastic component can be made independently of the viscoelastic component, it can be subtracted from the total response and a model for the viscoelastic component developed with confidence.

Firstly, if the models are grouped by the type of elastic function used, two groups emerge. Berg’s model [6] and the Triboelastic model [8, 9, 12] are grouped together because both have the simplest of constitutive relationships; a one-dimensional linear Hookean model at the component level described by the function: $F=kx$, where F is elastic force, k is a constant and x is displacement (extension or compression). In this model, the coefficient ‘k’ may be linear because of the components geometry or it may be an indication of relatively low strain (it is well documented that the elastic modulus of CBFNR is non-linear above 1% strain [45, 46]).

Similarly, Bergstrom and Boyce [13, 14], Miehe and Keck [16], Lion [18] and Haupt and Sedlan [19], are grouped together by the type of function used. All are three-dimensional constitutive material models that use 'finite strain energy functions' to describe the elastic element. These are functions that satisfy the following three constraints:

1. They are invariant to the axis orientation (x, y & z) i.e. the material is isotropic
2. At small strains the function reduces to a Hookean description, i.e. $\sigma = E\varepsilon$
3. Strain energy = 0 when $\lambda_x = \lambda_y = \lambda_z = 1$

Where E = Young's Modulus, σ = stress, ε = strain and λ = ratio of deformed length to original length in each orthogonal axis x, y & z. The strain energy functions used in these four models are the standard and modified, Neo-Hookean, Mooney-Rivlin and Ogden types [47]. The purpose of these functions is simply to introduce into the elastic description enough parameters so that the non-linear response of the elastomer at high strain is described. These four material models describe the materials elastic response up to 200% strain.

Alternatively, grouping the six models by considering the method used to determine the coefficients for the elastic functions results in three distinct groups. Firstly we can define a group that uses computer algorithms to determine coefficients from the total hysteretic stress-strain response. Here the fundamental in-phase modulus and phase angle are found by Fourier analysis of the response to sinusoidal strain histories at a number of frequencies. A minimisation algorithm is then used matches the models response to this result thereby determining values for the functions coefficients. In this group we have the Triboelastic models [8, 9, 12].

A second group can be defined where coefficients are determined by extracting ‘specific points on’ and/or ‘tangents to’ the CBFNR’s characteristic hysteresis loop (see Section 3.3). In this group we have, Berg [6], Bergstrom and Boyce [13, 14].

This leaves, Miehe and Keck [16], Lion [18] and Haupt and Sedlan [19] in a third grouping where points on the elastic force response curve are determined by direct measurement. Each element of the model (elastic, viscous and plastic) is described independently and so each can be measured independently by performing suitable tests. The coefficients for the strain energy function are found by a minimisation algorithm fit to a measure of relaxed strain at a number of points. The material is first strained by increasing deformation in steps, at each step the strain is held constant for a long time period; the strain is then decreased in steps, again holding the strain constant for a long period at each step. In this way the elastic stress response is approached from a positive and negative value of visco-elastic stress. The measurements made by, Miehe and Keck [16] and Lion [18] have a constant strain hold time of one hour. Haupt and Sedlan [19] held strain constant for 20,000 seconds (more then five hours). Haupt and Sedlan [19] assumed for their model that at a very long time period the value measured for steps of increasing strain would be identical to values measured for steps of decreasing strain, so the mean of the two values at 20,000 seconds is taken as a point on the elastic stress response line. Lion [18] includes elastic hysteresis in his model, Miehe and Keck [16] include plasto-elasticity in their model but both use stress relaxation to determine coefficient values for the elastic strain energy function.

Finally it should be mentioned that three of the six elastic force models discussed here include a description of the Mullins or Damage effect where the level of stress

decreases in successive cycles; rapidly for the first few cycles on virgin material then by a small amount over many cycles asymptotically to a stable response. This effect is described in, Haupt and Sedlan [18], Lion [17, 18], Miehe and Keck [16].

For comparison, the six CBFNR models discussed here are listed in Table 4.1-1 with a brief description of the function used to describe elasticity and the method by which coefficients for the function are determined.

Model name and Reference	Type of elastic description	Method by which the coefficients for the elastic function are determined
Berg [6]	Linear coefficient	Approximated as being the tangent to a large amplitude-damping loop.
Triboelastic [8, 9, 12]	Linear coefficient	Dynamic stiffness and phase angle are determining by Fourier analysis of response to sinusoidal excitation
Bergstrom and Boyce [13, 14]	Neo-Hookean based hyperelastic model.	Three material coefficients are required for this model. They are estimated from 'points on' and 'tangents to' the hysteresis loop [14].
Miehe and Keck [16]	Two term Ogden strain energy function	The elastic component for this model has 5 parameters, which are found by computer minimisation algorithm, fitting the function to relaxation points.
Lion [18]	Modified 3 term Mooney-Rivlin strain energy function	The three coefficients required are estimated [18]. Relaxation points are used to determine equilibrium stress.
Haupt and Sedlan [19]	Generalised 5 term Mooney-Rivlin model	The 5 coefficients are found by a least squares fit to relaxation points. These points are approached both by applying strain and by removing strain [19].

Table 4.1-1: *A Summary of recent Elastic Stress models developed for Carbon Black Filled Natural Rubber*

4.2 Descriptions for the viscous stress component

4.2.1 Berg's model

Berg's model [6] is predominantly time independent, the majority of damping loss being described by a non-linear friction force. A time dependent Maxwell element is used, but only to modify the models response to match small frequency dependent changes in the hysteresis loop shape. The model replicates the amplitude dependent stiffness (known as the Payne effect [17]) and the almost constant damping loss angle, which are characteristic features of CBFNR. Total force is described as the sum of three parts; an elastic force; a 'viscous' force and a friction force, shown schematically in Fig. 4.2.1-1.

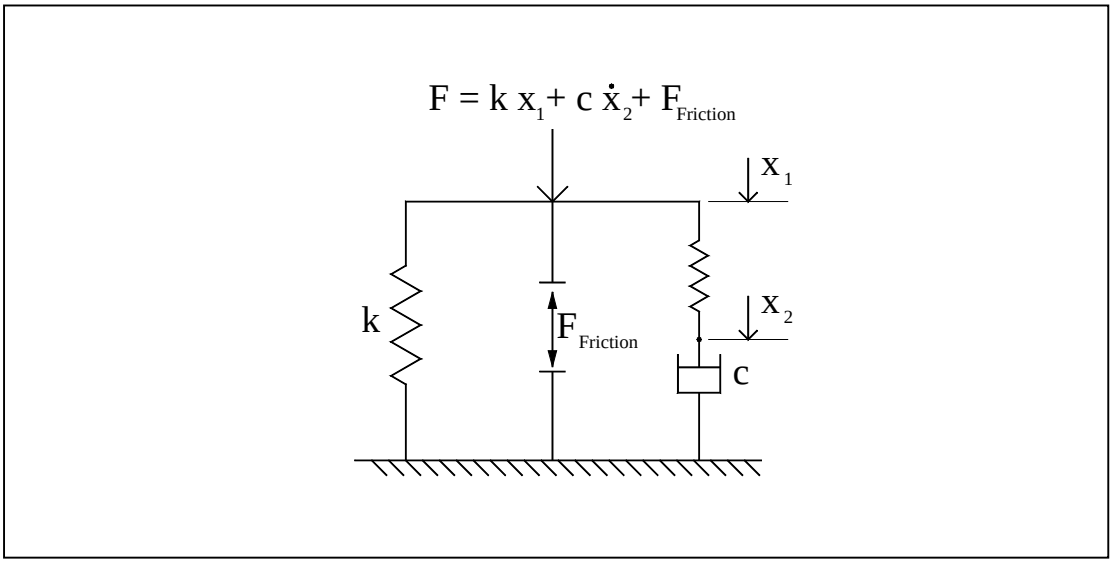

Fig. 4.2.1-1: *Schematic representation of Berg's model*

The elastic force is described by a linear stiffness (k), the viscoelastic force is described by a linear Maxwell element (dashpot and spring in series) and friction force described by a function that is zero at turning points (where velocity is zero) and increase non-linearly (taking the sign of velocity) to a constant value at infinity. Damping loss is predominantly described by the friction force, which is time independent and has the following basic form.

$$F_{Friction} \propto \frac{(x_1 - x_o)}{\beta + (x_1 - x_o)} . \mathrm{sgn}(\dot{x}_1)$$ **Equation 4.2.1-1**

Where, $F_{Friction}$ is the friction force, β is a constant, x_o is the displacement at the previous turning point and x_1 is the current displacement.

Berg's function has an additional scaling factor not shown in Equation 4.2.1-1 that changes the form of the friction function depending on the ratio of friction force at the previous turning point (x_o) to the maximum possible value of friction force at infinite strain. This element of the function has been excluded in Equation 4.2.1-1 for simplicity.

The benefits of using Berg's friction force function are that the asymmetric hysteresis loop shape commonly reported for CBFNR stress strain plots [6, 7, 8, 11] is easily replicated and coefficients for the function are easily determined by comparison with measured data by varying the constant β; but the model has limited application. Hysteresis is predominantly described by the time independent friction force, which means that realistic stress relaxation response is not well represented. Also, as Berg mentions himself, at high frequency the viscoelastic force described by a single linear Maxwell element tends to zero so that damping is described by the friction force function only.

The difficulty with a model of this type, where damping is described by a function that rises monotonically taking the sign of velocity, is its application in dynamic analysis software that uses the implicit Newton-Raphson Predictor Corrector method. The model requires storage of force and displacement values at each turning point. Turning points must be detected and then new values must be 'assigned' as described by Equations 4.2.1-2 and 4.2.1-3.

At a turning points; $F_o = F_o + \Delta F$ **Equation 4.2.1-2**

And; $X_o = X_o + \Delta X$ **Equation 4.2.1-3**

Where F_o and X_o are force and displacement at the previous turning point respectively, ΔF and ΔX are change in force and displacement since the previous turning point respectively.

Assigning values to variables is not a standard operation in dynamic analysis software that uses the Newton-Raphson Predictor Corrector method and if attempted will cause the algorithm to fail. It may be possible to overcome this difficulty by modifying the algorithm but this would require advanced programming and mathematical knowledge, and if it where achieved the result is likely to be inefficient; since turning points must be detected and the simulation halted, then restarted with the reassigned turning point values.

4.2.2 Triboelastic model

The Triboelastic model, introduced by Turner [7] and further developed by Coveney and Johnson [8] is a time independent model.

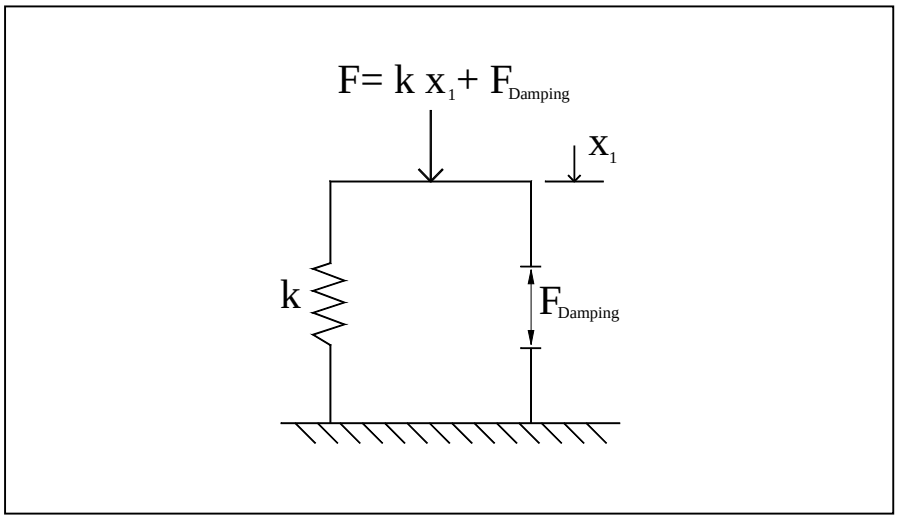

Fig. 4.2.2-1: *Schematic representation of the Triboelastic model*

Total force is described by the sum of two parts (Fig 4.2.2-1), a linear elastic element and an element that describes the shape of a velocity independent hysteresis curve that is zero at turning points (at zero velocity) and increases non-linearly (taking the sign of velocity) to a constant value at infinity.

The Triboelastic model is based on a phenomenological description that 'imagines' a large number of microscopic, one dimensional, Coulombic elements, linked by springs, resulting in an square root relationship between force and displacement that has the following form:

$$F_{Damping} \propto (x - x_o)^{1/2}.\mathrm{sgn}(\dot{x}) \qquad \textbf{Equation 4.2.2-1}$$

Where, $F_{Damping}$ is damping force, x is current displacement and x_o is displacement at the previous turning point.

The Triboelastic model however has the same limitation as Berg's model. Being time-independent stress relaxation is not modelled and the describing function requires values of force and displacement at the previous turning point to be stored and reassigned causing difficulty in implementation in automatic dynamic analysis software.

4.2.3 Rate dependent Triboelastic models

Coveney and Johnson [9] explore two possible modifications to the Triboelastic model described above. These are the 'Triboelastic visco-solid model' (TVS) and the 'Rate dependent Triboelastic model' (RT). For the TVS model a Maxwell element is added to the standard Triboelastic model making it almost identical to Berg's model (described in section 4.2.1). Since the TVS model is very similar to the Berg model it has the same limitations; limited ability to describe stress relaxation, no viscous

damping component at high frequency and a requirement for assigned variable values at turning points.

The RT approach is to replace the Triboelastic element with a non-linear Maxwell element that uses a 'power' relationship to achieve the predominantly rate independent damping force; this is shown schematically in Fig. 4.2.3-1.

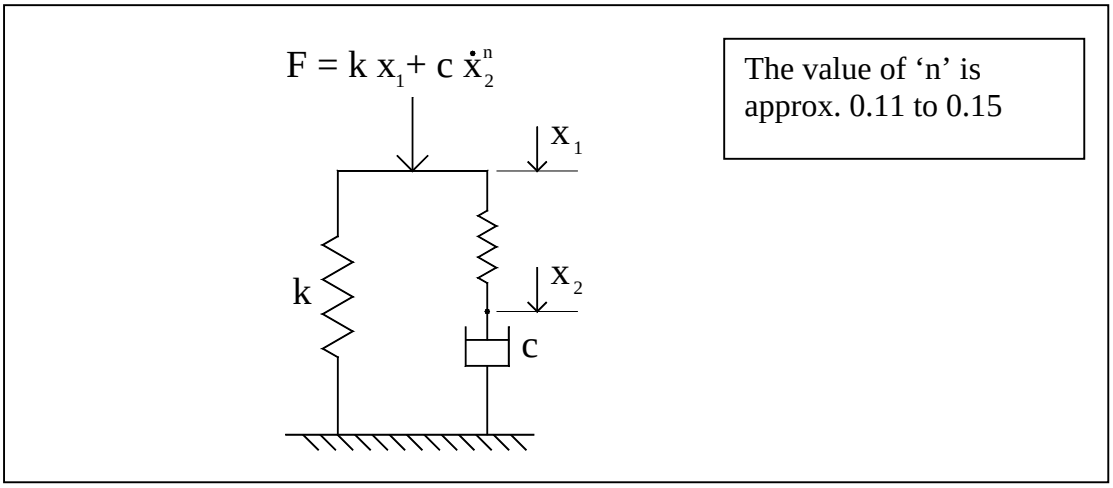

Fig. 4.2.3-1: *Schematic representation of the Rate Dependent Triboelastic (RT) model*

The RT model however has two failings; by describing damping with a power law the Triboelastic inverse square relationship, which approximates the asymmetric hysteresis loop shape of CBFNR, is lost and being a function of velocity only it does not have the flexibility of Berg's friction function which is easily adjusted, (by varying the constant β) to describe the measured hysteresis loop. Secondly when 'n' has a low value, which is required to describe the materials almost time-independent damping, sudden changes in the force vector at zero velocity (where $\frac{dF}{d\dot{x}} = \infty$) causes simulation difficulty. Numerical simulations using the Newton-Raphson Predictor Corrector method require smooth functions for trouble free operation [41, 44]. To achieve this in the RT model the power relationship must be changed to a standard linear Maxwell element at low velocity, i.e. below some value of $\dot{x}_2$, n=1. Although

this is easily implemented the question of…'at what velocity do we change the function from linear to non-linear so that a given simulation does not fail but the model still represents the components damping properties'…is an additional complication for a modeller to consider. Fig 4.2.3-2 illustrates this problem. The continuous line shows the form of a non-linear damping function dependent on x^n where 'n' has a low value. The dashed line represents linear damping where 'n = 1'.

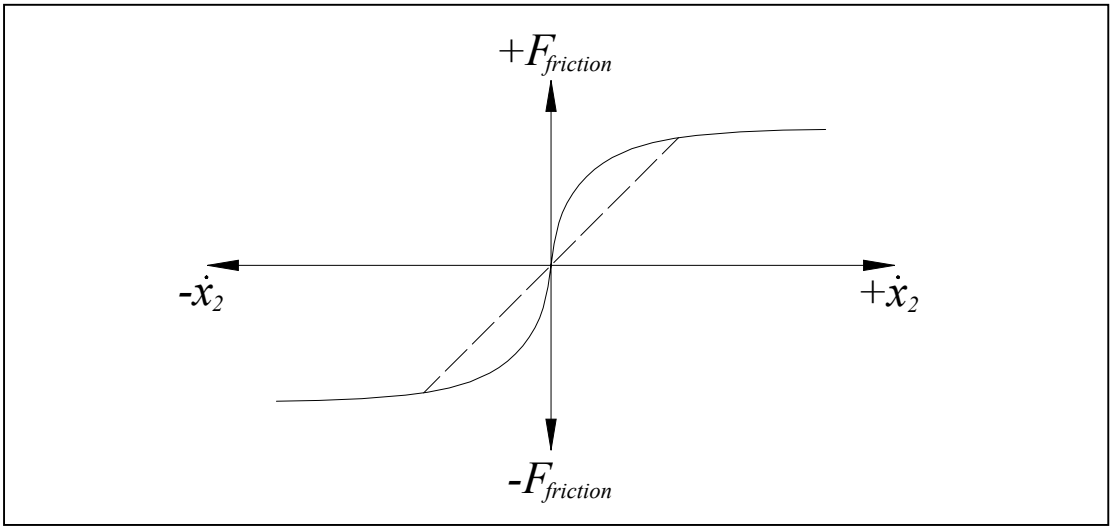

Fig. 4.2.3-1: *Illustration showing the requirement for a linear viscous relationship at low velocity to prevent rapid changes in the force vector*

4.2.4 Bergstrom and Boyce model

Bergstrom and Boyce [13] discussed the micro-mechanical behaviour of CBFNR and developed a constitutive model that is the sum of two parts, an equilibrium response (elastic force) and a 'time-dependent deviation from equilibrium' (visco-elastic force). This model is similar to the Triboelastic RT model (described above) with just two differences; equilibrium response is described by a hyperelastic model (see section 4.1) and time dependent response is a function of both velocity and displacement raised to a power; this is shown schematically below in Fig. 4.2.4-1.

Bergstrom and Boyce described the elastic force ($F_{Elastic}$) by a Neo-Hookean based hyperelastic function (see section 4.1) and the viscous force by a function that has the following form:

$$F_{Viscous} = c\left(|x| \dot{x} \right)^n$$

Equation 4.2.4-1

Where $F_{viscous}$ is the damping force, $|x|$ is displacement across the visco-elastic element, $\dot{x}$ is velocity across the viscoelastic element, 'c' is a damping coefficient and 'n' the power term is approx. 0.25

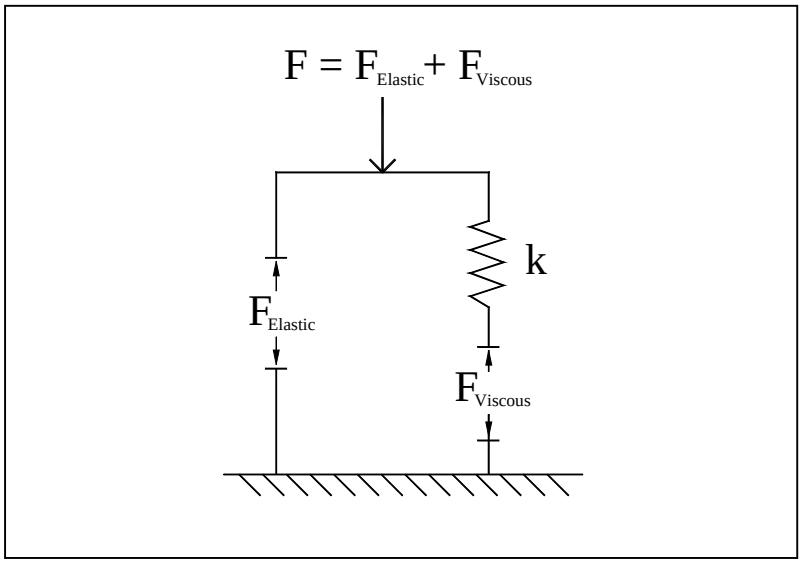

Fig. 4.2.4-1: *Schematic representation of the Bergstrom and Boyce model*

In their report [13] Bergstrom and Boyce show good correlation with measured data. The addition of displacement or strain dependence $|x|$ may help with the functions ability to fit measured data i.e. achieve the asymmetric hysteresis loop shape, but the description suffers from the same drawback as the rate dependent Triboelastic RT model regarding its application in dynamic analysis software. Where the Newton-Raphson Predictor Corrector method is used a non-linear Maxwell element using a power law with a value of n = 0.25 results in rapid changes in the force vector at low velocity causing computational difficulties.

4.2.5 Miehe and Keck

A one-dimensional interpretation of the constitutive model developed by Miehe and Keck [16] is shown schematically in Fig 4.2.5-1 with the relevant descriptive functions (Equations 4.2.5-1 & 4.2.5-1). This is similar to the 'Berg' and 'Triboelastic viscous solid (TVS)' models described above. Here though the visco-elastic and plasto-elastic elements are described by exponential functions of strain, which have a larger number of parameters and therefore give the model greater ability to match trends in the measured data.

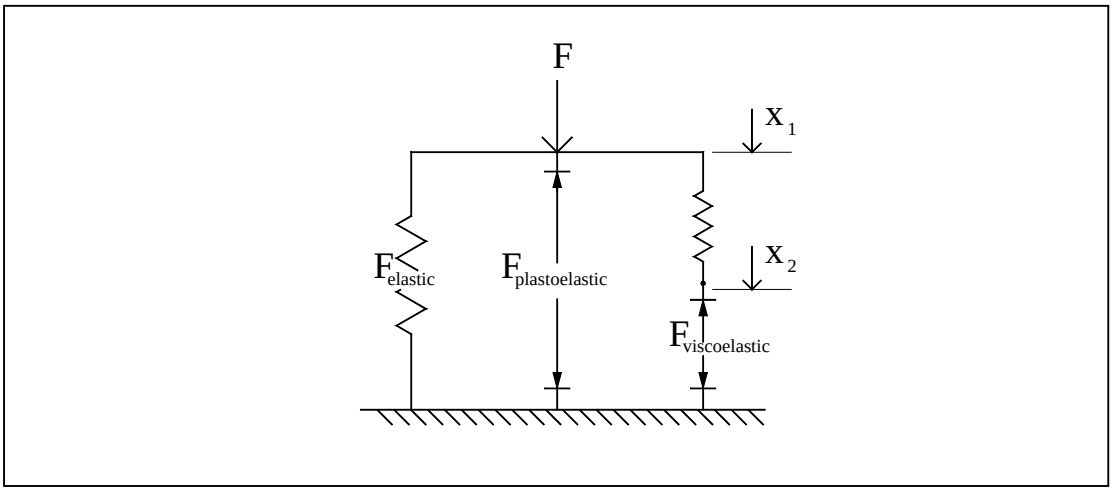

Fig. 4.2.5-1: *Schematic representation of the Miehe and Keck model*

$$F_{visco\text{-}elastic} = A \exp\left[Bx_1 + Cx_2\right]\dot{x}_2 \qquad \textbf{Equation 4.2.5-1}$$

$$F_{plasto\text{-}elastic} = P\exp\left[Qx_1\right] \qquad \textbf{Equation 4.2.5-2}$$

Where, $F_{visco\text{-}elastic}$ is the visco-elastic damping force $F_{plasto\text{-}elastic}$ is the plasto-elastic damping force *A, B, C, P & Q* are constants.

Miehe and Keck [16] showed good correlation between measured and modelled strain responses up to 200% in their report. The model describes elasticity using a two-term Ogden function, also 'Mullins effect': stress softening during the first loading cycles

is described, giving the model a total of 20 parameters. However, a description of Mullins effect is not required in a vehicle model because the rubber components undergo many strain cycles at all levels early in their long life, so that the stress softening effect becomes insignificant.

The nonlinear plasto-elastic and visco-elastic stress descriptions give this model the ability to match a wide range of data measurements, but the large number of parameters means that a computer minimisation algorithm is required to determine values for these functions.

4.2.6 Lion

Lion [18] presented a phenomenological model for carbon black filled natural rubber that described, non-linear elasticity, non-linear elastic hysteresis (plasto-elasticity), non-linear visco-elasticity and Mullins stress softening. This model has the same modular components as the Miehe and Keck model described above (Fig. 4.2.5-1), however the functions differ. Each element is described by a strain dependent function. Polynomial functions that include 'Neo-Hookean' and 'Mooney-Revlin' as special cases are used as non-linear multiplying terms in the description of each component i.e., elasticity, plasto-elasticity and visco-elasticity are all non-linear functions of strain. For the viscoelastic element this strain magnitude dependent term is combined with an exponential relationship that describes non-linear rate dependence, so that:

$$\sigma_v = f(\varepsilon, \dot{\varepsilon}) \qquad \textbf{Equation 4.2.6-1}$$

Where, σ_v, ε and $\dot{\varepsilon}$ are viscoelastic stress, strain and strain rate respectively.

The constitutive equations and viscoelastic description for this model given by Lion [18] are difficult to interpret and translate into a simple descriptive function that can

be implemented as discrete components in computer software or described by discrete components in a schematic representation. Because of its complexity this model has not been implemented and it is not possible to comment on its suitability for one-dimensional modelling of vehicle components in automatic dynamic analysis software.

4.2.7 Haupt & Sedlan

The model developed by Haupt & Sedlan [19] has elastic and viscoelastic elements only (referred to as ‘equilibrium stress’ and ‘over stress’ elements respectively). The Mullins effect is not described and experimental measurements show that plasto-elasticity is not significant. The final Haupt and Sedlan constitutive model has 15 parameters describing non-linear equilibrium stress in parallel with three visco-elastic elements that have strain-history dependent viscosity.

There are two features of this model that are not present in any of the models described above. These are the viscoelastic element, which naturally produces an asymmetric stress-strain response and is weakly time-dependent and ‘strain history’ dependent visco-elasticity. It was found that the non-linear Maxwell element used in this model reproduces the basic features of CBFNR and is easily described by discrete components and implemented in automatic dynamic analysis software. However, the ‘strain-history’ element of the Haupt and Sedlan model is complex and requires a great deal of experimental data to determine values for its coefficients. An interpretation of the ‘strain-history’ dependent function is given below in Equation 4.2.7-4 and a diagram showing how it could be implemented using discrete components in automatic dynamic analysis software given in Fig.4.2.7-2. A simplified model of the Haupt and Sedlan model with only a single visco-elastic

element and without strain-history dependent viscosity is shown schematically in Fig 4.2.7-1.

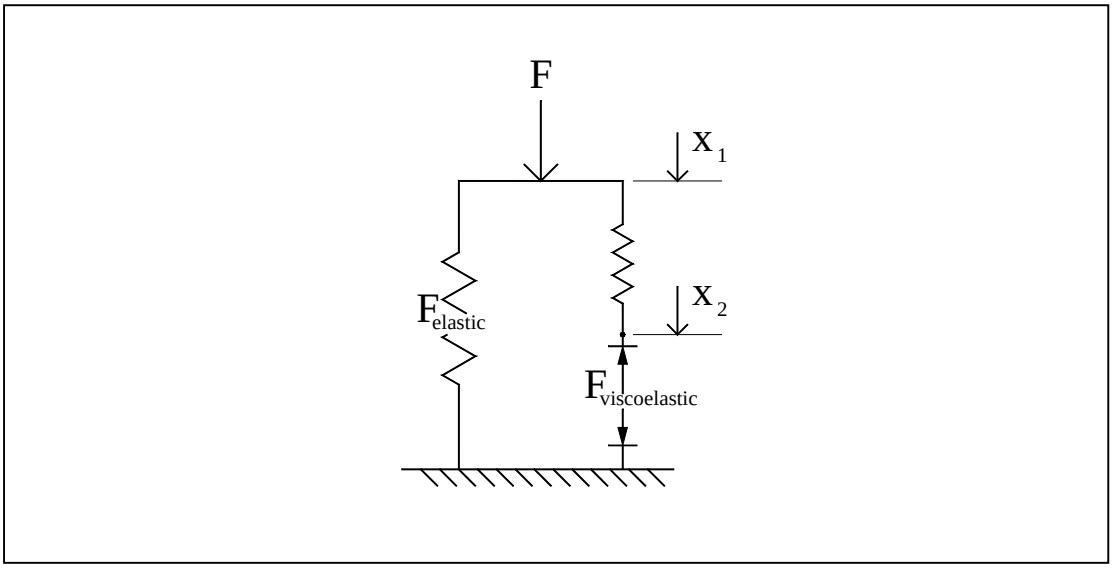

Fig. 4.2.7-1: *A one-dimensional and simplified schematic representation of the Haupt and Sedlan model (with a single viscoelastic element only)*

The elastic element is described by a five-term Mooney-Revlin function. The viscoelastic force is described by the following function:

$$F_{viscoelastic} = \frac{c\dot{x}_2}{|\dot{x}_1| + \xi} \qquad \textbf{Equation 4.2.7-1}$$

Where 'c' and 'ξ' are constants (the symbols used in this expression are not the same as those used by Haupt and Sedlan [19]). Strain-history dependence is not described; this function is a simplification of the Haupt and Sedlan model. The form used here is simply a standard linear Maxwell element where the viscous force is divided by the magnitude of strain rate ($\dot{x}_1$) plus a constant (ξ). In Haupt and Sedlan model 'ξ' is a 'process dependent variable' that has a low value at low strain rate and a high value at high strain rate to simulate strain history dependent viscoelasticity.

For a small value of ξ and/or high value of $\dot{x}_1$ Equation 4.2.7-1 produces an exponential response described by the following function (derivation given in Appendix 1):

$$F_{viscoelastic} = c.\mathrm{sgn}(\dot{x}_1) - (c.\mathrm{sgn}(\dot{x}_1) - F_0).Exp\left(-\frac{k.\mathrm{sgn}(\dot{x}_1)}{c}.(x_1 - x_0)\right)$$

Equation 4.2.7-2

And in response to a stepped input the visco-elastic element relaxes exponentially in the following way, (derivation given in Appendix 2):

$$F_{viscoelastic} = F_o.Exp\left[\frac{-\xi.k.t}{c}\right] \qquad \textbf{Equation 4.2.7-3}$$

For Equations 4.2.7-1, 4.2.7-2 and 4.2.7-3, ξ is a constant, c is maximum possible visco-elastic damping force, $\dot{x}_1$ total strain velocity, $\dot{x}_2$ strain velocity across the dashpot, F_o and x_0 viscoelastic damping force and displacement at the previous turning point respectively, x_1 is displacement, k stiffness coefficient and t time.

Equation 4.2.7-2 and 4.2.7-3 show that at high velocity this viscoelastic element produces a stable hysteresis loop enclosed by rising and falling exponential curves (see Fig 6.2-1) and at zero velocity the damping force decays exponentially. Thus the fundamental features of CBFNR are described. These are; an asymmetric hysteresis loop, predominately frequency independent damping and stress relaxation. In addition to this, the function is easily understood and easily implemented, it is also ‘smooth’ and continuous making it ideal for implementation in automatic mechanical system simulation software that uses the implicit Newton-Raphson predictor corrector method.

The Haupt and Sedlan model [19] uses three viscoelastic elements in parallel to achieve the required fit to measured data and in addition to this, values for 'ξ' are made 'strain-history' dependent so that stress relaxation measurements, (which showed differing decay rates depending on preceding strain history) could be modelled. We see in Equation 4.2.7-3 that rate of stress relaxation is partly determined by the constant ξ. In the Haupt and Sedlan model 'ξ' is made variable so that when stationary the value of ξ decrease over time to a constant low value, simulating high viscosity. As velocity ($\dot{x}_1$) increases the value of ξ increases to a constant high value, simulating low viscosity. The model prevents maximum and minimum values of ξ from being exceeded and the rate at which ξ changes depends on an independent relaxation time. This behaviour can be described schematically as discrete components by the use of an independent Kelvin element, which behaves as an exponentially decaying memory of strain rate ($\dot{x}_1$). The visco-elastic function (Equation 4.2.7-1) is modified as follows:

$$F_{viscoelastic} = \frac{c\dot{x}_2}{|\dot{x}_1| + Ax_{Kelvin} + \xi} \qquad \textbf{Equation 4.2.7-4}$$

Where c, A and ξ are constants, x_{Kelvin} is displacement of the Kelvin element to which the force applied (F_k) is equal to $|\dot{x}_1|$; $\dot{x}_1$ is total strain velocity; $\dot{x}_2$ strain velocity across the dashpot. This model is described schematically for a single viscoelastic element in Figure 4.2.7-2.

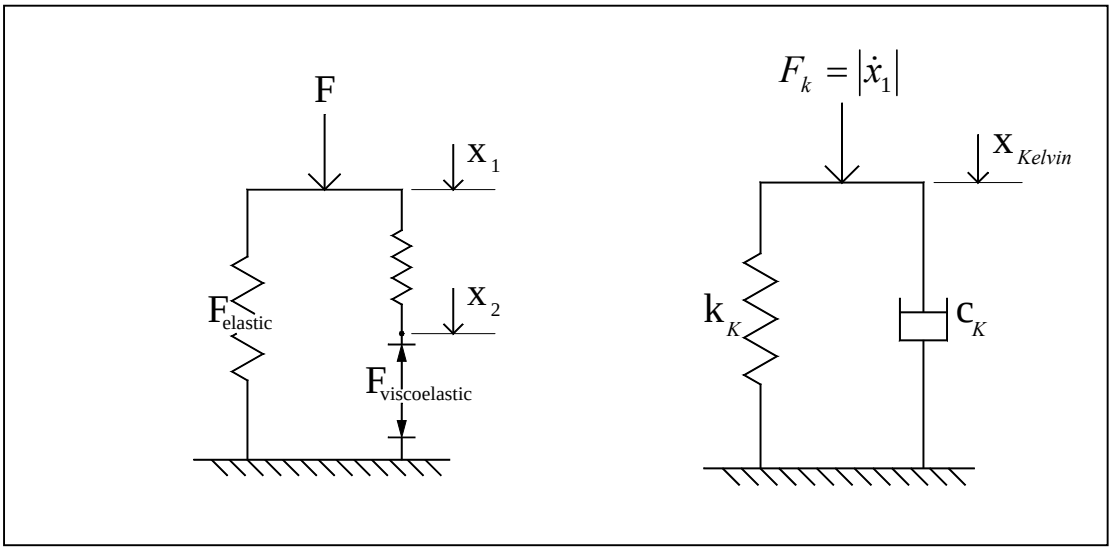

Fig. 4.2.7-2: *A one-dimensional schematic representation of the Haupt and Sedlan strain-history dependent viscosity model (with a single viscoelastic element only)*

In this interpretation (Equation 4.2.7-4) the viscosity variable has a range from 'ξ' minimum to '$A.x_{Kelvin} + \xi$' maximum and the 'rate of change of viscosity' is determined by $\frac{k_k}{c_k}$. To make this viscoelastic model identical to the Haupt & Sedlan model, force acting on the Kelvin element (F_k) would be given an upper limit thereby limiting the lowest possible viscosity.

The concept of 'strain history dependent viscosity' is further developed in a second paper by Haupt and Lion [20]; demonstrating that the description may need to be more complex then is represented here by the single linear Kelvin element shown in Fig 4.2.7-2.

4.3 Summary

1. Six models developed in resent years for modelling the dynamic response of Carbon Black filled Natural Rubber (CBFNR) have been reviewed. These are, Berg [6], Triboelastic [8, 9, 12], Bergstrom and Boyce [13, 14], Miehe and Keck [16], Lion [18], Haupt and Sedlan [19]. All these models describe total stress as the sum of an elastic (in-phase) stress and a damping (out-of-phase stress) where each element responds independently of the other.
2. 'Mullins' or 'Damage' effect is included in some of the models discussed here but this material behaviour is not relevant to vehicle components, which undergo many cycles in their long life.
3. We are able to group the various descriptions for elastic stress described in these six models in two ways. Either by the type of function used. Resulting in two groups: Linear elastic, and Nonlinear strain energy function. Or by the method used to determine coefficients for the elastic stress function. Resulting in three groups: Fourier analysis, 'Points on' and/or 'tangents to' the hysteresis loop, and a method where damping force is allowed to relax over a long period of time.
4. Models that describe damping by storing values of force and displacement at turning points (Berg [6] and Triboelastic [8, 9]) are not suited to use in dynamic analysis software simulations that use the Newton-Raphson Predictor Corrector method, as the algorithm does not allow for this operation.
5. Models that use a 'fractional power' to describe the predominately rate independent damping force of CBFNR (Triboelastic [12], Bergstrom and Boyce [13, 14]), are also not suited to this type of software because the rapid change in force vector at zero velocity can cause the algorithm to fail.

6. The models proposed by Miehe and Keck [16], and Lion [18] have a large number of parameters in their descriptive functions and as a result measured and modelled responses correlate over a wide range of strain (up to 200%). However the large number of constants means that a computer minimisation algorithm is required to determine their values. Also the descriptions can be complex and difficult to implement as discrete components in multibody dynamic analysis software.

7. Of the models reviewed here the most appropriate for the simulation of CBFNR components is that proposed by Haupt and Sedlan [19], since it is easily implemented as discrete components in dynamic analysis software and is computationally robust. It also reproduces the fundamental features of CBFNR which are; an asymmetric hysteresis loop, predominately frequency independent damping and stress relaxation.

   However, the strain history dependent viscosity described in this model is complex and requires a great deal of experimental data to determine values for its coefficients.

Chapter 5

Test rig design, experimental procedure and measurement for rubber components

5.0 Introduction

The characteristics of two Carbon black filled natural rubber components (CBFNR) from the Warrior Armoured Personnel Carrier (APC) Track Running Gear were measured. These two components were the ‘road wheel tyre’ and the ‘track link bush’. Road wheel tyre measurements are simply radial force-displacement responses where the load is applied perpendicular to the wheel’s circumference by a ridged flat steel surface to simulate contact with the tracks links. The wheel does not rotate; measurement and analysis of a rolling solid rubber tyre would be the subject of further work. The track link bush was measured in two directions, radial (perpendicular to the bush axis) and torsional (about the track bush axis). Of the six degrees of freedom, these two bush dimensions are the most relevant to the simulations of track motion and frequency response. These two track bush dimensions (radial and torsional) are treated here as two separate components; a three dimensional constitutive material model is not developed. This simplification can be justified because the objective here is to create a simple one-dimensional model that captures the components basic stiffness and damping characteristics. Therefore the responses of three carbon black filled natural rubber (CBFNR) components are investigated. These are; tyre radial characteristics; track bush radial characteristics and track bush torsional characteristics.

These three components have been chosen firstly because of their importance in any track running gear simulation but also because they provide good data for developing

a generic model that could describe any other rubber component in the Warrior APC running gear. Tyre measurements exercise the material in compression only but its geometric cross-section changes considerably as it is compressed against the flat surface. The track bush torsion measurement exercises the material predominantly in shear and the track bush radial measurement exercises the material predominantly in compression. A model that describes these three track components will be ‘general purpose’.

The response of each component to steady sinusoidal displacements with small amplitude and varying preloads, and with a varying amplitude and constant preload, has been measured to determine parameters for, elastic, geometric and viscoelastic descriptions. In addition to this, measurements were made at frequencies ranging from 0.1Hz to 20Hz to illustrate the components insensitivity to varying strain rate and stress relaxation to determine values for time-dependent parameters. Also the track bush torsional response to a dual-sine displacement history was measured for comparison with the response reported by Coveney and Johnson [8] and to simulate the type of strain history (combined high-frequency low-amplitude and low-frequency high-amplitude displacement) a component might experience on the vehicle.

Temperature effects are not studied since Warrior APC track components operate well above the materials glass transition temperature where modulus and loss angle are almost constant. The glass transition temperature for carbon black filled natural rubber occurs at around -40°C (see Figs. 3.1-2, 3.1-3).

5.1 Warrior APC track rubber components

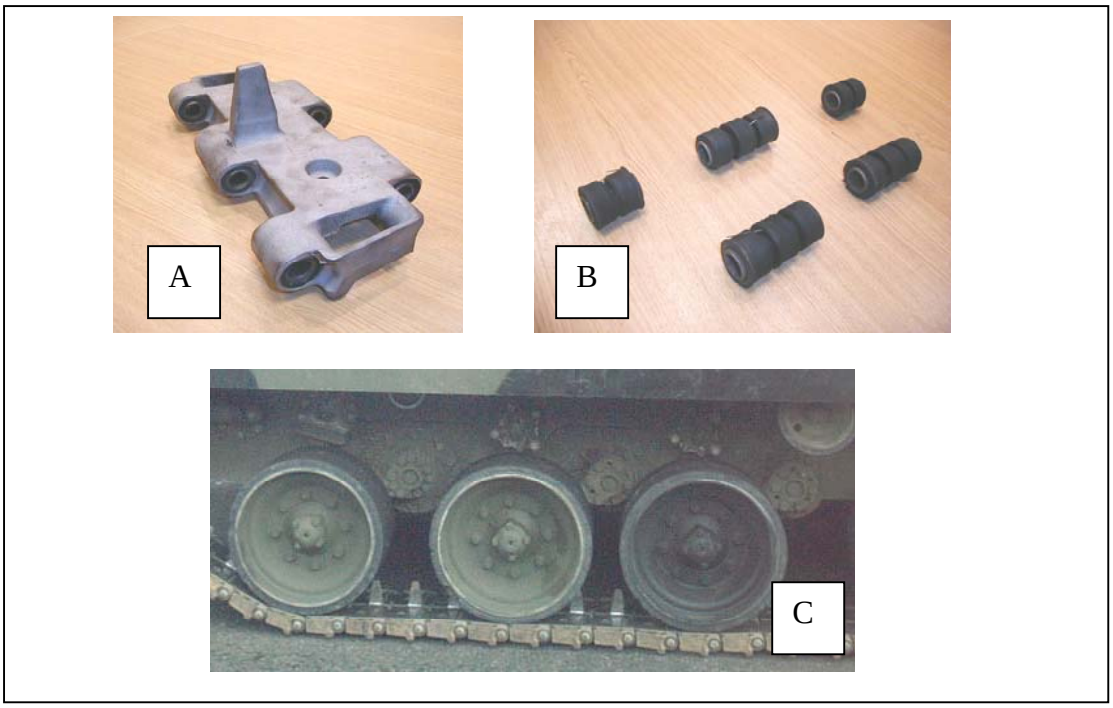

Fig. 5.1-1: *Warrior APC rubber track components; (A) A single Track link (B) Track bush sections removed from the track link casting (C) Road wheel tyres*

5.1.1 Road wheel Tyre

Road wheel tyres are made from a solid layer of CBFNR moulded onto the wheel's aluminium wheel hub. Road-wheel tyre material is 60phr (parts per hundred rubber by weight) N550 natural rubber (AVON compound code: 4X59). Tyre dimensions are; inside diameter = 538mm; outside diameter = 613mm; width = 128mm. Figure 5.1-C shows three road wheels on the vehicle. A wheel is made from an assembly of two identical cast aluminium hubs each with a moulded rubber tyre. These 'half-wheels' are bolted back-to-back so that the tyres run either side of the track horn. It is the tyre of one 'half-wheel' that is the subject of this study. The vehicle has twelve road wheels and weighs approximately 27 tonne therefore when stationary each tyre carries a load of around 11kN. The road wheel tyre measurements carried out in this study range up to 40kN, more then three times the tyres static load.

5.1.2 Track bush

Track bush material is 40pphr N200 natural rubber and when fitted into the track link casting its dimensions are; inside diameter = 31mm; outside diameter = 42mm; combined length of all five bushes (i.e. joint length) = 425mm. The joint between adjacent tracks links is made up of five individual sections of bush (Fig. 5.1-1B) each moulded onto a steel sleeve with an octagonal centre that engages with the track pin. The response of individual bush sections is not measured in this investigation; it is the response of the joint assembly that is measured. Therefore for the purpose of this study the term, 'track bush' refers to the assembly of five individual rubber sections. Before being fitted to the track link casting the bush sections have an outside diameter of 47mm. The material therefore has a high degree of pre-compression when the track is unloaded, being compressed from its relaxed state of 47mm diameter to 42mm diameter. It is assumed that the bush has been designed so that the material is under compression even when it experiences the maximum amount of torsion (approx 23°) when passing around the vehicles driving sprocket and idler wheel. This design ensures that the outer diameter of the bush does not rotate relative to the track link casting under normal operating conditions. Figure 5.1A shows the assembled track link casting and bush sections. All motion between adjacent links (neglecting pin clearance and small amount of strain in metal components) is possible only by torsional, radial and longitudinal motion of the track bush rubber.

Track link joints have a designed static equilibrium angle of 10°; this is commonly referred to as the tracks 'live-angle' and is the angle between adjacent track links at which there is no torsional strain about the track pin. The purpose of the 'live-angle' is to minimise the maximum amplitude of torsional strain in the bush rubber. So that maximum rotational amplitude occurs in one direction as the track joint passes over

drive sprocket and idler wheel, and in other direction as it is traverses the top span and ground contact.

When the track is assembled on the vehicle it is tensioned to approximately 13kN. Radial bush measurements carried out in this study range up to 50kN, more than three times static bush load.

5.2 Test rigs design and experimental procedure

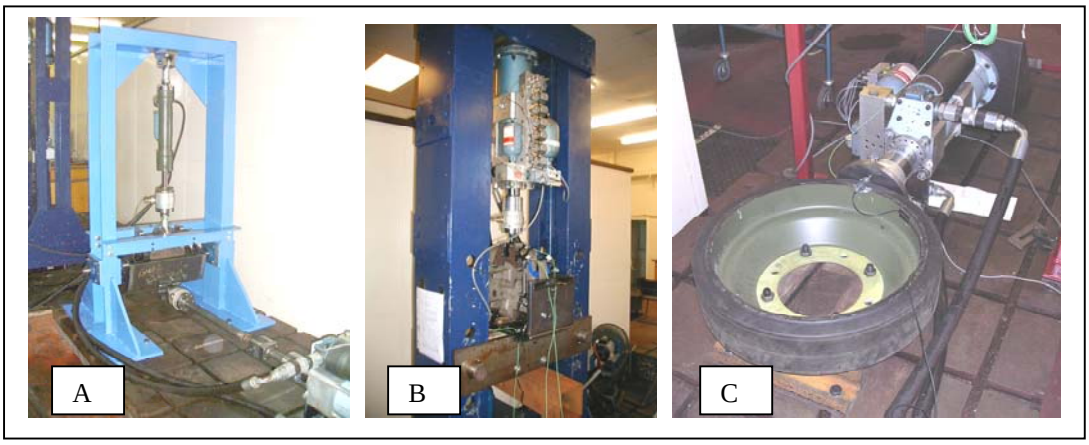

Fig. 5.2-1: *(A) Measurement of track bush torsional characteristics by rotation about the track bush axis (B) Measurement of Track bush radial force and displacement (C) Measurement of road wheel tyre radial force and compression*

Test rigs were constructed to measure each of the three track components: track bush torsion, track bush radial and road wheel tyre radial characteristic, shown above in Figures 5.2-1 A, B and C respectively. Each component was exercised by a displacement-controlled hydraulic cylinder. For drawings detailing test rig design, data acquisition and control see Appendix 7. In each case the effect of four variables were investigate, preload, amplitude, frequency and time. The four tests were as follows:

(I) Low amplitude at various preloads, 1Hz sinusoidal displacement

(II) Constant preload at various amplitudes, 1Hz sinusoidal displacement

(III) Constant amplitude and constant preload at, 0.1Hz, 1Hz, 10Hz and 20Hz sinusoidal displacement.

(IV) Stress relaxation: Response to a stepped displacement over time.

In addition to the tests listed above, two further measurements where taken. A measurement of the track bush torsional response at various radial loads has been made to investigate the degree of interaction between these two components, this result is presented in Section 5.7. Also the track bush torsional response to dual-sine displacement has been measured. This replicates the dual-sine test reported by Coveney and Johnson [8]. The frequency ratio between secondary and primary sine waves is 15:1, amplitude ratio 10:1. The dual-sine measurement is presented in Section 5.8.

Before the time domain measurements described above where conducted, components were allowed to normalise to room temperature (17° - 20°C).

Also the frequency response of each test rig was measured so that resonance effects would be avoided. These test rig frequency response measurements (and a short discussion of methodology and associated issues) are presented in Appendix 3. Track components time domain response measurements are shown to be valid up to the following frequencies:

- Track bush torsional force measurement (Fig. 5.2-1A) : 6Hz
- Track bush radial force measurement (Fig. 5.2-1B) : 75Hz
- Tyre radial force measurement (Fig. 5.2-1C) : 20Hz

5.2.1 Data Acquisition and Signal Processing

The following points cover the issues associated with data acquisition and signal processing.

- Force is measured by strain gauge load cell, displacement by Linear Variable Displacement Transducer (LVDT), acceleration by piezoelectric transducers.
- Calibrated force, displacement and acceleration signals were recorded to computer memory via a standard data acquisition board that has a maximum acquisition rate of 100kHz.
- Inline low-pass filters set to one quarter the sample rate frequency where used to prevent aliasing. For example: A 1Hz strain cycle was collected at a rate of 400 samples per second and the low pass filters set to 100Hz.
- Five cycles where averaged to ‘smooth’ cycle-to-cycle variation and sample rate set to collect 400 samples per cycle. Therefore the maximum sample rate required was 8000 samples per second for a 20Hz strain cycle frequency; well within the data acquisition board’s specifications.
- Particular care was taken to compensate for force due to the acceleration of test rig components that connect load cell and track component. This source of error is proportional to the amplitude of displacement and the square of acceleration. An accelerometer was attached to the load cell. Then the true force applied to the component measurement was found simply by subtracting the product of acceleration and the mass of components connecting load cell and component.
- Before taking measurements, the components where exercised through 20-30 cycles at maximum load to remove the stress softening (Mullins effect) seen on the first loading cycles of new unstrained rubber.

Attention to the above points enabled repeatable measurements to be made.

5.3 Measurement I:

Low amplitude displacement with various preloads, 1Hz sinusoidal displacement

The purpose of this measurement was to determine coefficients for polynomials that describe, elastic force and visco-elastic force relative to absolute strain (or absolute deformation) of the rubber component.

For a CBFNR model it is assumed that, in response to stable cyclic motion, the elastic force lays equidistance between the maximum and minimum damping force values. This assumption is best illustrated in the measured response of Figure 5.3.1-2, where the elastic response is taken as the ‘mean’ of two lines drawn through the turning points of small amplitude hysteresis loops of differing preload.

This assumption is common to all elastic stress models discussed in Section 4.1 and is an outcome of their descriptions for viscoelasticity, which have the same magnitude in both directions i.e. there are not differing damping coefficient depending on the direction of motion since the previous turning point.

Here the experimental method used to find a function that describes the elastic force differs from that used by, Mieche and Keck [16], Lion [18] and Haupt and Sedlan [19], who found equilibrium stress by a series of stress relaxation measurements (Table 4.1-1). It is assumed here that the effect of stress relaxation on the measured mean position of a small amplitude hysteresis loops can be removed by first setting the preload level then increasing the amplitude of a sinusoidal displacement so that a high level of both increasing and decreasing viscoelastic force is generated, then reducing the displacement to the small amplitude. It is assumed that this process stabilizes the hysteresis loop so that its mean value is stable from cycle to cycles (does not relax further) and lies on elastic force line. By this method the time required to collect data to determine the elastic force response is reduced from more then a day to

less then 60 minutes. However, this method has not been thoroughly validated. Validation would require careful measurement and would be the subject of further study.

This method of determining a polynomial relating force to displacement by taking the mean point through small amplitude hysteresis loops of varying preload has a secondary benefit. The measurements also provided data that enables the determination of a viscoelastic ‘geometric multiplier’ or ‘strain function’. Changing geometry as in the case of the radial compression of a solid rubber tyre not only produces a non-linear elastic component; viscoelastic force is also dependent upon absolute deformation. It is assumed here that the change in viscoelastic force due to a components changing cross-section can be measured by comparing the amplitude of hysteresis loops that have the same displacement amplitude but have different preloads. The effect of changing geometry is then modelled simply by multiplying the viscoelastic elements response by a function of displacement.

The procedure for the low-amplitude, varying displacement measurement was as follows:

- The preload was applied.
- The amplitude of a 1Hz sinusoidal motion was increased to a large value so that the viscoelastic force approaches a constant value in both the forward and reverse directions i.e. a fully developed hysteresis loop.
- Amplitude was slowly reduced to a low value and after a short settling time the data for five cycles was recorded.

This sequence of operations was repeated at each preload setting, with care taken each time to ensure that the low amplitude displacement was identical within the limits of the measurement and control system.

5.3.1 Elastic force description

The elastic force is taken as the least mean square fit to the mean of two lines; one connecting the maximum turning point of each low amplitude hysteresis loop, the other connecting the minimum turning points (Figures. 5.3.1-1, 5.3.1-2 and 5.3.1-3).

Figures 5.3.1-1 and 5.3.1-2 show the track bush response in each of the two dimensions, torsional and radial respectively. A linear fit has been used in both cases as this gives a good approximation and is sufficient for vehicle component simulation.

Notice that the response in torsion (Fig.5.3.1-1) is close to zero at 10° as it should be since the Warrior APC track links have a ‘live-angle’ (static equilibrium angle) of ten degrees. Also notice that the least mean square linear fit to the radial response (Fig. 5.3.1-2) does not pass though zero force at zero displacement. A possible explanation for this is that these measurements where taken early in the research before the ‘long relaxation time’ behaviour of CBFNR was fully appreciated. The procedure described above which removes this effect was not used in this case but it is expected that if these measurement where repeated with care the linear fit would pass through zero force at zero displacement.

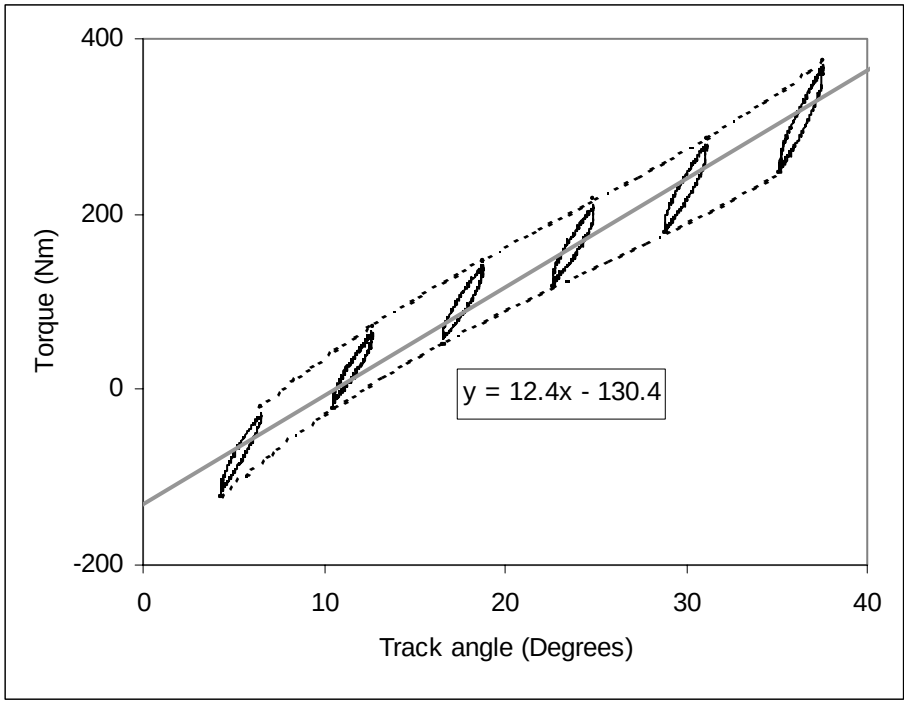

Fig. 5.3.1-1: *Track bush torsional elastic-force response*

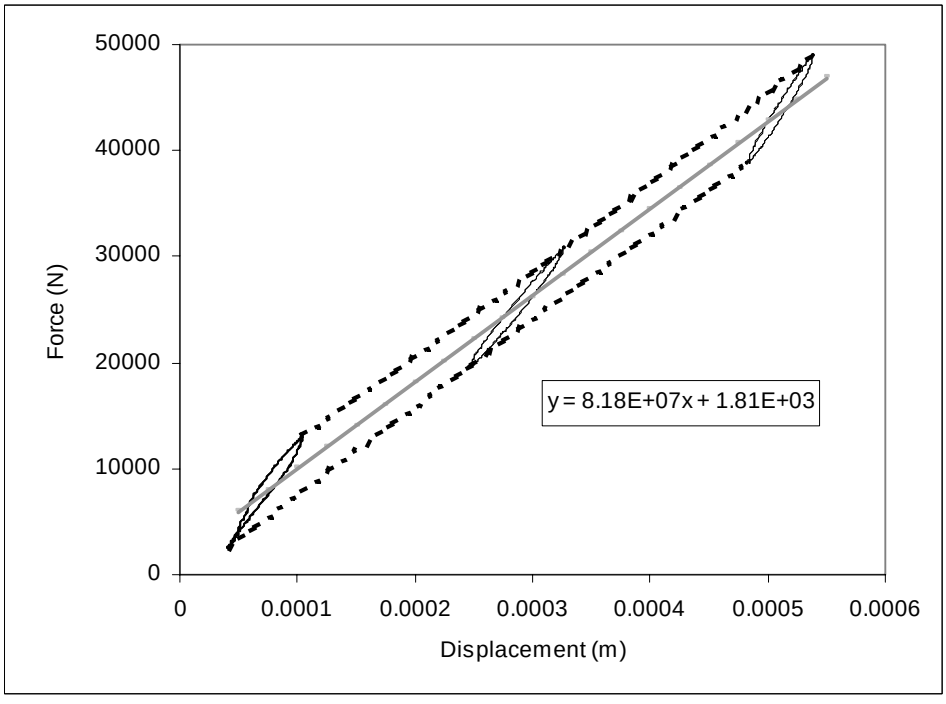

Fig. 5.3.1-2: *Track bush radial elastic-force response*

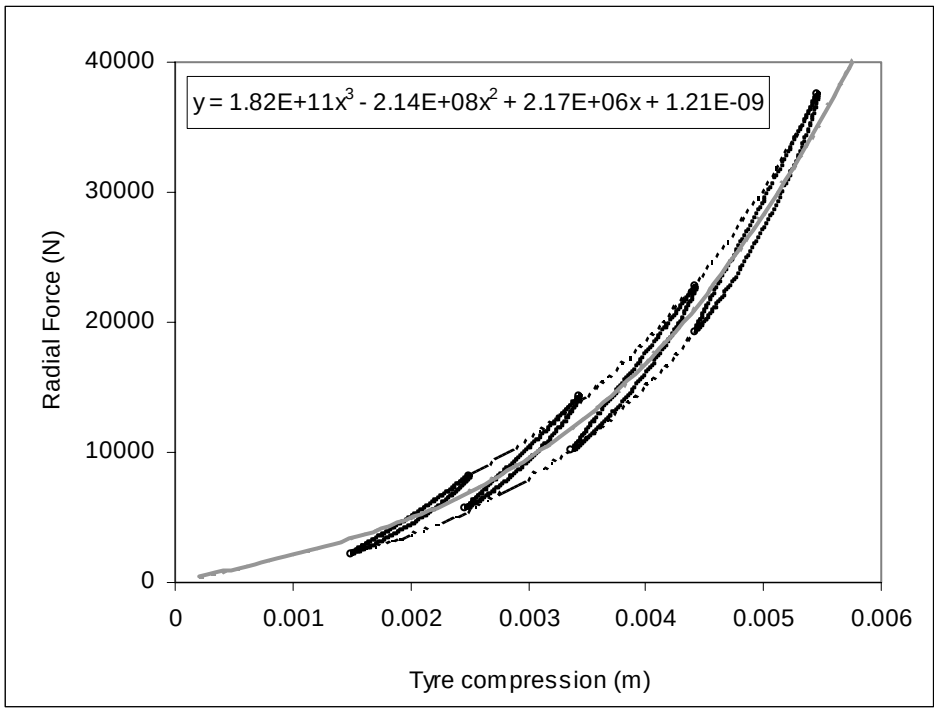

Fig. 5.3.1-3: *Road wheel tyre elastic-force response*

Figure 5.3.1-3 shows the road wheel tyre response to small amplitude sinusoidal displacements at varying preload but identical amplitude. In this case the elastic force response is described by a cubic polynomial. It is significant that the least mean square fit does pass through zero, since this gives confidence in this method of determining the elastic-force response.

In summary, from these measurements we have the following three functions, which describe the elastic force response of each component:

1. For track bush torsional elastic Torque:

$$F_e = 12.4\,\theta - 130.4 \quad Nm \qquad \textbf{Equation 5.3.1-1}$$

Where, F_e is the elastic torque component and θ is the angle between adjacent tracks.

2. For track bush radial elastic force:

$$F_e = 81.8 \times 10^6 x \quad N$$ **Equation 5.3.1-2**

Where: F_e is elastic force and x is track bush radial displacement.

3. For road wheel tyre radial elastic:

$$F_e = 1.82 \times 10^{11} x^3 - 2.14 \times 10^8 x^2 + 2.17 \times 10^6 x \quad N$$ **Equation 5.3.1-3**

Where: F_e is elastic force and x is tyre compression.

5.3.2 Geometric multiplying function

It is particularly noticeable in Figure 5.3.1-3 that the amplitude of the viscoelastic response increases with preload (hysteresis loops are larger at higher preloads). This is a geometric effect causes by the changing cross section of the tyre. A multiplying function that describes this effect for each of the three components was found by subtracting the elastic response (Equations, 5.3.1-1, 5.3.1-2, 5.3.1-3) from each low-amplitude varying-preload measurement (Figures, 5.3.1-1, 5.3.1-2, 5.3.1-3) then fitting a least mean square line to the maximum and minimum turning points. The result is shown below in Figures, 5.3.2-1, 5.3.2-2, and 5.3.2-3.

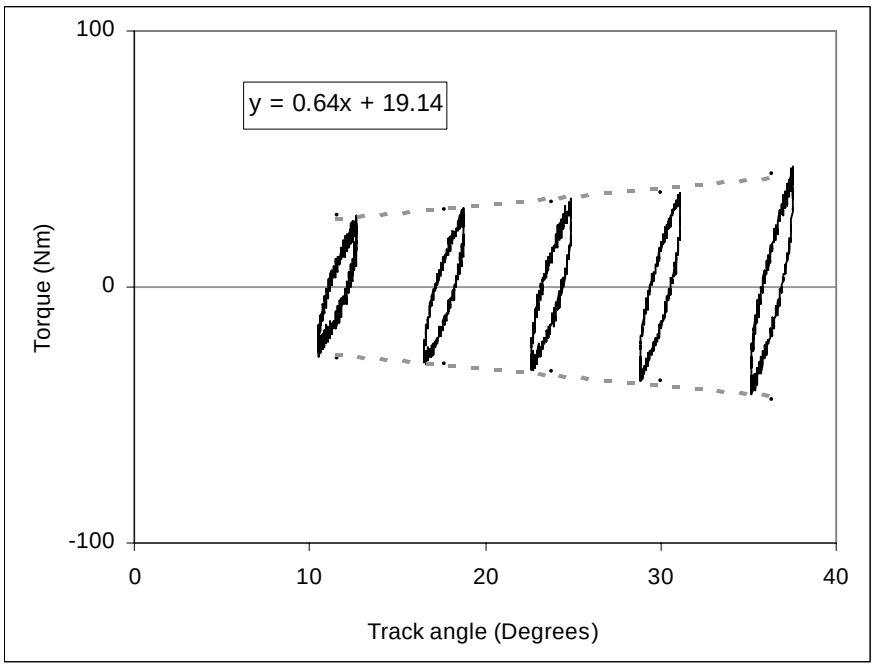

Fig. 5.3.2-1: *Track bush torsional geometric factor*

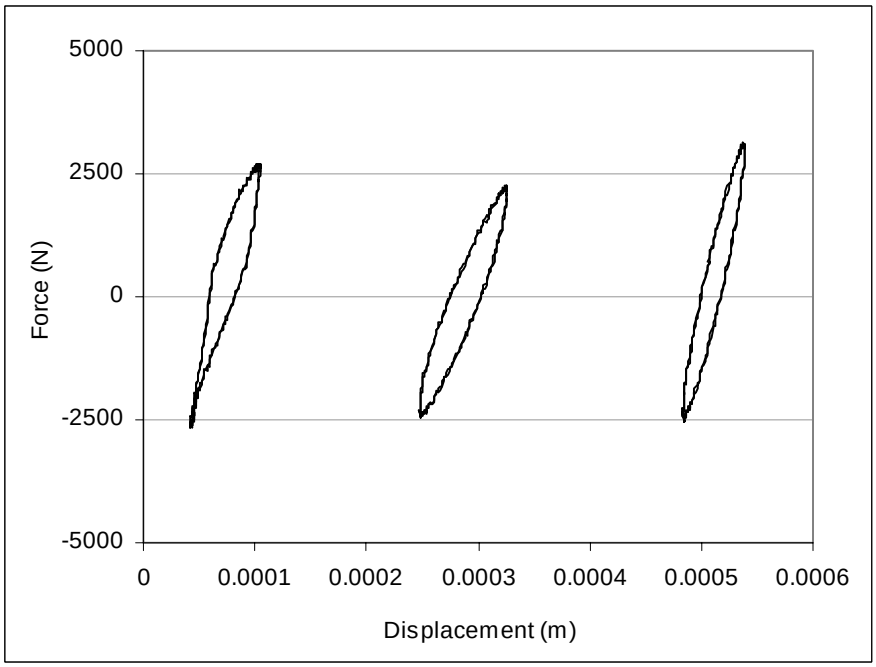

Fig. 5.3.2-2: *Track bush radial geometric factor*

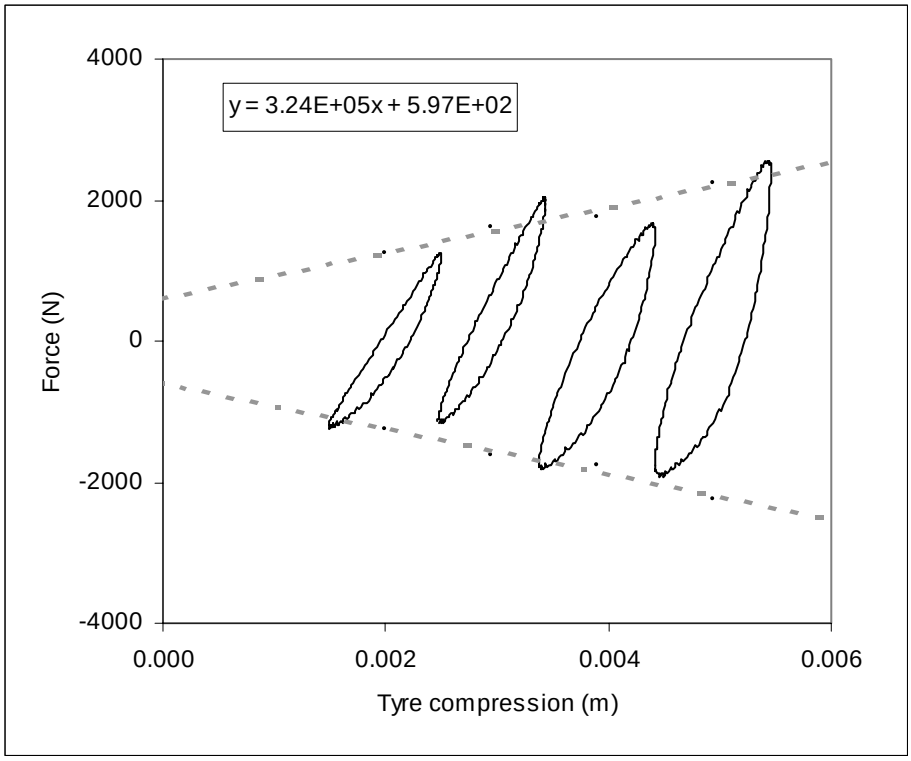

Fig. 5.3.2-3*: Road wheel tyre radial geometric factor*

We see from these graphs that the track bush radial response (Fig.5.3.2-2) does not show any significant geometric effect but that both the track bush torsional response and the road wheel tyre response do. To determine coefficients for these two geometric functions the hysteresis loops have been simply bound by a linear function. The multiplying function in each cases is therefore a linear scalar, so that $f(x_0)=\frac{mx_0+c}{c}$, where $f(x_0)$ is the multiplying function, x_0 is the components absolute displacement. 'm' and 'c' are constants. This function can be simplified to, $f(x_0)=h.x_0+1$, where x_0 is the components absolute displacement and $h=\frac{m}{c}$. Therefore from the measurements shown in Fig.5.3.2-1 and Fig.5.3.2-3 we have the following two functions describing change in visco-elastic force due to geometry:

1. Track bush torsional geometric multiplier.

$$f(x_0) = 0.033|x_0 - 10| + 1 \qquad \textbf{Equation 5.3.2-1}$$

In Equation 5.3.2-1 the reference angle (x_0 = 0) is taken as being the position where adjacent track link castings are inline. The addition of '10' in this equation is therefore to correct the function for track bush 'live-angle'.

2. Road wheel tyre geometric multiplier.

$$f(x_0) = 543.x_0 + 1 \qquad \textbf{Equation 5.3.2-2}$$

In both Equations 5.3.2-1 and 5.3.2-2, $f(x_0)$ is the geometric multiplying function and x_0 is the components absolute displacement.

5.4 Measurement II:

Constant preload at various amplitudes, 1Hz sinusoidal displacement

Each of the Warrior APC components was exercised at various amplitudes but constant preload by a 1Hz sinusoidal displacement. The purpose of this measurement is to produce data from which coefficients for the viscoelastic elements of the component model can be determined.

Measurements are presented below in Figs 5.4-1, 5.4-2 and 5.4-3. The elastic-force line (as determined in Section 5.3.1) is show on these charts so that the relationship between the viscous and elastic forces can be seen.

As was mentioned above, measurements of track bush radial response were carried out early in this research before the 'long relaxation time' characteristics of CBFNR where appreciated. It is believed that this is the reason that the measured response plots of Figure 5.4-2 do not lie equidistant about the elastic-force line.

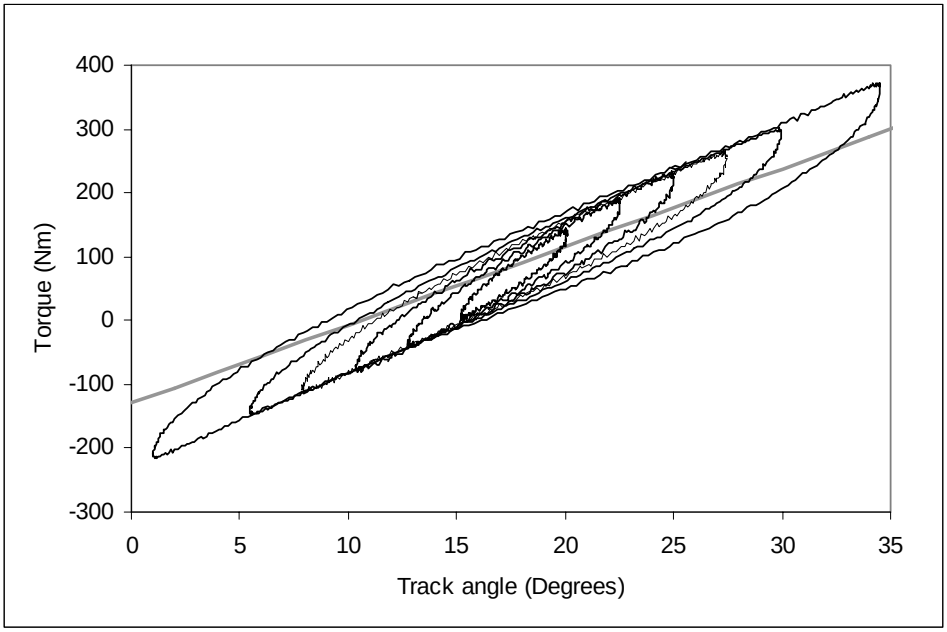

Fig. 5.4-1: *Track bush torsional force-displacement response*

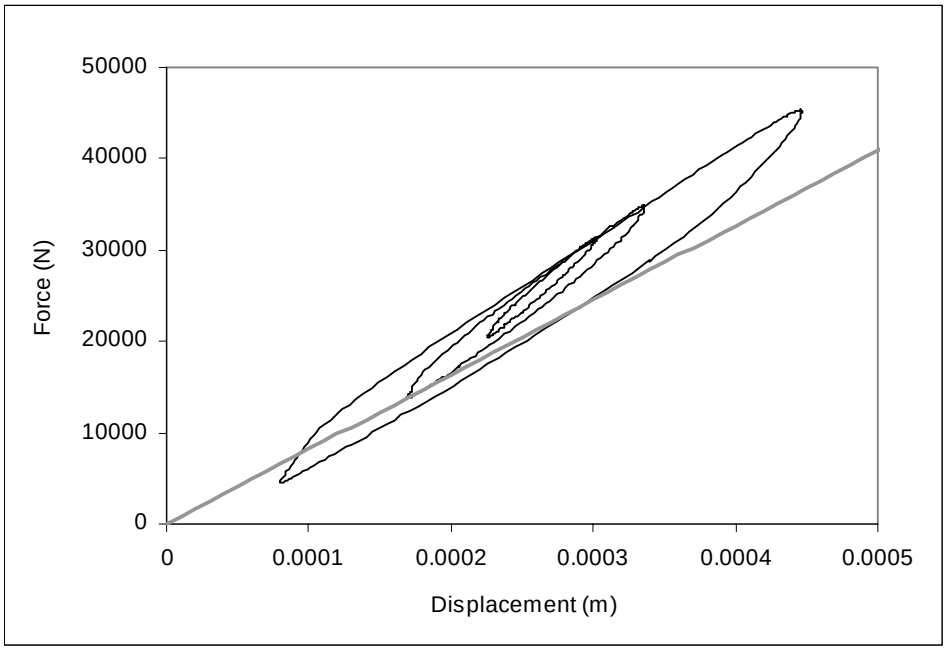

Fig. 5.4-2: *Track bush radial force-displacement response*

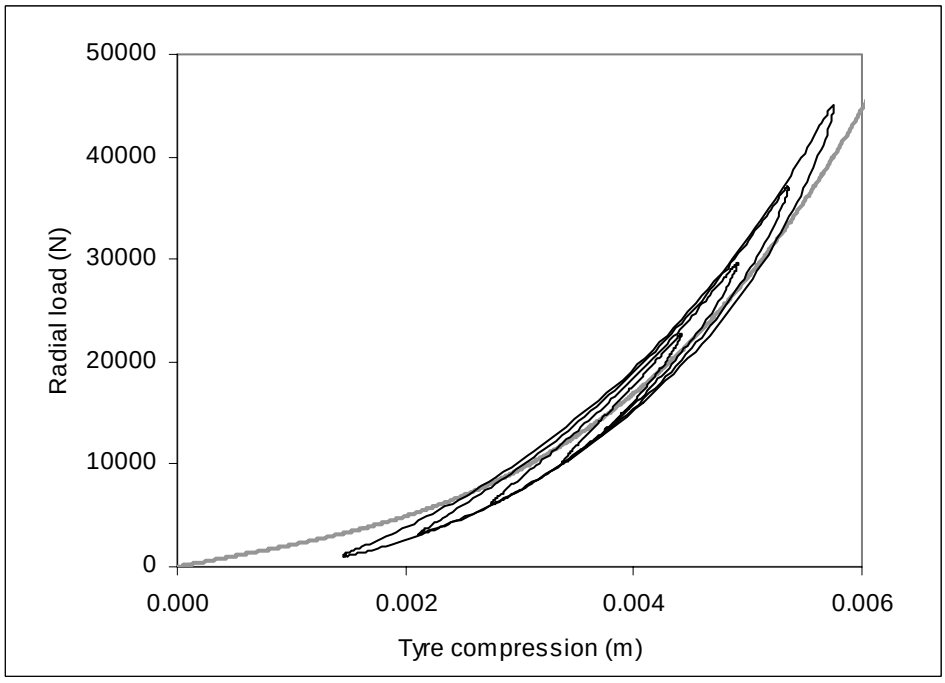

Fig. 5.4-3: *Road wheel tyre radial force-displacement response*

An important and consistent feature of these graphs (Fig 5.4-1, 5.4-2 & 5.4-3) is that at high amplitude the viscoelastic force response is not parallel with the elastic force line. The viscoelastic force continues to increase.

5.5 Measurement III:

Constant amplitude and constant preload at various frequencies

The object of this measurement is to demonstrate the insensitivity of carbon black filled natural rubber components to frequency variation. Measurements at constant amplitude and constant preload at 0.1Hz, 1Hz, 10Hz and 20Hz are presented in Figures 5.5-1 and 5.5-2. Measurements at higher frequencies where not possible due to the high force generated by accelerating test rig masses and test rig resonance.

Figures 5.5-1 and 5.5-2 show that the response of carbon black filled natural rubber components do not significantly change over the frequency range 0.1Hz to 20Hz. This is an expected result, agreeing with the frequency response of 'Truck Tread' shown in Figures. 3.1-4 and 3.1-5. We see here though that in detail the characteristic asymmetric shape shown in Figure 5.5-2 is unaltered by the changing frequency.

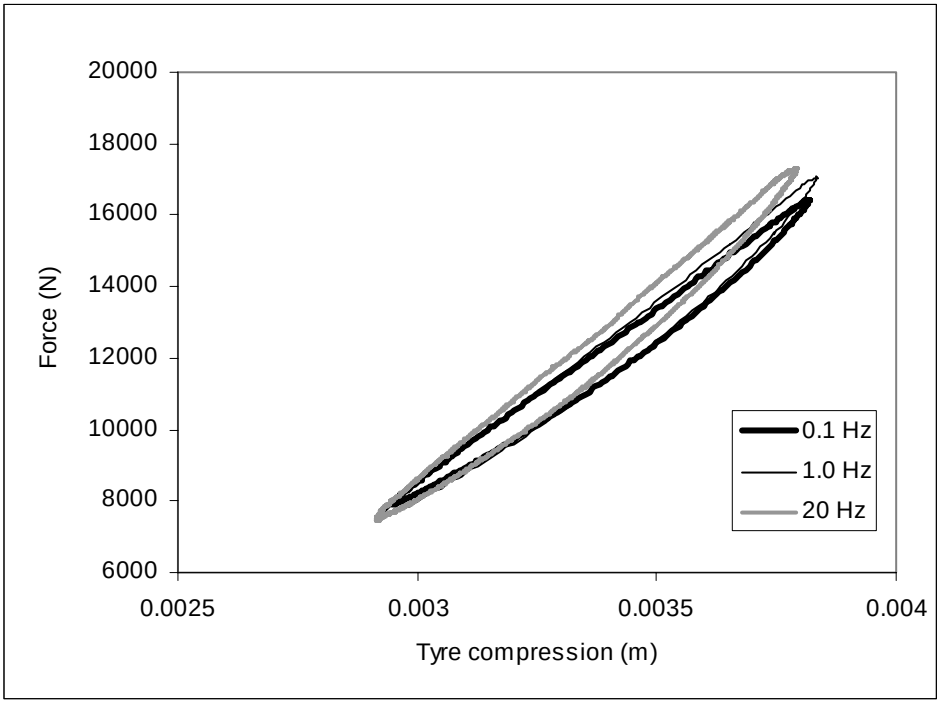

Fig. 5.5-1: *Road wheel tyre force-displacement response at several frequencies*

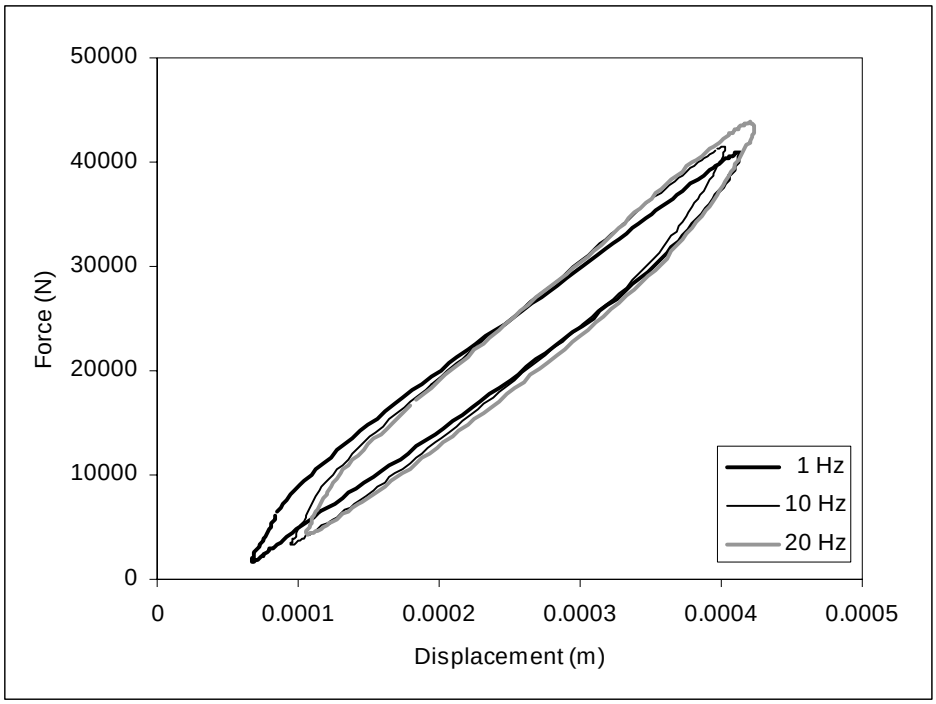

Fig. 5.5-2: *Track bush radial force-displacement response at several frequencies*

This result brings us to the conclusion that, as a first approximation damping would be represented by a frictional description not a viscous (velocity dependent) description. However, we will see in the next Section (5.6) that this material also exhibits stress relaxation; a feature that contradicts the frictional damping model.

5.6 Measurement IV: Stress relaxation:

Force response to a stepped displacement over time

Figure 5.6-1 shows the track bush response to a stepped torsional displacement, both total force and the elastic-force (determined by Equation 5.3.1-1) are shown for comparison. Only a few stress relaxation measurements were made: a comprehensive and detailed investigation of each track component's response to a variety of stepped inputs has not been undertaken. The reason for this is that it has been shown by Haupt and Sedlan [19] that stress relaxation response depends upon strain history and a 'strain history dependent viscosity model' is needed to describe it. This level of complexity is excessive for a Warrior APC track component model.

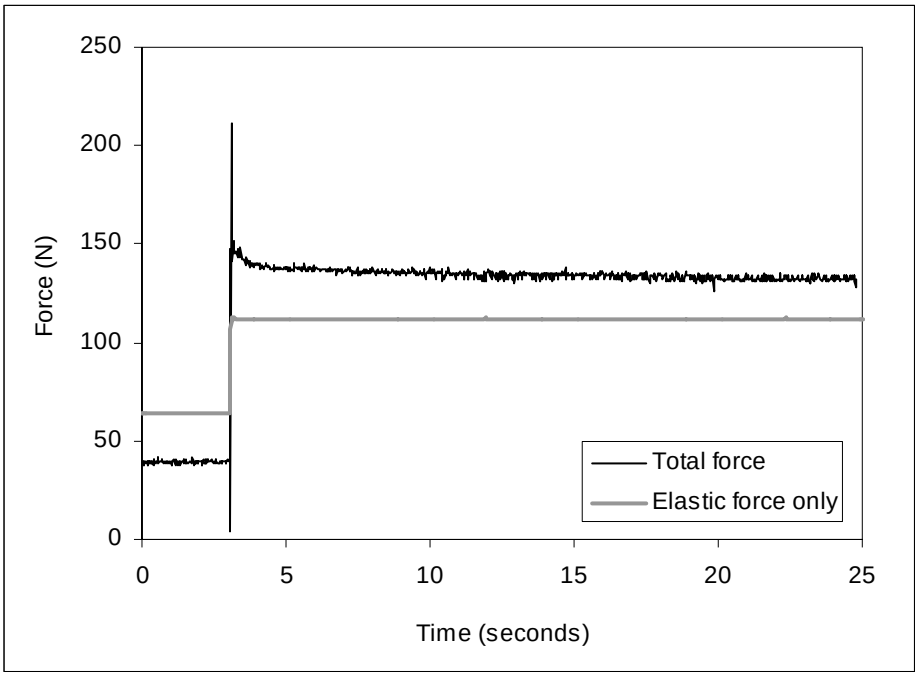

Fig. 5.6-1: *Track bush torsional stress relaxation*

Figure 5.6-1 shows the characteristic features of a CBFNR stress relaxation response. These are an immediate rapid fall in force in a short time followed by a slow fall in force at long time. This response is not described by a single decaying exponential function.

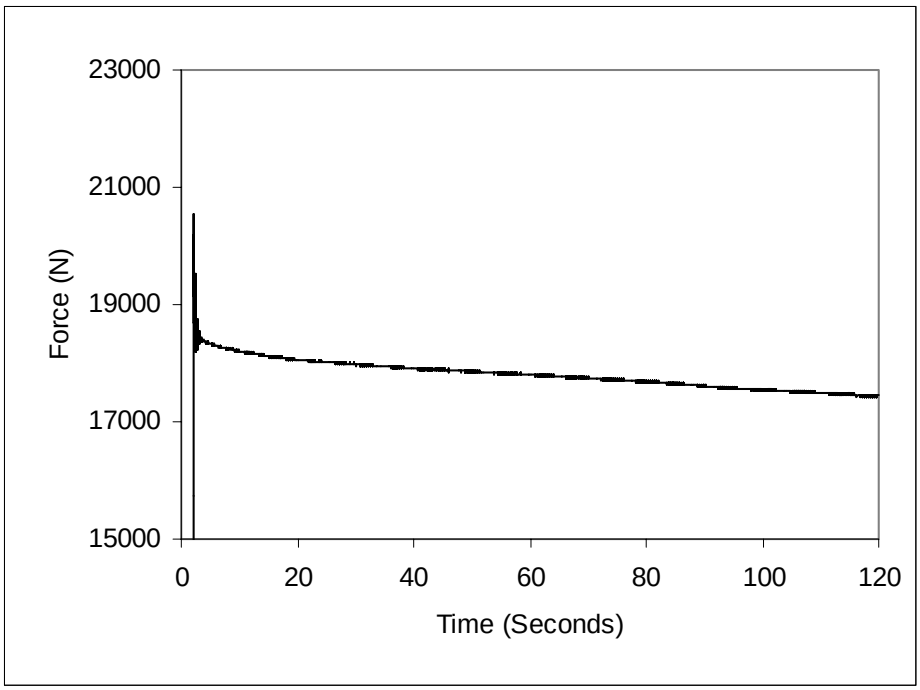

Fig. 5.6-2: *Road wheel tyre stress relaxation*

Figure 5.6-2 shows a stress relaxation measurement for the road wheel tyre, again a typical carbon black filled natural rubber response

5.7 Track bush torsional response at various radial loads

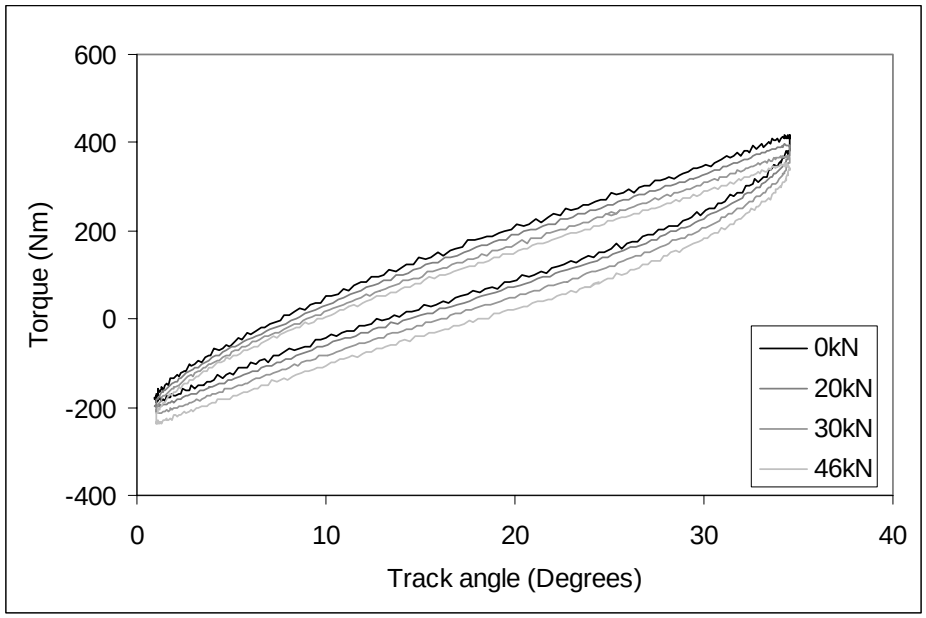

Fig. 5.7-1: *Track bush torsional response at varying radial loads*

Figure 5.7-1 shows the effect that changing track bush radial load has on the track bush torsional response when subject to stable sinusoidal motion at 0.2Hz. At each setting the radial load was applied with the bush stationary at a track angle of 10°; the tracks 'live-angle' where the bush is not strained in torsion.

This measurement shows that although these two track link bush dimensions are modelled and measured as independent components they do interact, but that the interaction is not so excessive that its exclusion from the model will produce an unrepresentative description. The measurement shows that for steady sinusoidal motion and constant radial preload, torque about the bush axis decreases slightly by a constant value as track tension (radial load) increases but also that stiffness and damping are not significantly affected.

An equivalent measurement showing the effect on radial response of changing torsional load has not been made but this could be the subject of further work.

5.8 Track bush torsional response to duel-sine displacement

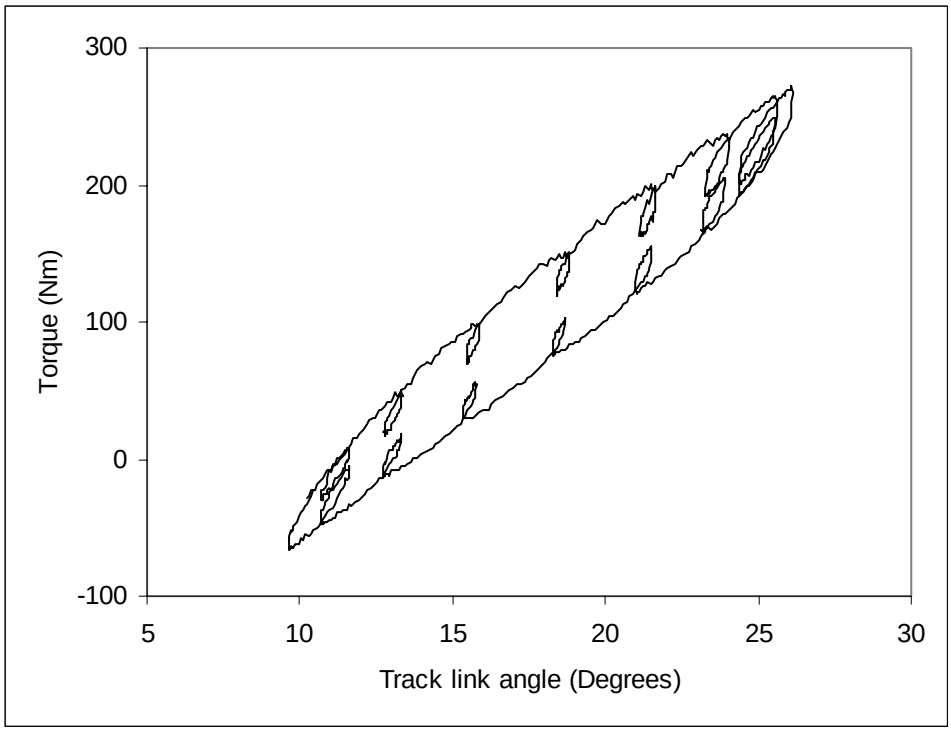

Fig. 5.8-1: *Track bush torsional response to dual-sine displacement*

Figure 5.8-1 shows track bush torsional response to duel-sine displacement. The amplitude and frequency ratios are taken from Coveney and Johnson [8] so that a comparison could be made with this work. Secondary to primary frequency ratio is 15:1; secondary to primary amplitude ratio is 10:1.

Primary frequency = 0.1Hz, Primary amplitude = 7.5°, Secondary frequency = 1.5Hz, Secondary amplitude = 0.75°.

The purpose here is to simulate the type strain history (combined high-frequency low-amplitude and low-frequency high-amplitude) a component might experience on a vehicle.

Chapter 6

Development of a model for rubber components

6.0 Introduction

The literature review of models developed for carbon black filled natural rubber (CBFNR) components (Chapter 4) showed that a viscoelastic model based on the work of Haupt and Sedlan [19] best describes the characteristics of (CBFNR) and is suited to software that uses the Newton Raphson Predictor Corrector method. In Chapter 5 functions that describe the elastic force and the increase in viscoelastic force due to changing geometry where found.

The objective here in Chapter 6 is to develop a generic model that can describe the behaviour of all CBFNR components in the Warrior Armoured Personnel Carrier (APC) running gear by simulating one-dimensional force-displacement response. It is important to note that the model developed here is a phenomenological description and therefore cannot be guaranteed to simulate the response to stain rates or strain amplitudes that have not been measured.

It is response at the component level that is described by the model; material is not considered at the micro-mechanical level and constitutive equations are not developed. Hyper-elastic constitutive models, which describe the nonlinear elastic behaviour of rubber, are not used; elasticity is described by a polynomial fit to measured data (Section 5.3.1). Damage; the reduction in viscoelasticity over time (also known as the Mullins effect) is not modelled nor are thermal effects or plasto-elasticity (also known as equilibrium stress hysteresis). The model is deliberately simplified as far as possible but retains elements that are important for vehicle

component simulations so that it describes the force-displacement response to high amplitude, low amplitude, multiple frequency and transient strain histories.

Coefficients for descriptive mathematical functions used in the model developed here are found by manually changing their values and by visual comparison matching the modelled response to the measured response. Computer algorithms are not used other then 'least mean square fit polynomials' common to most standard graphical software packages.

6.1 The simplified Haupt and Sedlan model

The viscoelastic elements of the CBFNR model developed here are based on the work of Haupt and Sedlan described in Section 4.2.7. Haupt & Sedlan use three parallel visco-elastic elements to describe the response of CBFNR in their model [19] but at this stage (before comparing the models response with experimental data) it must be assumed that any number of these elements maybe required for the Warrior Armoured Personnel Carrier (APC) track components.

The simplified model used here differs from that used in the Haupt & Sedlan [19] model in two ways. Firstly, the viscoelastic element does not including a description of 'strain history dependent viscosity' and secondly; the elastic force (F_e) and a viscoelastic geometric multiplying term $f(x_0)$ are described by polynomial fits to direct measurements, whereas in Haupt and Sedlan's model, elasticity is described by a strain energy function and geometric effect by a three-dimensional constitutive material model.

The use of a geometric multiplier means that the model developed here has two parts (Fig 6.1-1), one part that sums the elastic and viscoelastic force (Equation 6.1-1), the other that models viscoelastic behaviour only. The reason for this is that the geometric

multiplier multiplies the viscoelastic force (Equation 6.1-3) before it is added to the elastic force (Equation 6.1-1). The total response (*F*) is constructed in reverse to the way that it was deconstructed in the measurements of Sections 5.3.1 and 5.3.2.

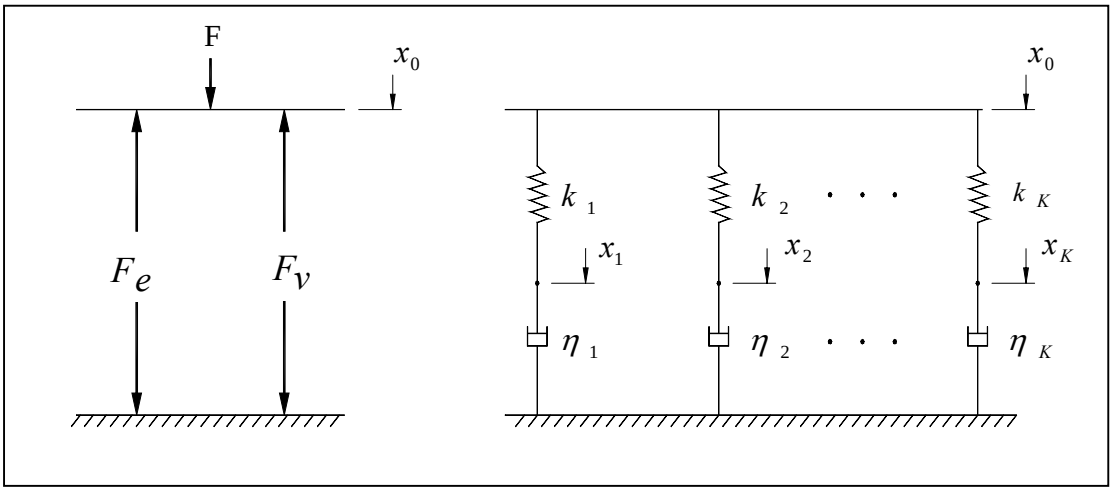

Fig. 6.1-1: S*chematic representation of the simplified Haupt and Sedlan carbon black filled natural rubber component model*

$$F = F_e + F_v \qquad \textbf{Equation 6.1-1}$$

$$\eta_K = \frac{c_K}{|\dot{x}_0| + \xi_K} \qquad \textbf{Equation 6.1-2}$$

$$F_v = f(x_0)\sum_{K=1}^{N} \eta_K \dot{x}_K \qquad \textbf{Equation 6.1-3}$$

Where, K = 1, 2, …N and $f(x_0)$ is the geometric multiplying function

$$F_e = Ax_0^3 + Bx_0^2 + Dx_0 + x_0 \qquad \textbf{Equation 6.1-4}$$

Where, A, B and D are coefficients for the elastic force polynomial. η is the coefficient of viscosity, ξ_k and c_k, are the viscoelastic element constants, x_0 is displacement across the component and '*F*' is applied and reaction force, F_e is elastic force and F_v is viscoelastic force.

6.2 The time dependent viscoelastic element

The non-linear Maxwell element use to describe time depended viscoelastic response is a simplified version of that used by Haupt and Sedlan [19]. Viscoelasic force is described by the following function:

$$F_{viscoelastic} = \frac{c\dot{x}_2}{|\dot{x}_1| + \xi} \qquad \textbf{Equation 4.2.7-1}$$

Where 'c' and 'ξ' are constants, $\dot{x}_1$ is strain rate across the viscoelastic element and $\dot{x}_2$ strain rate across the dashpot (see Fig 4.2.7-1).

It was shown in Sections 3.3, 5.4 and 5.5 that CBFNR components produce an asymmetric hysteresis loop in response to stable cyclic strain and although the material has almost total stress relaxation at infinite time [19], it is insensitive to frequency and velocity variation over a wide range (Figs. 3.1-4, 3.1-5, 5.5-1 and 5.5-2). A Maxwell type element where the viscous part is described by Equation 4.2.7-1 has these same features when 'ξ' has a low value. But for a small value of ξ or a high value of $\dot{x}_1$ a Maxwell element where the viscous force is described by Equation 4.2.7-1 produces a time-independent exponential response of the following form (derivation given in Appendix 1):

$$F_{viscoelastic} = c\,\mathrm{sgn}(\dot{x}_1) - (c\,\mathrm{sgn}(\dot{x}_1) - F_0).Exp\left(-\frac{k\,\mathrm{sgn}(\dot{x}_1)}{c}(x_1 - x_0)\right)$$

Equation 4.2.7-2

Where, 'c' is maximum possible viscoelastic damping force, 'F_o' and 'x_0' viscoelastic damping force and displacement at the previous turning point respectively, 'k' is the stiffness coefficient for the Maxwell spring, x_1 displacement and $\dot{x}_1$ velocity of displacement.

Equation 4.2.7-2 produces a loop enclosed by exponentially rising and falling curves centred about the, zero displacement, zero viscous force point (Fig 6.2-1).

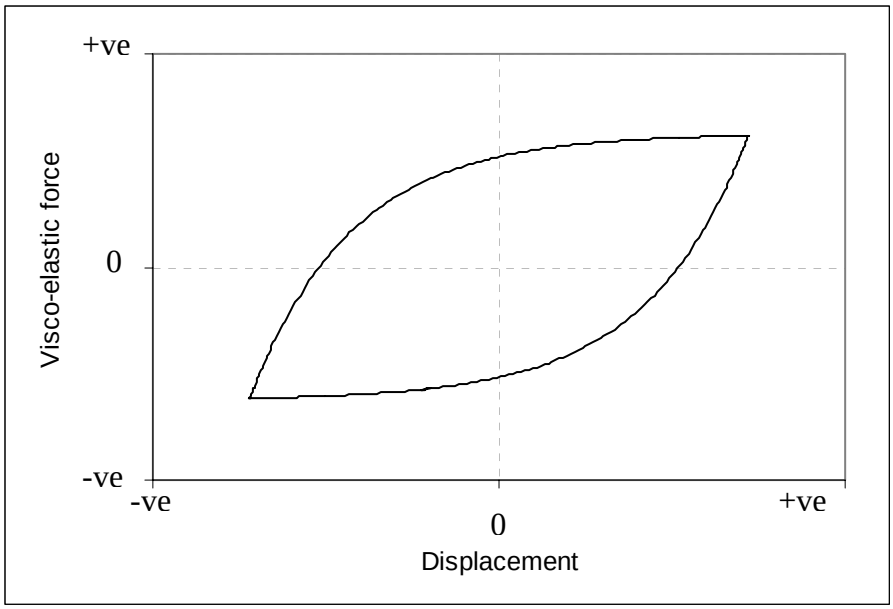

Fig. 6.2-1: *Rising and falling exponential curves produced by Equation 4.2.7-2*

Coefficients ‘c’ and ‘k’ in Equations 4.2.7-1 and 4.2.7-2 are determined by comparing measured data (where the elastic and geometric components of the response have been removed) with a plot produced by Equation 4.2.7-2 (Fig 6.2-2).

This method of determining ‘*c*’ and ‘*k*’ is evidently an approximation because it is assumed that ξ is small, but if it were not then Equation 4.2.7-1 becomes time-dependent and simple visual comparison between the measured and modelled viscoelastic force component would not be possible. Also the integration required to determine Equation 4.2.7-2 (see Appendix 1) would be far more complex.

When the predominately time independent behaviour of carbon black filled natural rubber is considered the additional accuracy achieved by developing a ‘true’ descriptive time dependent function and the effort required to measure and match data to this type of function cannot be justified since some approximation is adequate for vehicle component simulation.

The coefficient ξ is determined separately by comparing Equation 4.2.7-3 with stress relaxation measurements.

$$F_{viscoelastic} = F_o Exp\left[\frac{-\xi\ k\ t}{c}\right] \qquad \textbf{Equation 4.2.7-3}$$

In figure 6.2-2 the viscoelastic response of four track bush torsional measurements of constant preload and varying amplitude (see Fig 5.4-1) are compared with plots produced by Equation 4.2.7-2. Viscoelastic response has been determined by removing the elastic component and the geometric multiplying component then offsetting the hysteresis loops so that their mean displacement and viscous force are at zero.

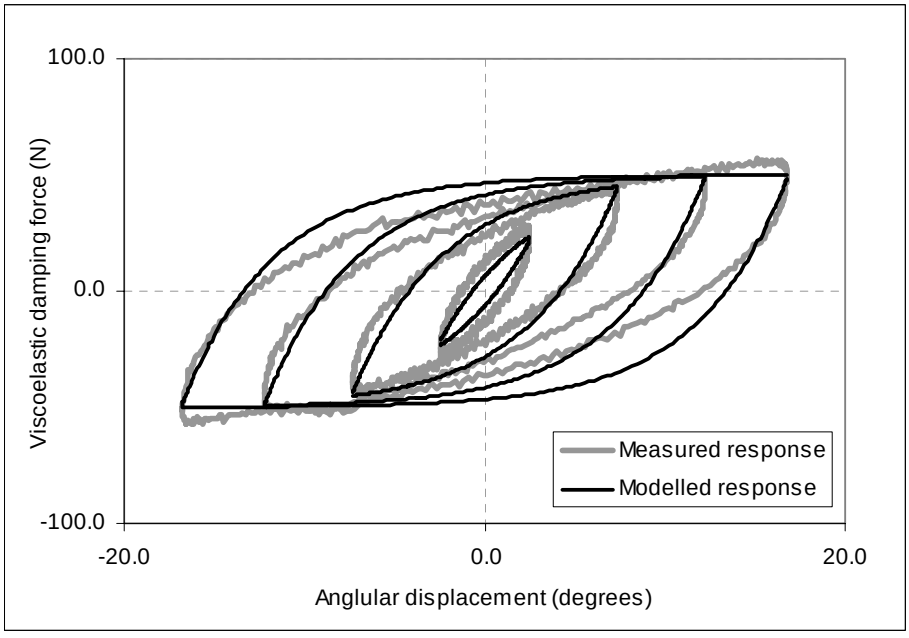

Fig. 6.2-2: *Track bush torsional viscoelastic force. Modelled using a single viscoelastic Element (Equations 4.2.7-2)*

The values of constants ‘k’ and ‘c’ are the same in each of the four plots and have been adjusted by visually comparing the measured and modelled response to achieve the ‘best fit’ to both small and large amplitude displacements.

Figure 6.2-2 illustrates two difficulties that are encountered when trying to match the function for a single viscoelastic (*N=1*) element to measured hysteresis loops of varying amplitude. Firstly, the modelled response is a compromise between describing a 'rounded loop' at small amplitude, which requires a high stiffness coefficient (k) value and a 'flatter loop' at high amplitude, which requires a low stiffness coefficient value. Secondly, it is qualitatively evident that the measured viscoelastic damping force continues to increase as amplitude increases and is not constant relative to the X-axis at high amplitude, but the modelled response does approach a constant value at high amplitude. These two points are important if we are to develop a general purpose CBFNR model for vehicle components that describes damping and stiffness over a range of amplitudes.

A better fit is possible by the addition of a second (parallel) viscoelastic element of (the same non-linear type described by Equation 4.2.7-2) but that has lower stiffness. The result is shown in Figure 6.2-3.

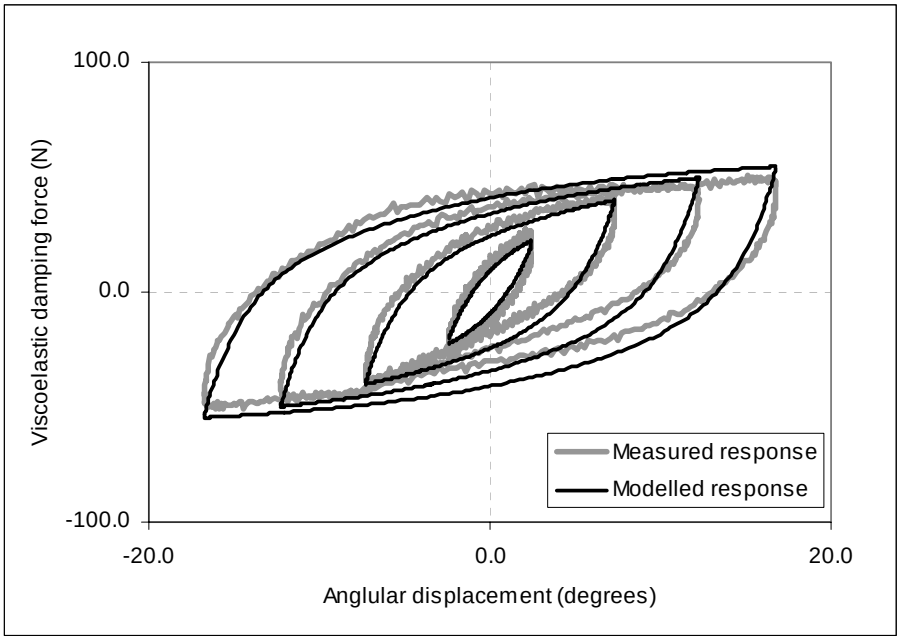

Fig. 6.2-3*: Track bush torsional viscoelastic force. Modelled using two parallel viscoelastic elements (Equations 4.2.7-2)*

With the additional viscoelastic element the model has twice as many coefficients; two stiffness values (k), two damping force values (c) and two time-dependent parameters (ξ). Again these values have been found by manual adjustment and visual comparison between modelled and measured hysteresis loops. The values found by this method are subjective but the method is not excessively time consuming, values that produce a 'good' match are easily found. The result achieved by using two parallel viscoelastic elements (Figure 6.2-3) are qualitatively an improvement over those in Figure 6.2-2, representing the measured response much better over the range of amplitudes measured. The additional complexity is justifiable but adding further parallel elements would not significantly improve the match. Two parallel time-dependent viscoelastic elements are sufficient to model the response to steady cyclic motion. Therefore for the proposed model (Figure 6.1-1), the value of '*N*' in Equations 6.1-3 is two.

Equivalent two-element viscoelastic force response plots are presented for the track bush radial and road wheel tyre, Figures 6.2-4 and 6.2-5 respectively.

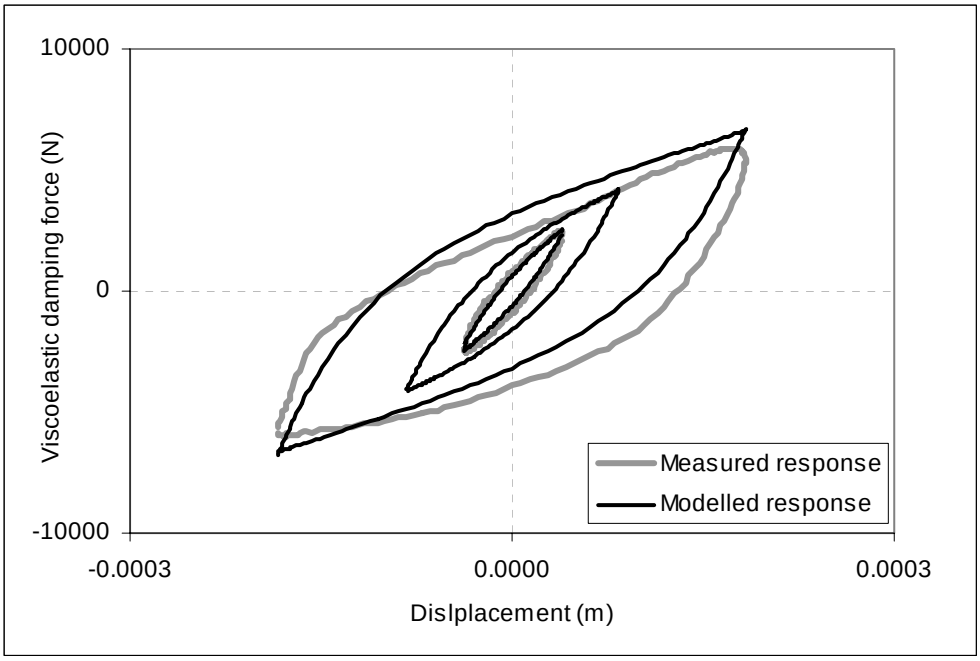

Fig. 6.2-4: *Track bush radial viscoelastic force. Modelled using two parallel viscoelastic elements (Equation 4.2.7-2)*

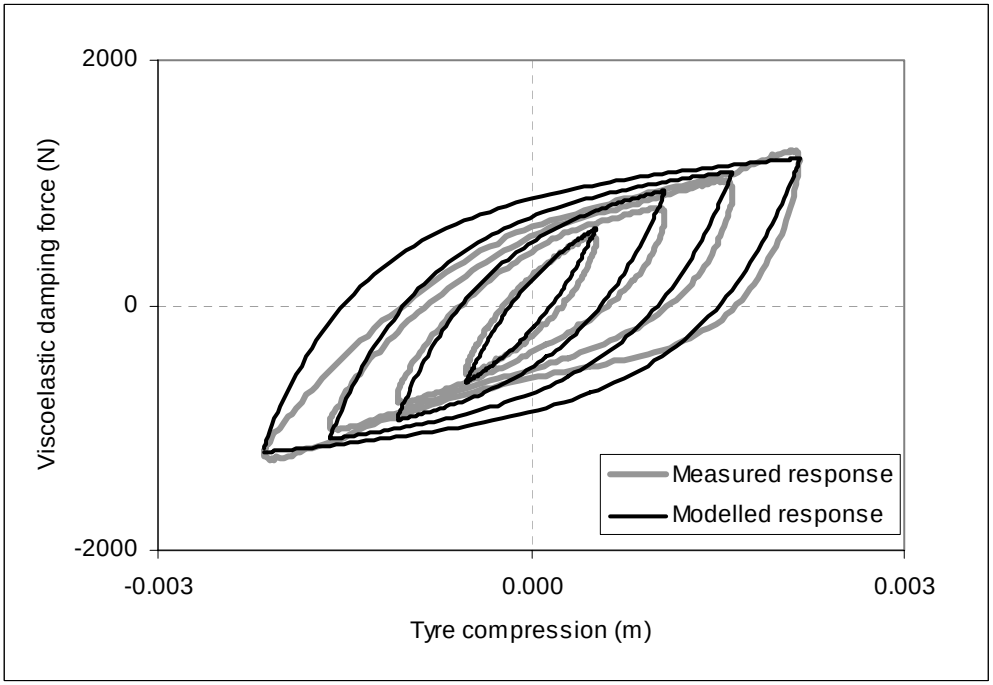

Fig. 6.2-5: *Road wheel tyre viscoelastic force. Modelled using two parallel viscoelastic elements (Equation 4.2.7-2)*

It is evident that at large amplitudes the modelled road wheel tyre viscoelastic force (Fig. 6.2-5) represents the measured response less well then either the track link bush

torsional or radial viscoelastic force models (Figs. 6.2-3 and 6.2-4, respectively). The reason for this is likely to be due to one of the following characteristics, which are unique to the tyre.

1. The tyre is unique among the components investigated here because of its 'contact' with the flat steel surface. The track bush is compressed into the track link casting so that its outer diameter cannot slip under normal operating conditions and its inner surface is moulded to a steel insert, whereas contact between the tyre and the flat steel surface compressing it is likely to have some slip. As the tyre is loaded and unloaded the contact patch size and the distribution of stress in the tyre depends on the coefficient of friction between the two surfaces. Slip and stiction between these surfaces may explain the change in hysteresis loop shape at large amplitude displacement.

2. The tyres highly non-linear geometric shape may also contribute to the changing hysteresis loop form.

3. Also compression between the rigid round wheel hub and rigid flat steel surface cause some regions to be highly strained while others are unstrained. The track bush is compressed into the track link so that is it highly strained before any load is applied. The tyre is not preloaded; the tyre is totally unstrained before it makes contact with the ridged flat surface so that the relative change in strain is large.

It should be emphasised though that it is only at the very larges amplitude displacement that the tyres damping loop is poorly represented in its detail. In general and over a wide range of amplitudes, the damping loops are well represented. At maximum amplitude displacement the tyre load varies from approximately 1,300N to 45,000N (see Figure 5.4-3). This is large variation in load but the method being used to describe damping is simply the sum of two exponential curves.

To study tyre contact and material strain a simple finite element analysis (FEA) was undertaken. For simplicity hyper-elasticity strain energy material functions, which describe non-linear elastic behaviour at large strains, were not used. The material is simply described by a constant modulus, E = 20Mpa. Poisson ratio (ν) = 0.499 (G=6.67) and coefficient of friction between steel and rubber (μ) = 0.8.

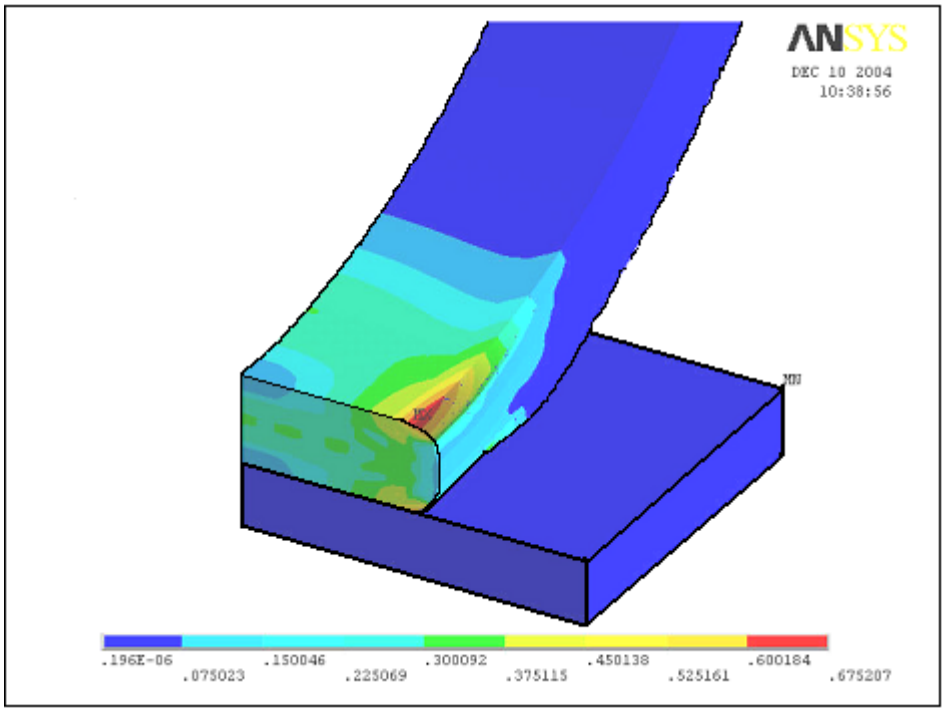

Fig. 6.2-6: *Quarter model of the tyre contact showing von Mises strain. Tyre compression is 8mm. Produced using ANSYS FEA software.*

Figure 6.2-6 illustrates the type of tyre deformation we might expect at high load (approx 60kN). Strain within the tyre ranges from zero to 60%. The FEA model has not been investigated in detail, its purpose here is to aid understanding, but it is clear that the contact patch size and consequently the stress-strain relationship are partly dependent on the contact surface coefficient of friction.

6.3 Stress relaxation and the response to dual-sine motion

Introduction

In Section 6.2 a time-independent approximation (Equation 4.2.7-2) was compared with the response to stable sinusoidal motion to determine stiffness and damping coefficients *k* and *c* for the model. This was possible because of the predominantly time-independent behaviour of CBFNR. Here in Section 6.3 the model is further developed to describe the materials response to stepped displacement and duel-sine motion. These very different strain histories are discussed together because it was found that the variable 'ξ', that partly determines the rate of stress relaxation (Equation 4.2.7-3) is also important in the description of duel-sine response.

It is shown that it is possible to closely simulate the response to both duel-sine motion and a stepped displacement (stress relaxation) by momentarily stiffening each of the parallel viscoelastic elements of the simplified Haupt and Sedlan model (Fig. 6.1-1) using 'nested', rapidly decaying, viscoelastic elements of the same type. But by doing this the models response to stable sinusoidal motion developed in Section 6.2 is compromised. The solution to this problem would be to introduce a 'strain velocity dependence' that describes; high viscosity at low velocity and low viscosity at high velocity similar to that used by Haupt and Sedlan [19] (see Section 4.27). It is suggested here though that this complexity is not necessary for the simulation of Warrior APC CBFNR track components in a full vehicle model, where the individual component models should be simple track and easy to apply and some approximation to real behaviour can be justified. Therefore the final model presented in Section 6.4 is a compromise. It has only a single stiffened viscoelastic element that is not strain history dependent. This model approximates the response to, sinusoidal, dual-sine and stepped displacements.

To study time dependence, the model was implemented in dynamic analysis software. Measurements of the CBFNR response to dual sine and stepped displacement motion were compared with equivalent simulations using MSC.ADAMS^{TM} (*Automatic Dynamic Analysis of Mechanical Systems*). The details of how the model was implemented in this software are discussed in Section 7.1.

Model development

Fig 6.3-1 shows the measured track bush torsional response to a stable dual-sine displacement history (see Section 5.8).

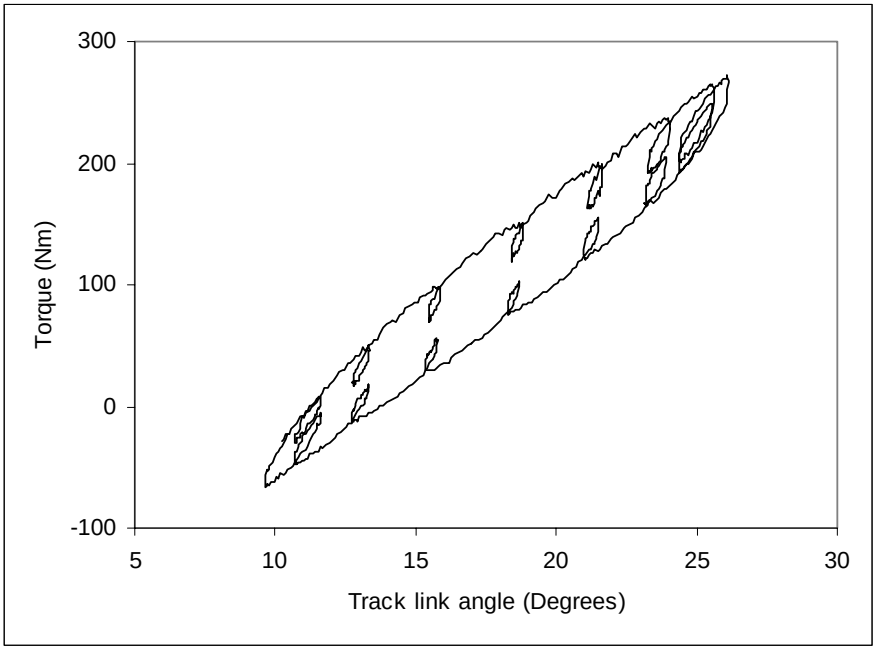

Fig. 6.3-1: *Measured track bush torsional response to dual-sine displacement.*

This response (Fig 6.3-1) agrees (qualitatively) with measurements reported by Coveney and Johnson [8]. The loops produced by the secondary sinusoidal waveform are a feature of carbon black filled natural rubber that cannot be describe by the simplified Haupt and Sedlan model.

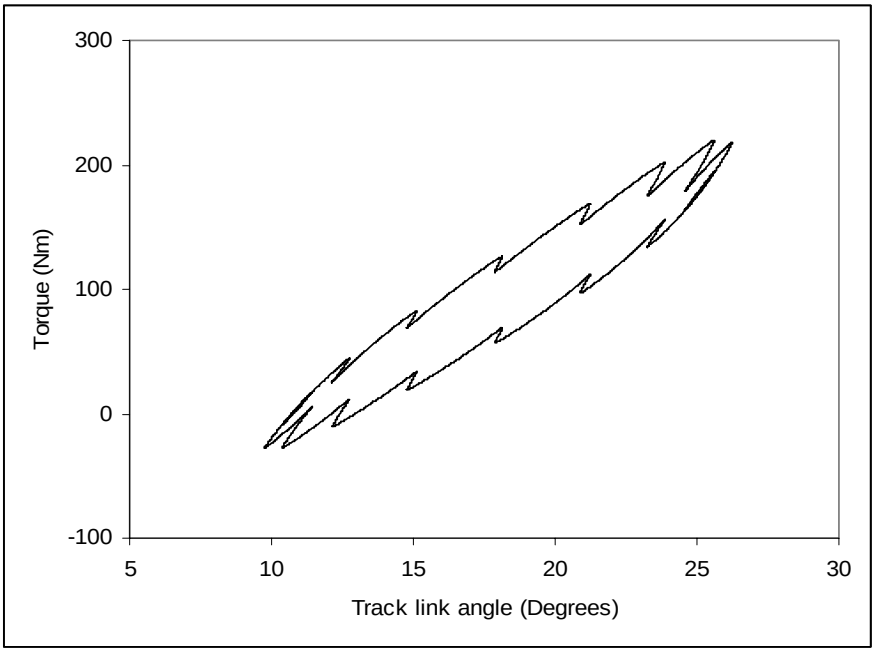

Fig. 6.3-2: *Simulation of track bush torsional response to dual-sine displacement produced by ADAMS simulation of the simplified Haupt and Sedlan*

Figure 6.3-2 shows the response of the Simplified Haupt and Sedlan model (developed in Section 6.2) when simulating the dual-sine measurement of Fig. 6.3-1. Evidently the correlation between Figs. 6.3-1 and 6.3-2 is poor. It is not possible for a model that has viscoelastic elements of the type used in the proposed model, to produces the characteristic enclosed loops we see in dual-sine measurements. The model must be modified. This becomes evident when considering Equation 4.2.7-2.

$$F_{viscoelastic} = c\,\mathrm{sgn}(\dot{x}_1) - (c\,\mathrm{sgn}(\dot{x}_1) - F_0)Exp\left(-\frac{k\,\mathrm{sgn}(\dot{x}_1)}{c}(x_1 - x_0)\right)$$

Equation 4.2.7-2

Where, 'c' is maximum possible viscoelastic damping force, 'F_o' and 'x_0' viscoelastic damping force and displacement at the previous turning point respectively, 'k' is the stiffness coefficient for the Maxwell spring, x_1 displacement and $\dot{x}_1$ velocity of displacement.

The first term in Equation 4.2.7-2, $\left(c\,\mathrm{sgn}(\dot{x}_1)\right)$, determines maximum possible damping force and has constant magnitude. The multiplying term; $\left(c\,\mathrm{sgn}(\dot{x}_1) - F_0\right)$; and the exponential, $Exp\left(-\frac{k\,\mathrm{sgn}(\dot{x}_1)}{c}\left(x_1 - x_0\right)\right)$, are both variable, dependant on F_0 and x_0 respectively. This dependence on F_0 and x_0 'scales' the exponential so that this function (Equation 4.2.7-2) could not produce the loops that we see in the dual-sine measurement. The only possible solution is to make the coefficient 'k' variable so that the exponentially described viscoelastic force increases more rapidly under certain circumstances. This can produce the loops we see in Figure 6.3-1 and to do this additional nonlinear viscoelastic elements have been introduced into the model; the same type as those used in the simplified Haupt and Sedlan model where viscoelastic force is described by the following function:

$$F_{\textit{visco-elastic}} = \frac{c\dot{x}_2}{\left|\dot{x}_1\right| + \xi} \qquad \textbf{Equation 4.2.7-1}$$

'c' and 'ξ' are constants, $\left|\dot{x}_1\right|$ is the magnitude of velocity across the Maxwell element and $\dot{x}_2$ is velocity across the dashpot.

A simple dashpot and a linear Maxwell elements were also considered as possible ways to increase the stiffness coefficient momentarily. However the same type of nonlinear viscoelastic element has been used because it is limited to a maximum possible force (unlike a simple dashpot), it does not reduce to a spring element at high frequency (like a linear Maxwell element) and its decay rate is controllable by 'ξ'. These additional stiffening elements are placed in parallel with each spring and are given a relatively high value of 'ξ' so decay is rapid and its influence has short

duration. A schematic representation of this ‘four-element model’ for duel-sine simulation is shown below in Figure 6.3-3.

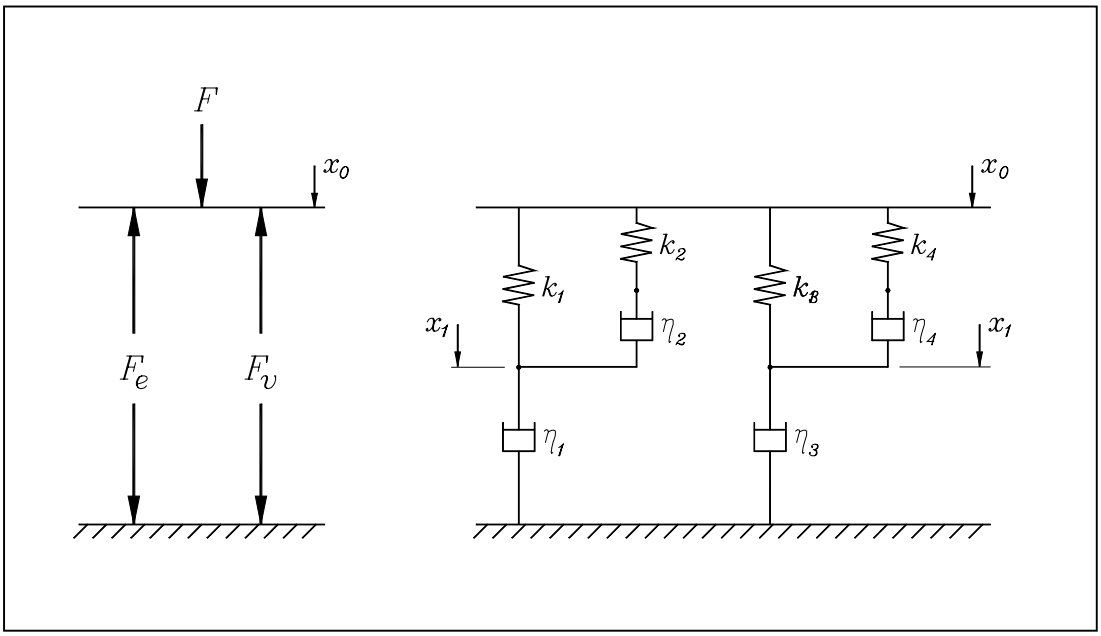

Fig. 6.3-3: *Four-element model: Two nonlinear viscoelastic elements each with a nested rapidly decaying nonlinear stiffening viscoelastic element*

As for the Simplified Haupt and Sedlan model (fig. 6.1-1) the following equations apply:

$$F = F_e + F_v \qquad \textbf{Equation 6.1-1}$$

$$\eta_K = \frac{c_K}{|\dot{x}_K| + \xi_K} \qquad \textbf{Equation 6.1-2}$$

$$F_v = f(x_0)(\dot{x}_1\eta_1 + \dot{x}_3\eta_3) \qquad \textbf{Equation 6.1-3}$$

$$F_e = Ax_0^3 + Bx_0^2 + Dx_0 + x_0 \qquad \textbf{Equation 6.1-4}$$

Where, K = 1, 2, 3 and 4, $\dot{x}_K$ is the velocity across viscoelastic element K, $f(x_0)$ is the geometric multiplying function. c_K, ξ, A, B and D, are constants.

Tests have shown that this four-element viscoelastic model represents the response of CBFNR to dual-sine motion and stepped displacement very well (Figures 6.3-4 and 6.3-5). Values for the variables used in these simulations are given in Appendix 4a.

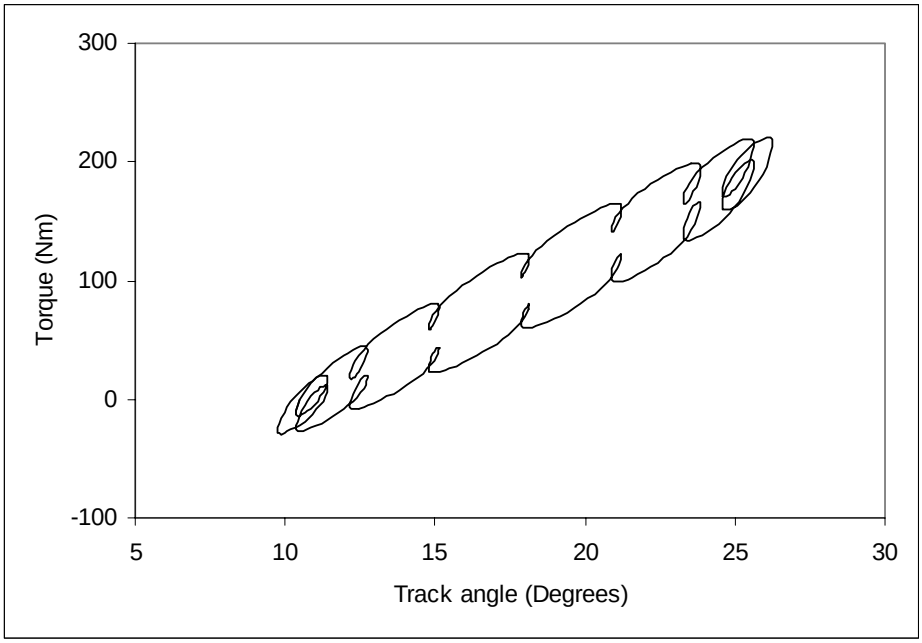

Fig 6.3-4: *Simulated track bush torsional response to dual-sine displacement produced by ADAMS simulation of the four-element viscoelastic model*

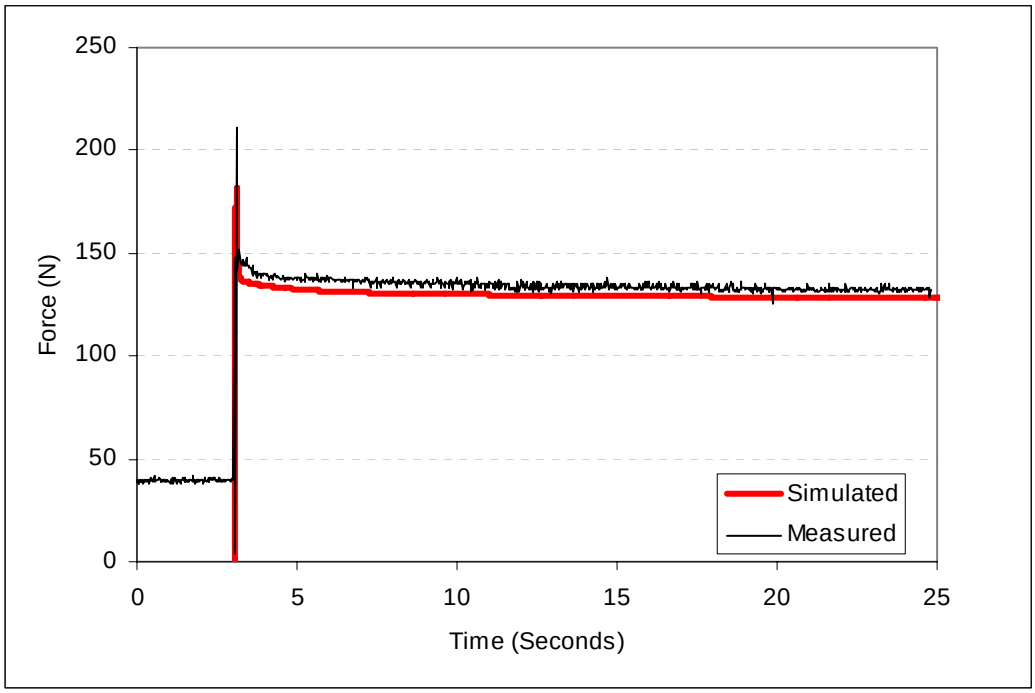

Fig. 6.3-5: *Measured and simulated track bush torsional stress relaxation produced by ADAMS simulation of the four-element viscoelastic model*

The model has four stress relaxation variable parameters and is therefore able to very closely simulate the stress relaxation plot but it is the nested element that has produced the very rapid, almost instantaneous relaxation that is a feature of CBFNR, being observed by Haupt and Sedlan [19] and Lion [18]. This stress relaxation response is not so easily achieved if the nested elements are not used.

We have shown that the 'four element model' (Fig.6.3-3) simulates dual-sine response and stress relaxation well but the model has a drawback that prevents its implementation in this simple form. The same stiffening that produces the 'looped' response to dual-sine histories and rapid relaxation in response to stepped displacement 'corrupts' the response to stable sinusoidal motion that was developed in Section 6.2. By stiffening the viscoelastic elements at high velocity, the additional nested elements change the models so that a simulation of the 'constant amplitude

varying frequency' measurement (Section 5.5) produces damping loops of changing shape. Not the constant profiles shown in Figures 5.5-1 and 5.5-2.

It may be possible to produce a 'compromise' or 'best fit' to all data by determining coefficients using a computer minimisation algorithm but it appears from tests that the next step in the development of this model should be to make the coefficients k_2 and k_4, in Figure 6.3-3, dependent upon stain rate. This is a process (or history) dependence of the type suggested by Haupt and Sedlan [19]. This has not been pursued however. A model of this type requires extensive development and would be the subject of further work.

The approach taken here is to develop a compromise model. The final model presented in Section 6.4 has a single stiffening element only, so that each of the strain histories (dual-sine, single sine, and stress relaxation) is approximated. It is considered that this compromise is sufficient for a vehicle component model where each rubber component is a small part of a complex system. In addition to this an effort has been made to simplify the model and make it 'general purpose' by using constant ratios between variables in the viscoelastic force elements and by using identical time constants in each of the three track components. This has reduced the number of variables that have to be found for the viscoelastic component of the model to just four. The final model for Warrior APC CBFNR components is presented in Section 6.4.

6.4 Final model for carbon black filled natural rubber components

The final model (presented in Figure 6.4-1) describes viscoelastic damping using three non-linear viscoelastic elements. Geometric non-linearity is described by a multiplying function and elastic force by a polynomial. As for the 'four-element' model described in Section 6.3, Equations, 6.1-1, 6.1-2, 6.1-3 and 6.1-4 apply.

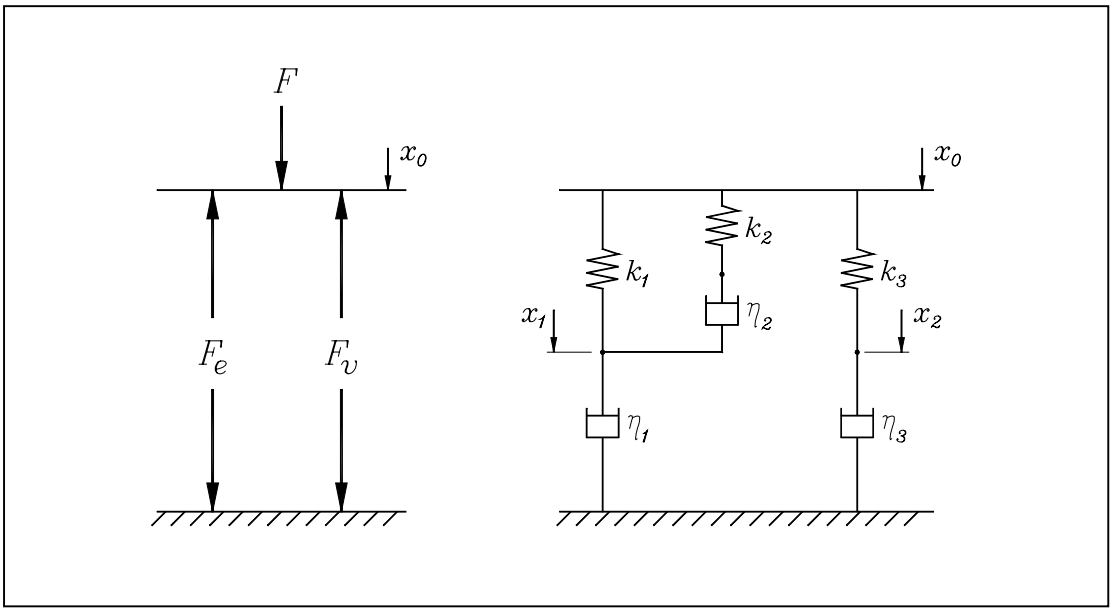

Fig. 6.4-1: *Final model containing three non-linear viscoelastic elements*

This model is a compromise between the simplified Haupt and Sedlan model described in Section 6.1 and the 'four-element' model describe in Section 6.3 In this model the coefficients, 'k_2' and 'η_2' are given the same values as 'k_1' and 'η_1' respectively. It was found that this allowed some stiffening so that dual-sine response and stress relaxation are approximated but the effect is not sufficient to significantly change the response to sinusoidal strains of differing frequency. Values for k_1, k_2, c_1 and c_2 are found by the method described in Section 6.2.

A further simplification has been achieved by giving the time constant of each viscoelastic element an identical value in each of the three component models, i.e. the tyre, the track bush radial response and the track bush torsional response.

Equation 4.2.7-3 shows that the time constant (τ) of the viscoelastic elements $\tau = \frac{c}{k.\xi}$.

By empirical investigation; comparing simulated relaxation and dual-sine response with measured response it has been found that suitable values for τ_1, τ_2 and τ_3 in each of the models three nonlinear viscoelastic elements are 100, 0.1 and 1.0 respectively. The result is that the number of variables in the viscoelastic model have been reduced from nine to four: k_1, c_1, k_3 and c_3. Values for each of the three component models are given in Appendix 4b.

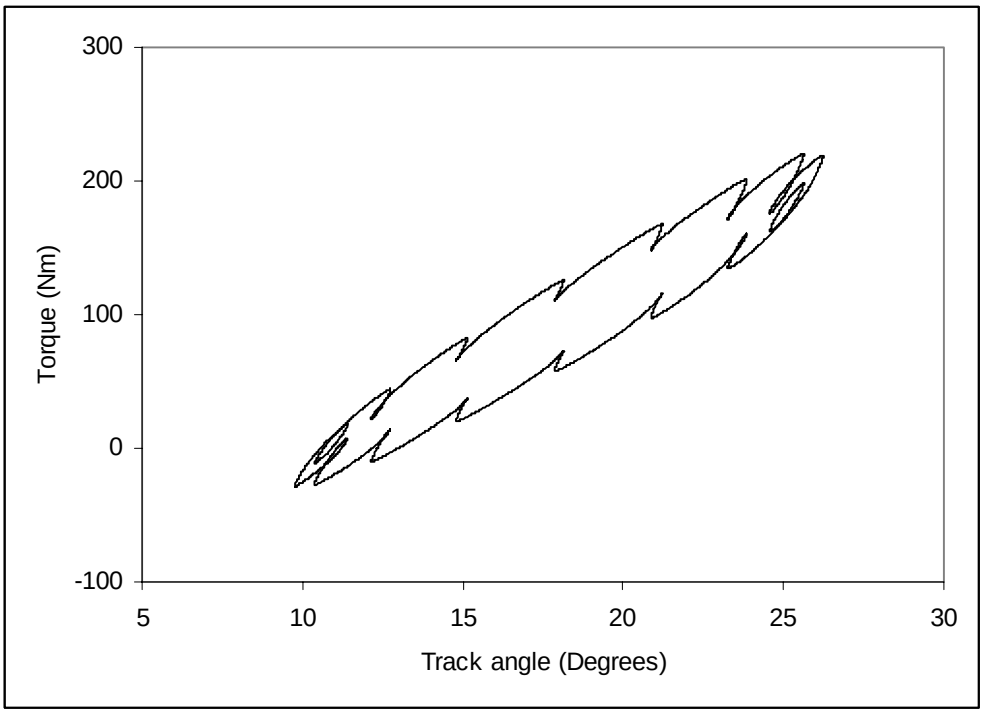

Fig 6.4-2: *Simulated track bush torsional response to dual-sine displacement. Produced by ADAMS simulation of the final three viscoelastic element model*

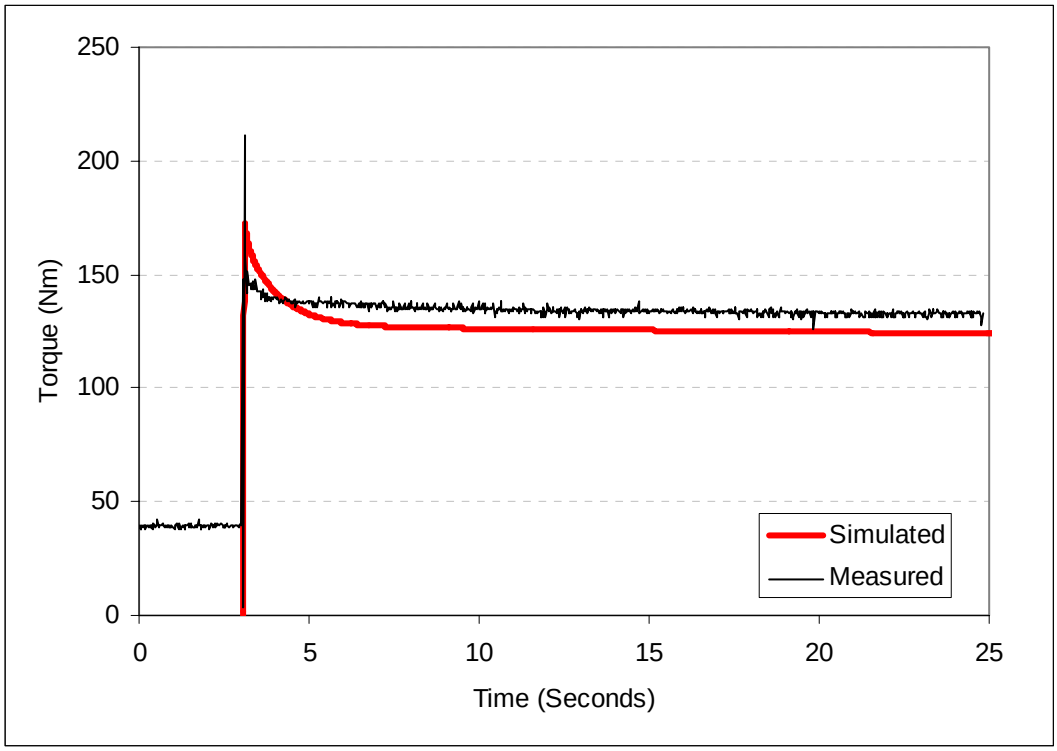

Fig. 6.4-3: *Measure and simulated track bush torsion stress relaxation, produced by* ADAMS simulation of *the final 'three viscoelastic element' model*

Figures 6.4-2 and 6.4-3 show the final three-element model response to dual-sine motion and stress relaxation respectively.

Evidently the three-element model does not describe the measured response to dual-sine and stepped displacement as well as the four-element model. Large loops are not formed in the dual-sine simulation and stress relaxation does not show the characteristic initial rapid relaxation. However we do see a number of small loops in Figure 6.4-2 and the dual-sine response is significantly 'better' then that produced by the simplified Haupt and Sedlan model (Fig 6.1-1).

6.5 Summary

The model developed here for simulation of Warrior APC, carbon black filled natural rubber components is a compromise between the simplified Haupt and Sedlan model described in Sections 6.1 and the four-element model developed in Section 6.3 The final model has three nonlinear Maxwell elements. These are two parallel elements and one that is nested.

Parameters for the time-dependent viscoelastic component are found by the method described in Section 6.2 where coefficients are adjusted to fit measured damping loops by visual comparison.

The number of coefficients required for the three nonlinear viscoelastic elements in the final model have been reduced from nine to four by two methods. Firstly, the 'nested' Maxwell element is given identical values to the element to which it is applied. Secondly, the time constant of each nonlinear Maxwell element is predetermined, having the same value in each component model.

Coefficients for the 'four-element' and 'three-element' models are given in Appendix 4a and 4b respectively.

Chapter 7

Comparison between measured and simulated rubber component response

7.0 Introduction

Here the 'final model' developed in chapter 6 is implemented in MSC.ADAMS^{TM} software and simulations compared to the measured response for each of the three Warrior APC CBFNR components. Parameter values for each of the component models are given in Appendix 4b.

7.1 Implementation of the final model in ADAMS software

Various measured force-displacement graphs are presented in Section 7.2 with their respective simulations. These simulations are produced by implementation of the 'final model' for CBFNR components (presented in Section 6.4) using MSC.ADAMS^{TM} software. However, because of a technical difficulty caused by the software's algorithm it is not possible to describe the 'final model' as show in Figure 6.4-1. Instead it is implemented as show here in Figure 7.1-1.

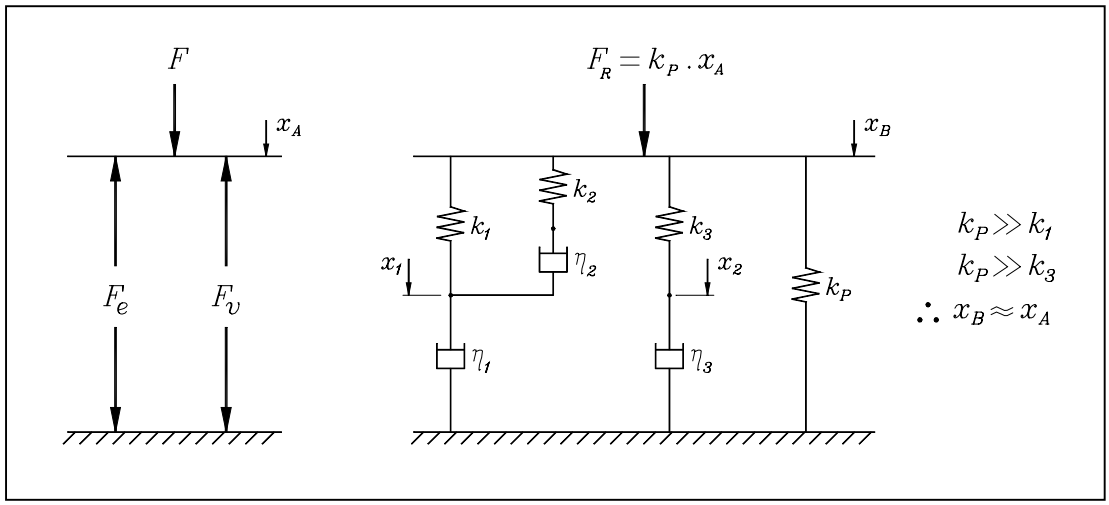

Fig 7.1-1: *Implementation of the 'final model' in ADAMS software so that* $x_B \approx x_A$.

The model has these two separate parts because the viscoelastic response is multiplied by a geometric factor (see Sections 5.3.2 and 6.1). The difficulty is that it is not possible to describe a motion in ADAMS software as being equal to a variable. A function that describes motion must be time dependent. This causes a problem because the model is made up of two parts that have the same displacement, x_A and x_B (Fig 7.1-1). But $x_B = x_A$, is not an allowable definition of motion.

The solution used here is to add an extremely stiff spring element (k_P) in parallel with the viscoelastic part of the model and apply a force equivalent to displacement x_A multiplied by this stiffness coefficient. The displacements of both parts are then the same to within a small error which depends on the ratio $\frac{k_1}{k_P}$ and $\frac{k_3}{k_P}$. For the simulations presented below in Section 7.2 the highest value ratio is 0.001.

7.2 Comparison between measured and simulated response plots

For all graphs presented in this section the grey line represents the elastic force (as described in Section 5.3.1) and the black lines represent total force.

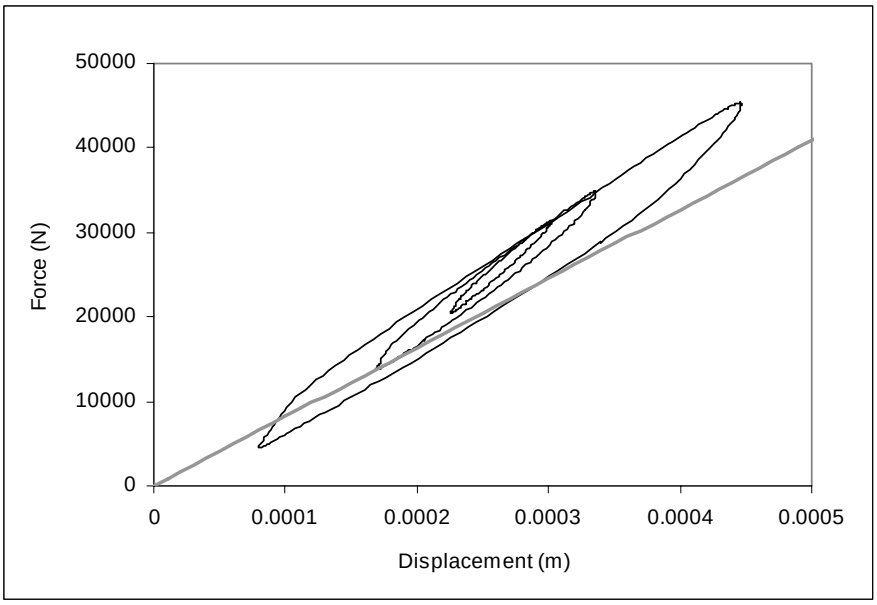

Fig 5.4-2: *Measured track bush radial force-displacement response*

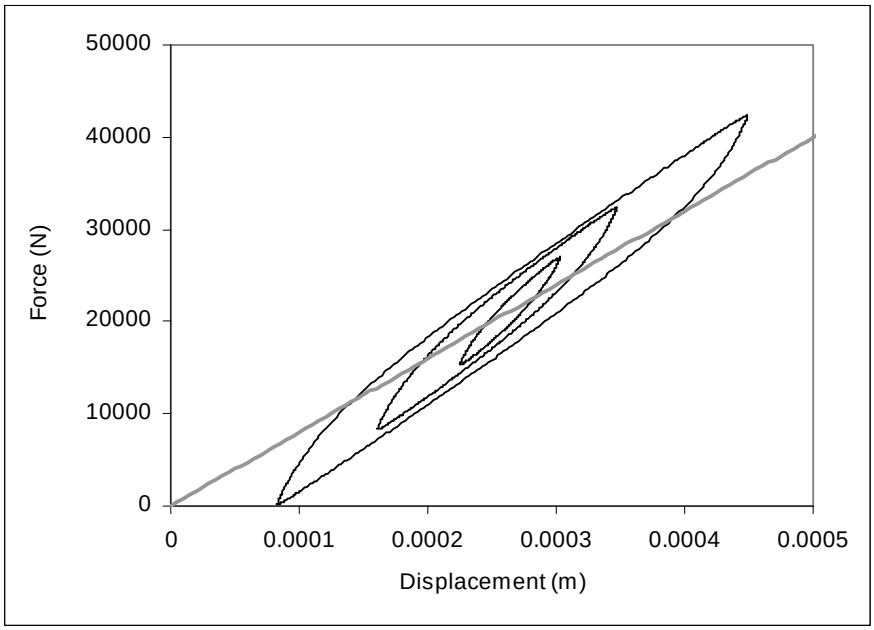

Fig 7.2-1: *Simulated Track bush radial force-displacement.*

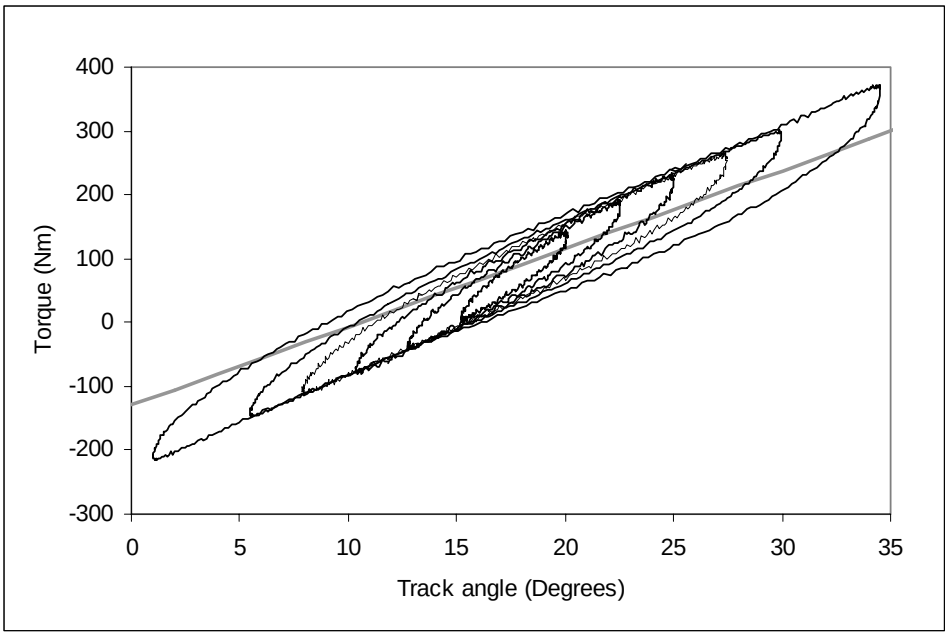

Fig 5.4-1: *Measured track bush torsional force-displacement response*

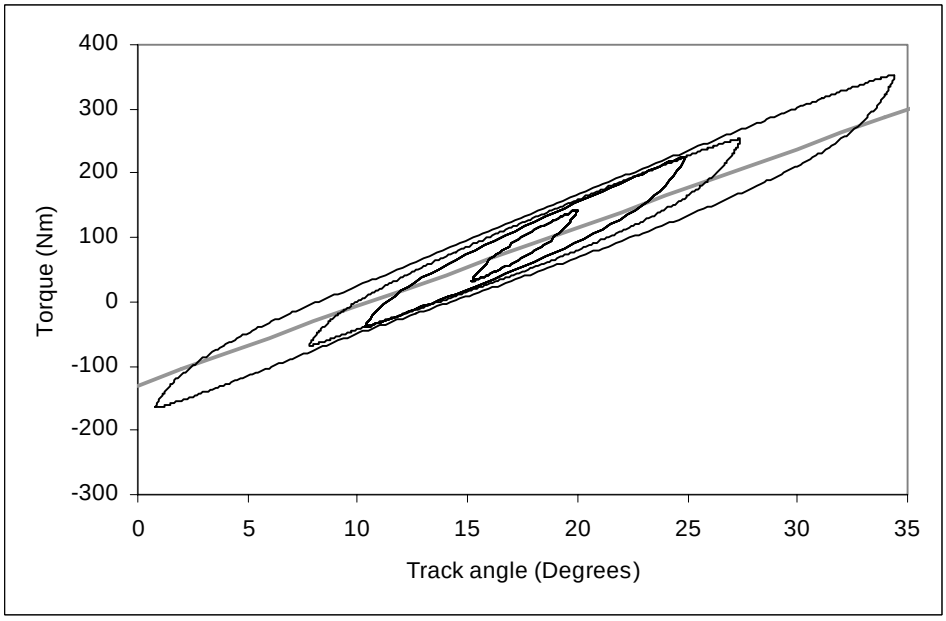

Fig 7.2-2: *Simulated track bush torsional force-displacement response, (Several of the loops have been omitted here for clarity).*

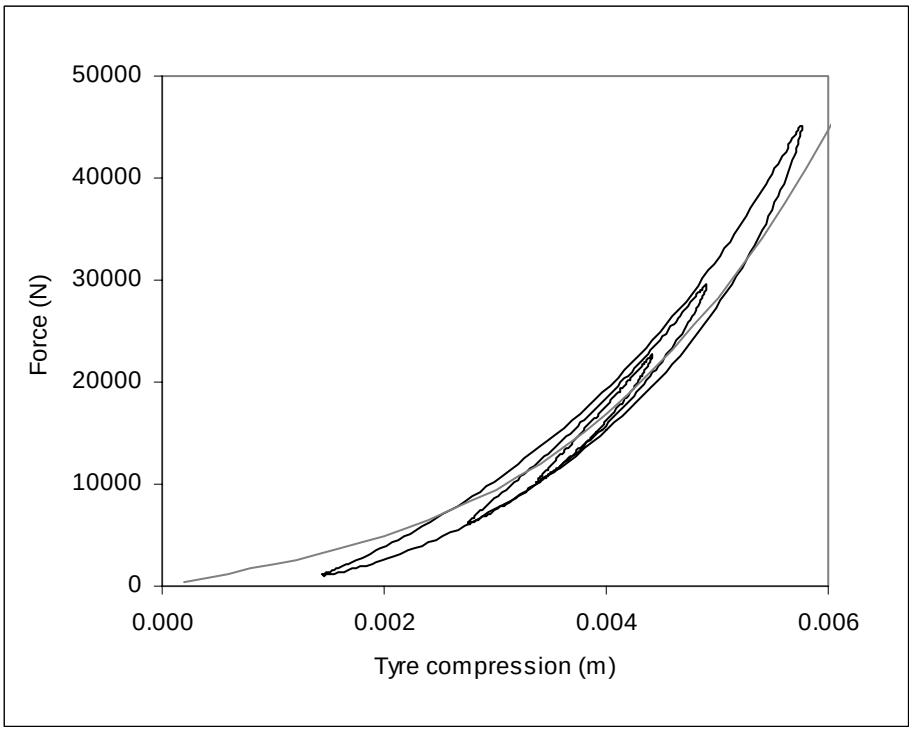

Fig 5.4-3: *Measured road wheel tyre radial force-displacement response*

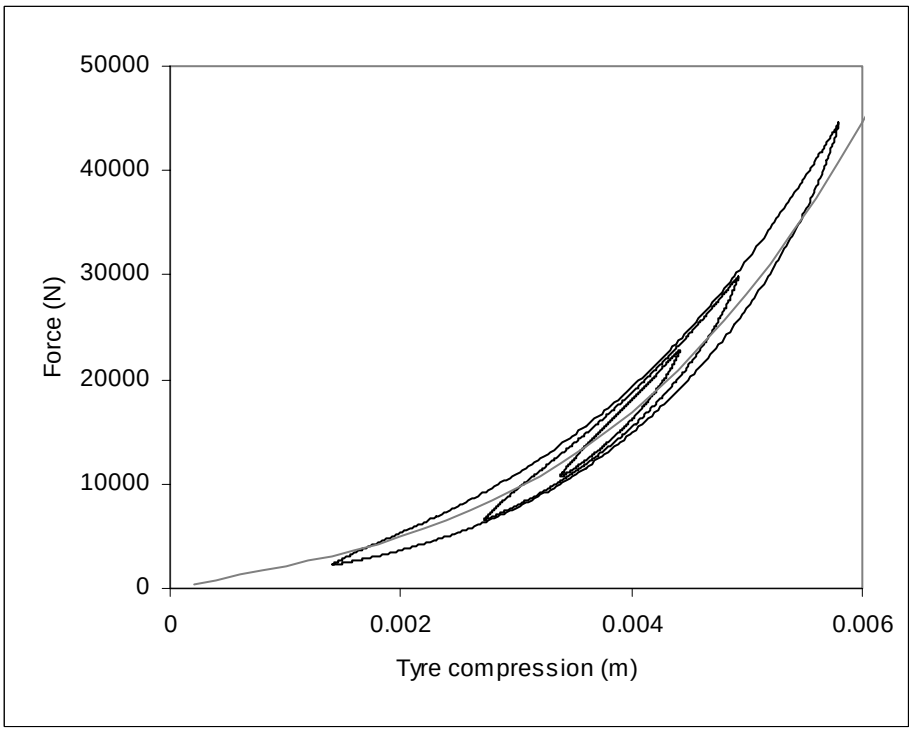

Fig 7.2-3: *Simulated road wheel tyre radial force-displacement response*

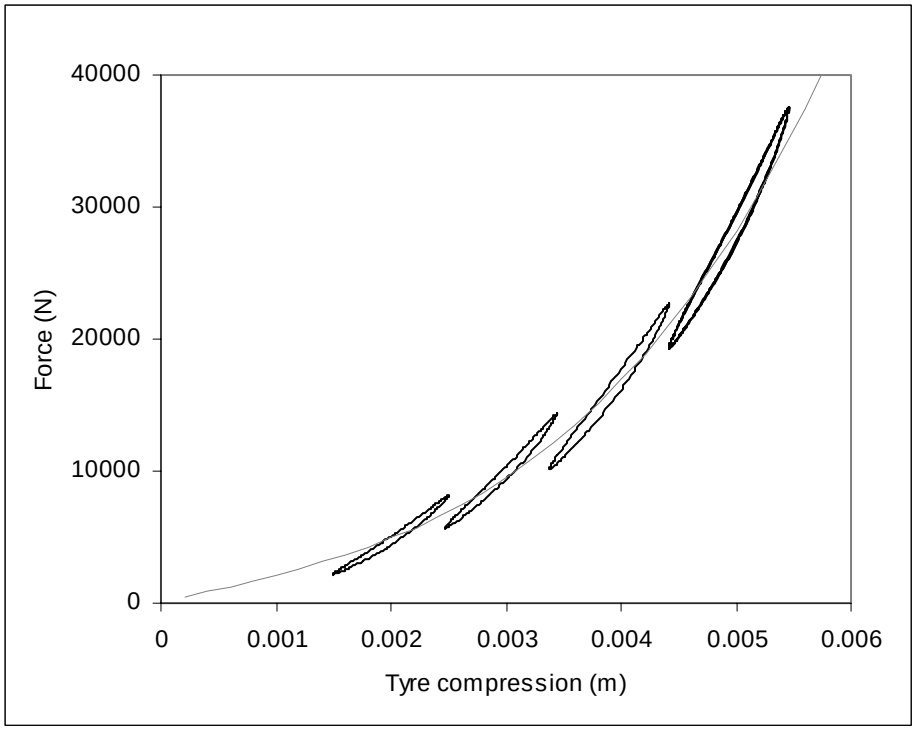

Fig 5.3.1-3: *Measured road wheel tyre displacement*

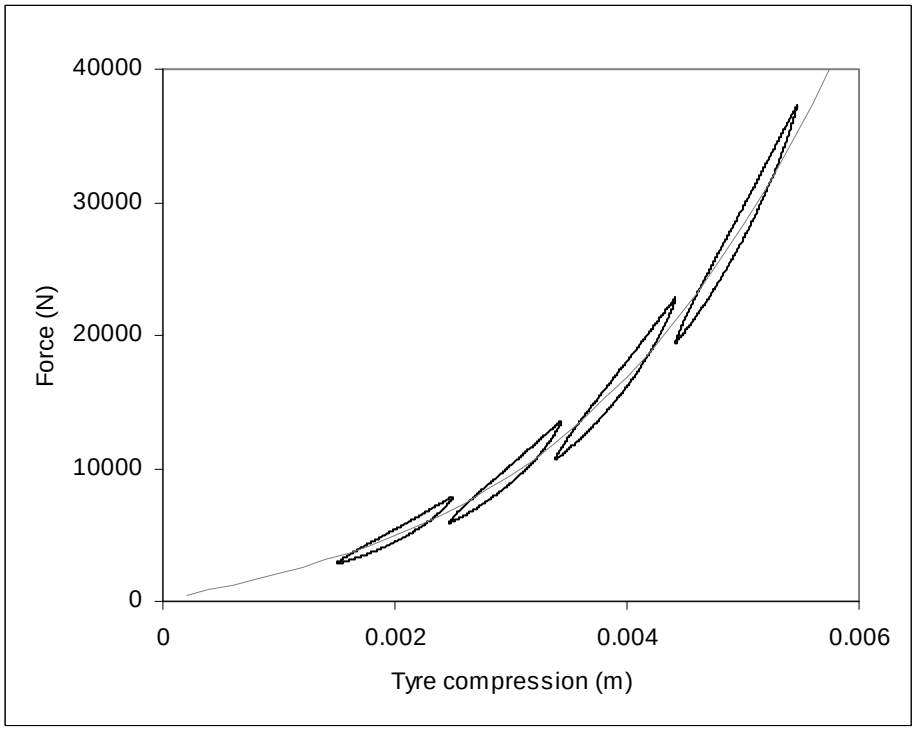

Fig 7.2-4: *Simulated road wheel tyre displacement-force response*

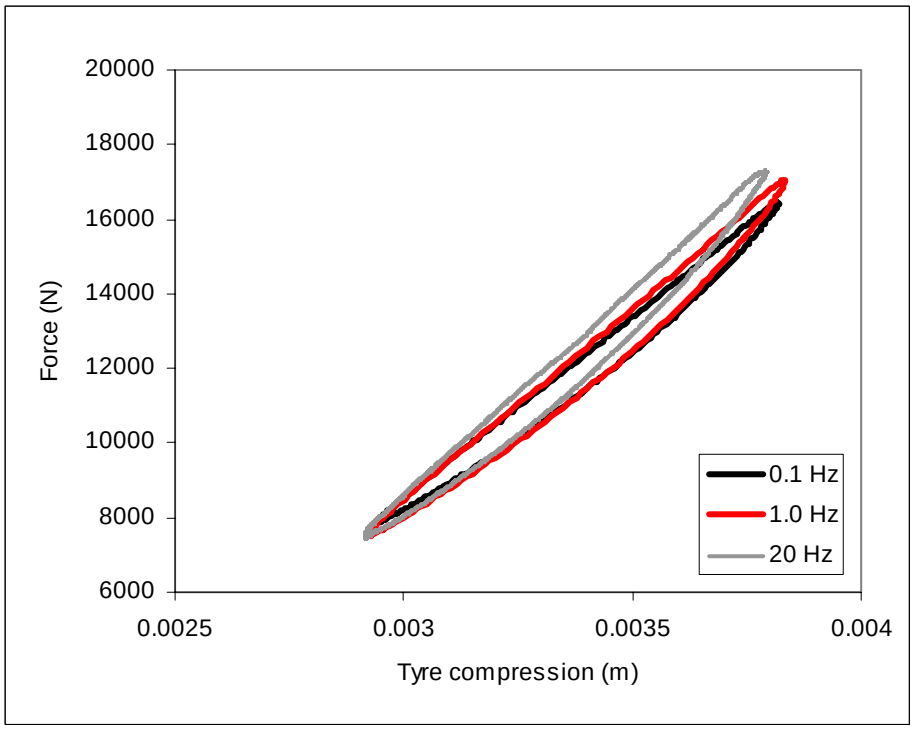

Fig 5.5-1: *Measured road wheel tyre force-displacement response at several frequencies*

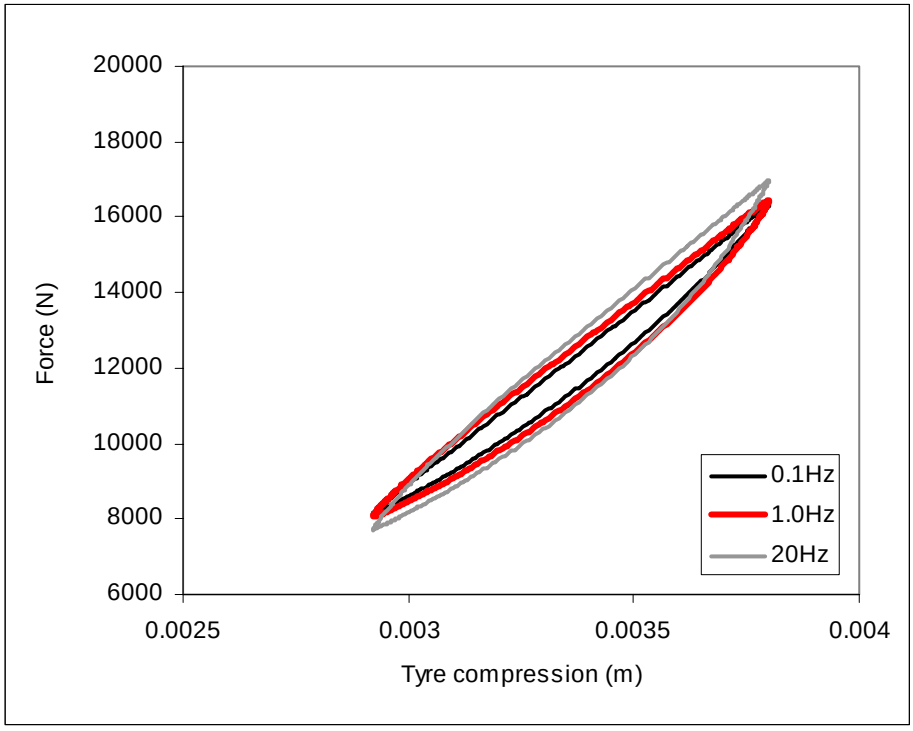

Fig 7.2-5: *Simulated road wheel tyre force-displacement response at several frequencies*

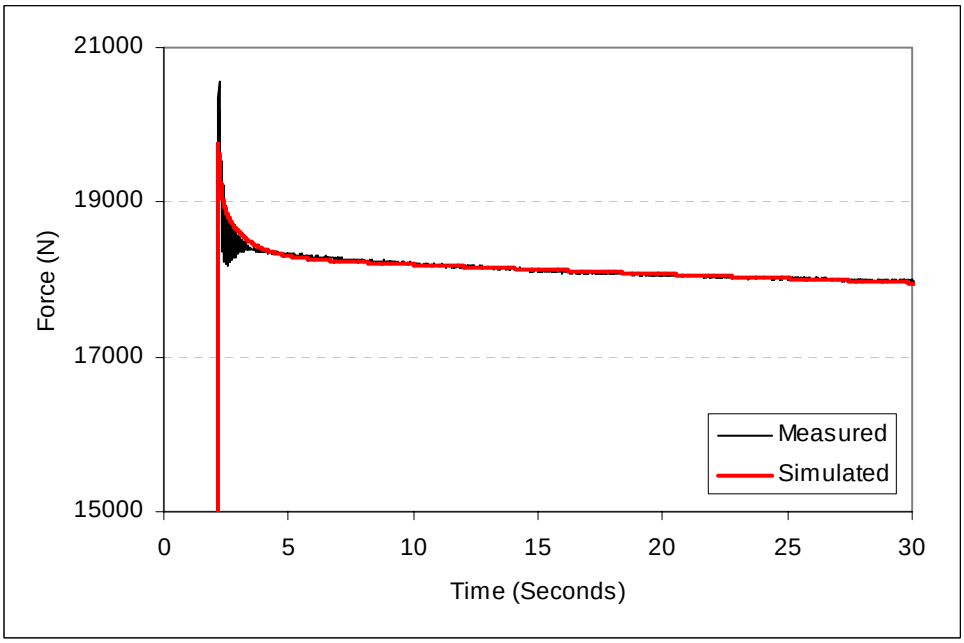

Fig. 7.2-6: *Measure and simulated road wheel tyre stress relaxation*

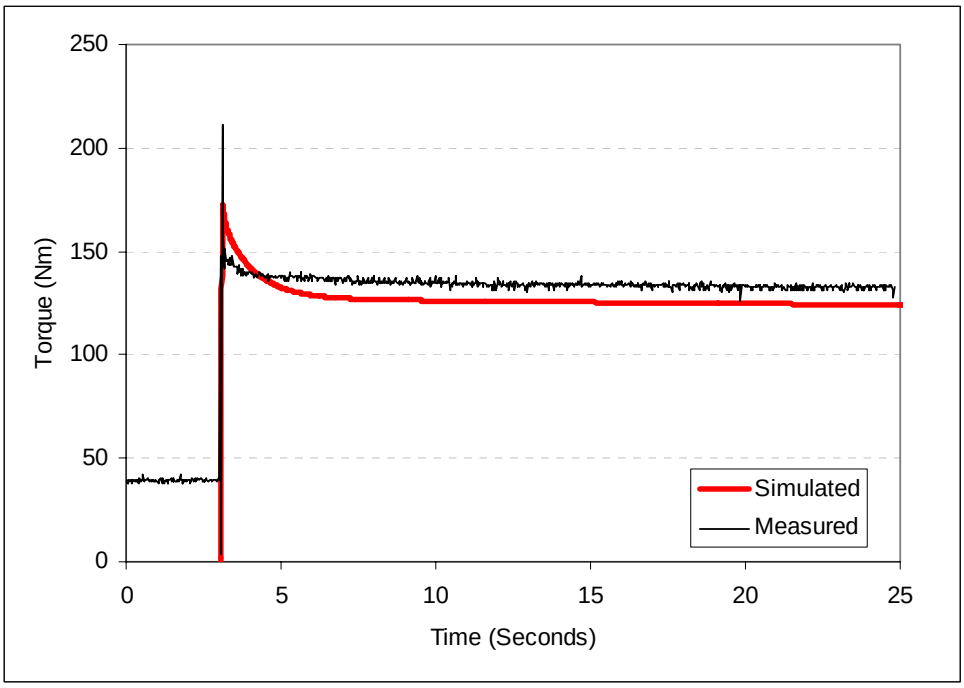

Fig.7.2-7: *Measure and simulated track bush torsion stress relaxation*

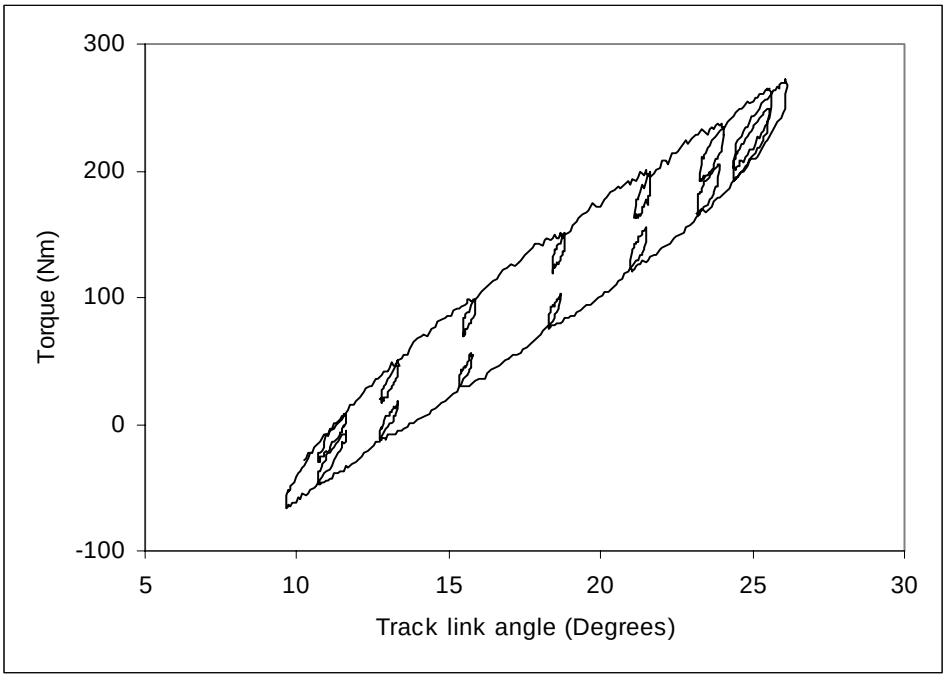

Fig. 5.8-1: *Measured track bush torsional response to dual-sine displacement*

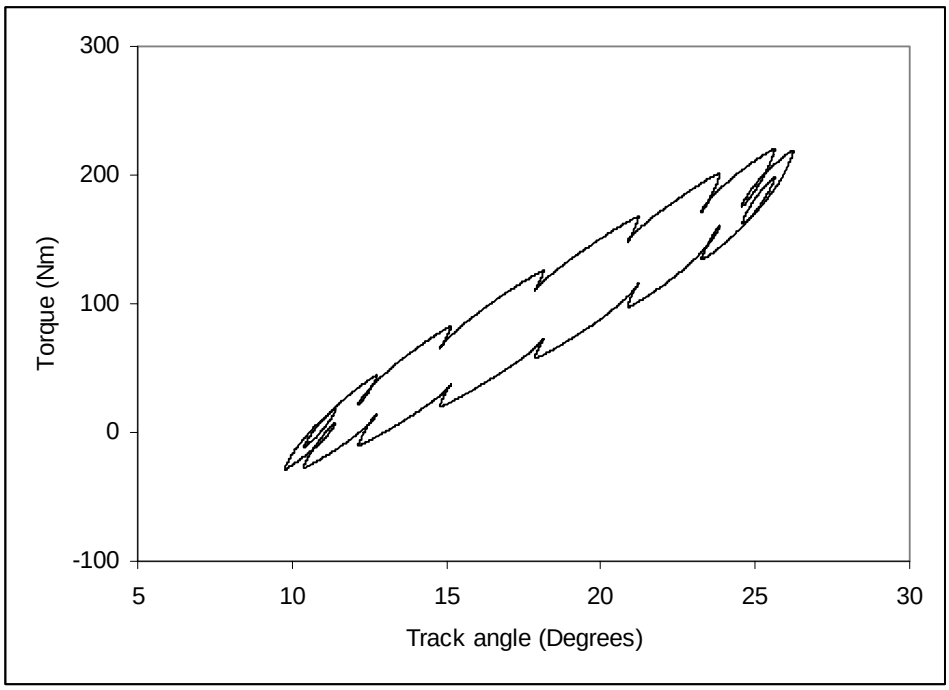

Fig. 7.2-8: *Simulated track bush torsional response to dual-sine displacement*

7.3 Summary

The comparisons between measured and simulated responses show that the model closely approximates the response to steady sinusoidal motion and that damping and stiffness are described sufficiently accurately for used in vehicle component models. Stress relaxation and the response to dual-sine displacement are less well described but this has been justified in Sections 6.3 and 6.4 by the requirement for a reasonably simple model. A more precise simulation would require strain history dependence (as described in Section 6.3), where the coefficients values k_2 and k_4 in Figure 6.3-3 would be variable. A model of this type would be the subject of further work if a high degree of accuracy were required. The results presented here shows that the model is satisfactory for simulation of Warrior APC CBFNR components in the first instance, where the development of a full vehicle model is at an early stage.

Chapter 8

Summary of the rubber components investigation

8.0 Summary

A ‘general purpose’ time-dependent model for carbon black filled natural rubber components has been developed for implementation in ‘dynamic simulation software’ that uses the Newton-Raphson Prediction Corrector algorithm. No attempt has been made to describe the materials microstructure. Force-displacement measurements have simply been deconstructed into three elements, an elastic force, a viscoelastic force and geometric multiplier.

A number of models developed in recent years for carbon black filled natural rubber have been reviewed and the response of three Warrior Armoured Personnel Carrier components to various displacement histories presented. These components are, the track link bush radial response, track link bush torsional response and road wheel tyre radial response.

A novel method has been used to determine values for a polynomial that describes elasticity and a function describing the effect of changing geometry. This depends upon the assumption that by following careful measuring methodology; the magnitude of viscoelastic force in response to small amplitude sinusoidal displacement lies equidistant about the elastic force line.

It has been shown that for dynamic simulation software that uses the Newton-Raphson Predictor Corrector algorithm; viscoelasticity is best described by a non-linear Maxwell element based on that presented by Haupt and Sedlan [19]. Primarily this is because values at turning points do not have to be stored, the element naturally reproduces an asymmetric shape and the element has ‘stress relaxation’. The Haupt and Sedlan model has been significantly changed though by the addition of a ‘stiffing

element' producing a model that better describes dual-sine motion and stress relaxation. The viscoelastic description developed requires only four parameter values that are found simply by manually changing values of a time-independent function and visually comparing the damping loop produced with measured data. Computer minimisation algorithms are not used. The final model developed here is a compromise. It is satisfactory for use in vehicle models, being able to describe the three fundamental features of carbon black filled natural rubber response, these are its; predominantly frequency independent damping, asymmetric hysteresis loop shape and stress relaxation. Also viscoelasticity is described by a 'smooth' continuous function that is easily implemented in automatic dynamic analysis software. The model has been implemented using ADAMS software and results show good correlation with the measured response to stable sinusoidal motion. However, dual-sine motion and stress relaxation are less well described.

The model could be further developed by introducing 'strain history dependent parameters' such as strain-rate dependence similar to that used by Haupt and Sedlan [19] and Haupt and Lion [20] which would improve the dual-sine and stress relaxation simulations but this would be the subject of further research. Other possible areas for further work are:

- The development of a three-dimensional constitutive material model based on the one-dimensional model developed here.
- An investigation into road wheels response when rolling over a surface.
- Further validation of the technique used here to determine the elastic force response and a geometric multiplier by taking a line through the mean point of small amplitude hysteresis loops.

- Investigate the effect of temperature on the dynamic response of CBFNR and how the model developed here could describe this behaviour. For simplicity temperature effects were not studied in this work; all measurements were made at room temperature (approx. 20°C).
- Further work is required to determine whether the model developed here (for the purpose of describing CBFNR components in simulation software that uses the Newton-Raphson Predictor-Corrector algorithm) has wider range of applications. Answering the following questions: Is the model suitable for use in other types of simulation software? Does the model describe internal damping in materials other than CBFNR?
- Another important area of study for further work is CBFNR response to transient vibration. This has not been explored in depth in this study; only a few measurements of the rubber component's response to a stepped displacement where made. This is an area where further work is required to developed the model and understand the materials behaviour.
- The CBFNR component models developed here should be applied in a full vehicle simulation and the results assessed by comparison with measured data to determine whether the use of these models improves the accuracy of the full vehicle simulation.

Chapter 9

The Warrior APC rotary damper

9.0 Introduction

The objective here is to develop a model of the Warrior Armour Personnel Carrier (APC) suspension rotary damper for use in a full vehicle simulation. The model will be implemented in multi-body simulation software such as MSC.ADAMS^{TM} that computes response by the implicit Newton-Raphson, Predictor-Corrector method. An important feature for robust and trouble free operation in this type of software is that the descriptive function produces smooth and continuous; force, displacement and velocity responses. The damper model is one component in the complex multi-body mechanical system and it is important that it functions well.

The Warrior's rotary damper is designed and manufactured by Horstman Defence Systems Limited and has been proven on test rigs and in the field to fulfil all performance and endurance requirements. The damper has remained unchanged throughout the Warrior's production history from 1979 to the present day. In general the purpose of a suspension damper is to dissipate energy imparted to the road wheels by undulating road surfaces, vehicle acceleration and turning. But for the Warrior APC the primary purpose is to minimise the vehicle's pitching motion. Tracked vehicles are particularly susceptible to pitching motion because of their high pitching inertia and relatively high suspension compliance. Pitch mode natural frequencies are typically very low (circa 1.0Hz) and are a main source of ride discomfort, severely reducing the vehicles off-road performance if not damped [21].

The Warrior has twelve road wheels (six on either side of the vehicle) each mounted on a 400mm trailing wheel arm. Transverse horizontal torsion bars allow the wheel

arm to rotate in response changing ground profiles. Rotary dampers act in parallel with torsion bars at six of the twelve wheel stations. Numbering pairs of wheel stations from 1 to 6 along the vehicle from the front to rear (Fig 9.0-1), dampers are installed at stations 1, 2 and 6. The three central stations (3, 4 and 5) are undamped. It is damping at the stations furthest from the centre of gravity that offer most resistance to pitching motion.

The 3D solid model of a Warrior's APC running gear (Fig 9.0-1) shows the drive sprocket at the front of the vehicle, six pairs of road wheels, six pairs of torsion bars, idler wheels, support rollers and the track.

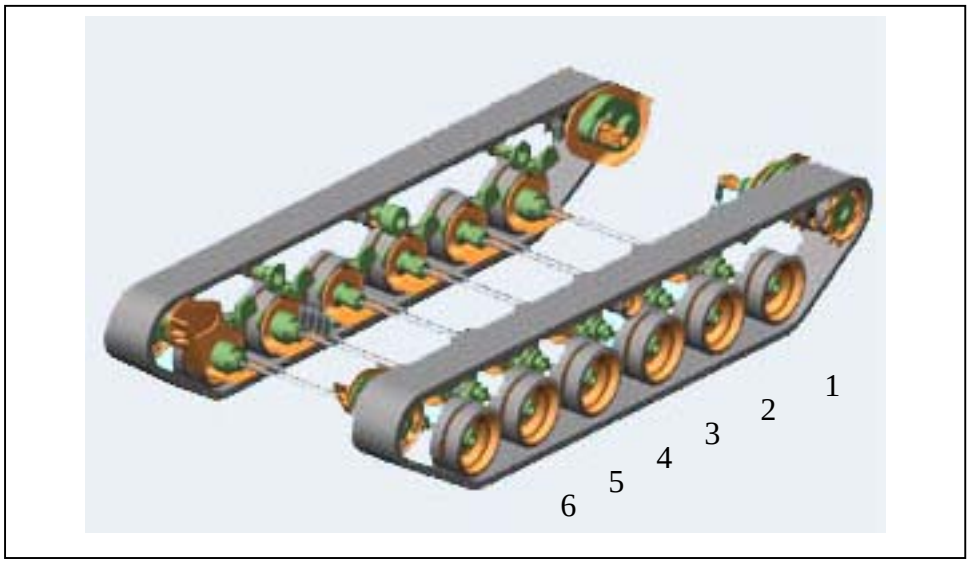

Fig. 9.0-1: *Warrior Armoured Personnel Carrier running gear (Horstman Defence Systems Ltd). Wheel stations are numbered 1 to 6 from front to rear*

9.1 Design of the Warrior APC Rotary damper

In principle the Warrior's rotary damper has the simplest possible design. It is an un-pressurized passive device with a single simple orifice determining the resistance to flow between chambers in both directions. Pressure relief valves restrict damping force to maximum compression and rebound values.

For its purpose, the damper requires a maximum rotation angle of approximately 90° (±45°). Therefore, to optimise space, the design has two identical chambers 180° apart. The chambers have identical, vane pistons, orifice and pressure relief valves (see Figure 9.1-1).

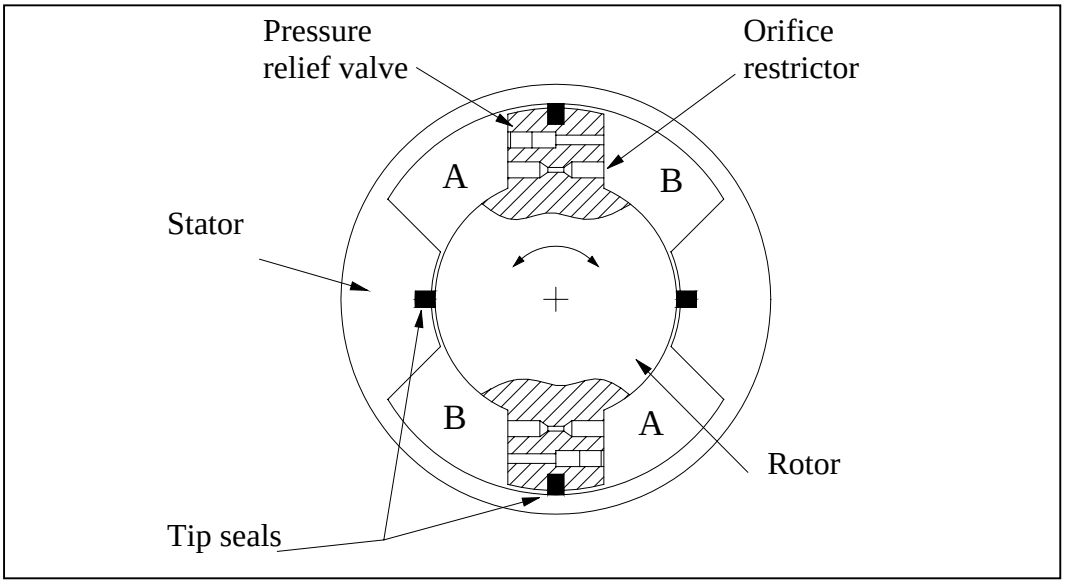

Fig. 9.1-1: *Section through rotary damper*

Passageways connect the chambers labelled ‘A’ and the chambers labelled ‘B’ so that oil pressure is balanced. The damper’s rotor is connected directly to the road wheel arm and torsion bar so that it rotates at the same angular velocity.

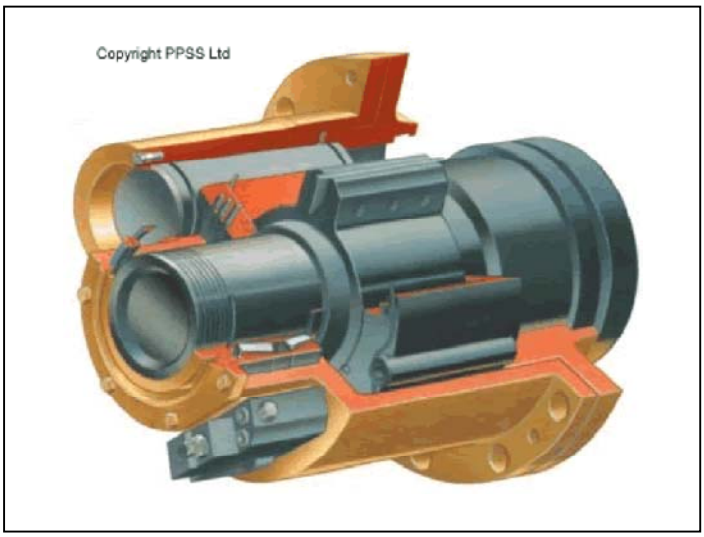

Fig. 9.1-2: *Sectioned view of the rotary damper*

Damper resistance is caused by the restriction to oil flow through both orifices and seals. *'The damping rate is determined by the rate at which fluid is allowed to leak from the pressurised chambers across the rotor vanes, via seals orifices and valves…perfect sealing is not of paramount importance'*…[21].

Although the principle behind the damper is simple its design in detail and its construction are not. The sectioned 3D image (Fig 9.1-2) illustrates this. The damper incorporates wheel arm bearing and is designed to withstand high torsional and radial loads. Rotating components are mounted in a cast-steel housing, which supports the bearings outer race and the dampers stator.

A complex labyrinth of channels is necessary to connect the chambers, to fill the damper with oil and purge it of entrapped air. Priming is a lengthy procedure requiring, specialist tools, hydraulic pump and heavy lifting equipment that can rotate the damper into various orientations.

Because damping force is generated by oil flowing through a single simple orifice the damping rate is the same in both bounce and rebound up to where the pressure relief valves operate. This is unusual in damper design. It is more common for damping rate in compression to be higher than the rate in rebound.

Figure 9.1-3 shows the envelope to which the damper has been designed. The upper and lower bounds allow for nonlinearities such as, variation in valve coefficient, transition from laminar to turbulent flow, flow past seals, mechanical backlash, friction, viscosity variation and expansion due to temperature change.

In response to exceptionally rapid motion in bounce the pressure relief valves acts to restrict maximum force transmitted to the hull. In rebound following a bump when the only restoring force is that of the torsion bar the relief valve allows the road wheel to return quickly to its normal position.

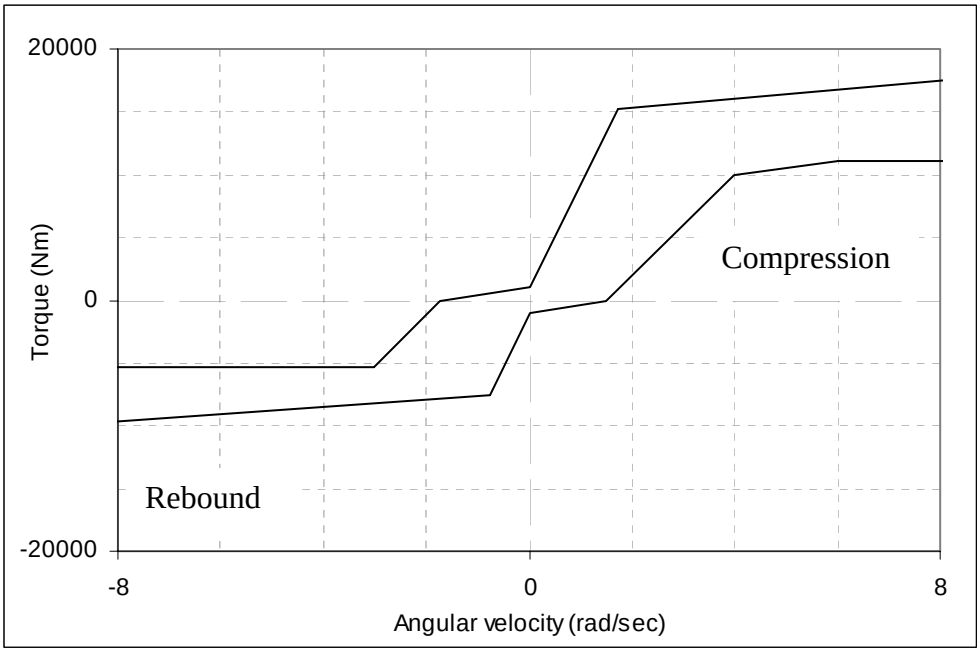

Fig. 9.1-3: *Design specification showing the allowable range of damper torque*

An additional design requirement for the damper is that low displacement amplitudes have low resistance. This is so that the transmitablity of high frequencies to the Warrior's hull is low. As explained here in an excerpt taken from Holman [21].

'The main source of ride discomfort is vehicle pitching. This results from excitation of the pitch mode natural frequency of the vehicle. This is typically very low (c 1 Hz). Oscillations of this type must be adequately damped. However, it is undesirable that a damper should respond positively to the higher frequency, small amplitude oscillation induced by passage over cobblestone surfaces (or, in the case of tracked vehicles, track links). Response to these would result in unwanted energy dissipation' [21].

Holman goes on to state that this requirement has been satisfied: *'Frequency response testing has shown that, although the damper responds very effectively to frequencies normally associated with pitch oscillation, energy dissipation at high frequencies (30Hz) is very low' [21].*

Data from test conducted by Horstman Defence Systems Limited show that the damper satisfies the requirements. Torque lies within the limits specified in Figure 9.1-3 and power dissipation falls at low amplitude as required.

The results produced by Horstman Defense Systems Ltd however are not ideal for the development of a damper model for vehicle simulation. The Horstman characteristic torque verses angular velocity graph is produced by constant velocity excitation (triangular waveform) producing an individual point on the graph for each measurement (Fig. 9.1-4) rather then the continuous plot produced in response to sinusoidal excitation, which would show nonlinearity and hysteresis in detail.

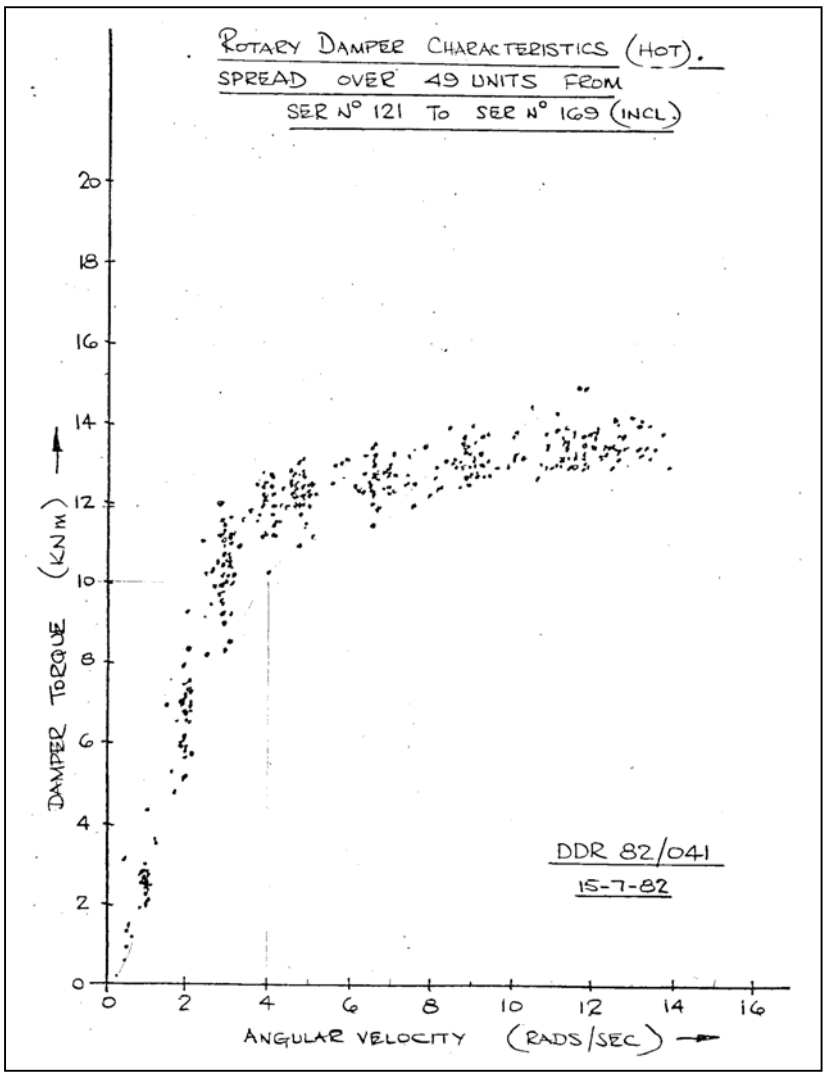

Fig. 9.1-4 *Characteristic graph of torque verses angular velocity, produced by Horstman Defense Systems Ltd*

To investigate the nonlinearities and hysteresis for the development of a damper model a test rig was built, measurements of torque versus angular velocity in response to sinusoidal excitation have been undertaken and these are presented in Chapter 12. However because the test rig that was built has limited range, the Horstman data (Fig 9.1-4) is used to develop the model at high velocities.

Chapter 10

Literature review of automotive suspension damper models

10.0 Introduction

Many papers have been published on the topic of automotive damper modelling [22-36] and although each may describe a different damper design (monotube, dual tube or gas pressurized) all agree that damper response is significantly non-linear. Physical models attributed non-linearity primarily to, turbulent flow, gas compressibility and friction. Although other nonlinearities that may also be described are: pressure relief (blow-off), temperature/viscosity variation, cavitation, aeration and mechanical backlash.

Here in Chapter 10 four descriptive techniques for vehicle damper models are discussed. These are: equivalent linearization, restoring force method, physical models and models which use discrete spring, damper and friction elements.

10.1 Linear equivalent models

Linearization is effectively an averaging technique where parameters for a linear single degree of freedom mass-spring-damper system are determined from the true non-linear damper response. This type of model is described by the following linear equation.

$$m_{eq}\ddot{x} + c_{eq}\dot{x} + k_{eq}x = F \qquad \textbf{Equation 10.1-1}$$

Where, m_{eq} is the equivalent mass of reciprocating parts, c_{eq} is the equivalent damping coefficient, k_{eq} is equivalent spring coefficient, F is the reaction force, $x, \dot{x}\ and\ \ddot{x}$ are displacement, velocity and acceleration, respectively. The coefficients c_{eq} and k_{eq}

maybe derived by harmonic excitation or by a broadband excitation that simulates the motion the damper will experiences as a vehicle component. But whichever type of excitation is used when testing the damper, the experimental method by which the coefficients are determined is the same (requiring measurements of $F(t), x(t)$ and $\dot{x}(t)$). However due to the dampers non-linearity, the coefficients in each case are likely to have different values.

The theory of 'linearization of nonlinear systems' is covered in detail by Worden and Tomlinson [50]; who in turn refer to the work of Hagegorn and Wallaschek with regard to determining linearised coefficients by experimental methods. Hagedorn and Wallaschek [24] derive linearised equations for an automotive damper that equate the coefficients c_{eq} and k_{eq} to measured, force $F(t)$, displacement $x(t)$ and velocity $\dot{x}(t)$. These equations can be interpreted as Equations 10.1-2 and 10.1-3 below, where the 'bar' notation $\overline{f(t)}$, has been used to indicate 'mean value' rather then 'expected value' $E[f(t)]$ as in Hagegorn and Waklaschek.

Linerarized damping coefficient

$$c_{eq} = \frac{\overline{\left(F(t) - \overline{F(t)}\right)\dot{x}(t)}}{\overline{\dot{x}^2(t)}}$$

Equation 10.1-2

'*Equation 10.1-2 describes a power balance: In the mean all power provided by external force (F) is dissipated in the damper of the linearized system*' [24].

Linearized stiffness coefficient

$$k_{eq} = \frac{\overline{F(t)x(t)} + m\overline{\dot{x}(t)} + \overline{F(t)}\,\overline{x(t)}}{\overline{x^2(t)} - \overline{x(t)}^2}$$

Equation 10.1-3

'*Equation 10.1-3 can be interpreted as an energy balance stating that in the mean kinetic and potential energy of the linearized system are equal to each other*' [24].

Hagedorn and Wallaschek [24] compare the equivalent linearized harmonic and broadband coefficients for a monotube automotive damper and recognise that the result is dependant upon the test signal, suggesting that motion of the damper while on the vehicle should be recorded and used to determine these coefficients. But Hagedorn and Wallaschek suggest that a linearized model is most useful in comparative tests where the effect of design changes or ageing are explored.

Assessing linear and bilinear models, Hall and Gill [22] compare the ride performance predicted by a physical model that described both non-linearity and hysteresis with a model that excluded hysteresis and a linearized model. The conclusion was that models that do not describe hysteresis or which linearize the data '*are inappropriate and lead to over-optimistic estimates of ride performance'.*

10.2 Restoring force maps

A restoring force map is a three dimensional plot with force response on the vertical axes, displacement and velocity on the horizontal axes. Values for the map are most often determined by damper tests at constant frequency of varying amplitude. The map maybe described by either a grid of flat surfaces connecting measured points or a continuous smooth surface profile produced by a three-dimensional curve fitting technique. When used to simulate damper response data is retrieved from the stored map for the given displacement and velocity conditions.

The restoring force map method has limited application because of damper non-linearities, which produce a frequency dependent response.

Examples of restoring force maps are given by, C.Surace. et. al. [26] and Duym [33].

Duym states that restoring force maps are unsuccessful for broadband excitation but that they are useful in modelling the response to harmonic motion. C.Surface. et. al. simply use the restoring force map method to compare measured response with the response produce by a physical model. The map is not used for damper simulation.

10.3 Parametric or physical models

The most common type of damper model is the physical or parametric model. This method describes damper response by equating formulas for physical phenomena and the kinematics of the mechanism. For example: laminar flow through an orifice is proportional to pressure drop, turbulent flow approximately proportional to pressure drop squared. Flows are equated to volumetric change, displacement and compliance. Gas laws are applied where appropriate and friction is described by a suitable function.

This modelling method produces a set of non-linear differential equations that are suited to Newton-Raphson Predictor Corrector numerical simulation, however a drawback is that precise parameter identification for the many values requires repeated simulation and automated minimisation algorithm techniques. A number of papers, which use physical parametric damper models, are: [22, 26, 27, 30, 31, 34, 35 and 36]. These models are all very similar in principle, however they differ in some details. Summaries of their characteristics are listed in Table 10.3-1. But this table presents only an overview of the physical phenomena described in each model; the detailed description of any component may differ in each case. For instance, turbulent flow maybe described by $\Delta P \propto \dot{V}^2$ or $\Delta P \propto \dot{V}^{1.75}$; friction may be described as Coulombic, include stiction or be a function of displacement and/or velocity.

Author/s & Reference	Hall & Gill [22] (1986)	Surace et. al. [26] (1991)	Kwang-jin [27] (1997)	Purdy [30] (2000)	Yung & Cole [31] (2002)	Duym [36] (1997)	Duym [34] (1998)	Duym [35] (2000)
Type of automotive damper	Dual-tube	Mono-tube	Mono-tube	Dual-tube	Mono-tube	Dual-tube	Dual-tube	Mono & Dual-tube
Friction	√	√	√	√	√		√	√
Oil and chamber compliance	√	√	√	√	√	√	√	√
Adiabatic gas compression			√	√	√	√	√	√
Cavitation / Vapour pressure	√	√		√				
Gas solubility - Henry's law						√		
Laminar flow				√				
Turbulent flow	√	√	√	√	√	√	√	√
Pressure relief (Blow-off)					√	√	√	√
Thermal effects			√				√	

Table 10.3-1: *A summary of the various physical phenomena that are described in a selection of parametric models*

10.4 Spring and dashpot models

The parametric models described above in Section 10.3 can also be represented as a nonlinear spring in series with a nonlinear dashpot, plus a frictional element. Turbulent flow through an orifice is then represented by the nonlinear dashpot and the nonlinear spring represents, chamber compliance, compression oil and compression of entrapped gas. This approach suits the implementation of a physical model in software packages such as MSC.ADAMS where discrete components are assembled to represent the mechanical system. Figure 10.4-1 illustrates this approach.

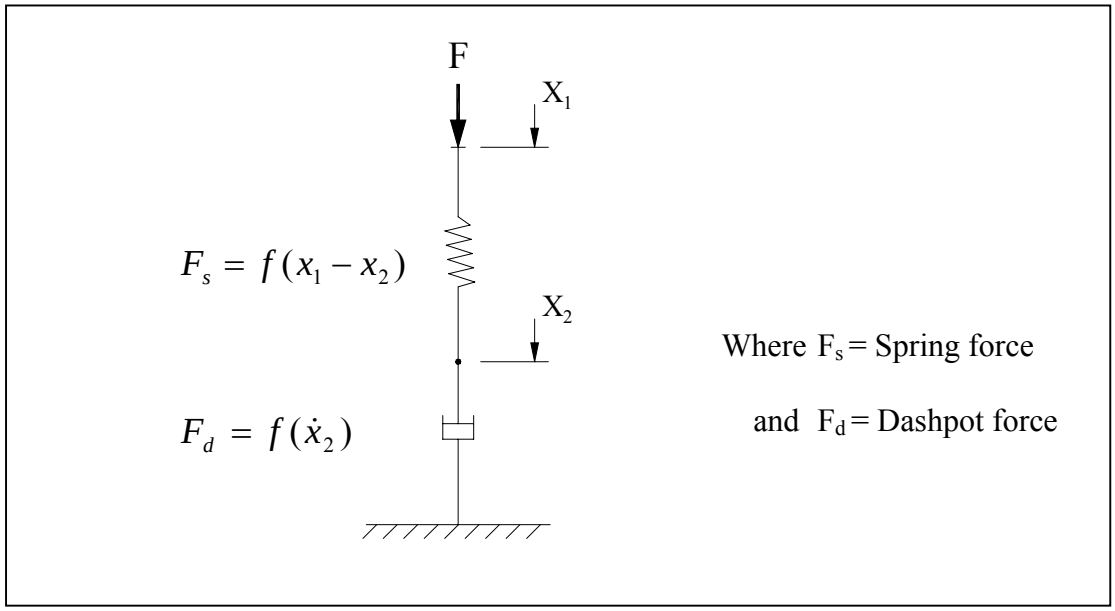

Fig. 10.4-1: *A physical damper model represented by non-linear dashpot and non-linear spring in series.*

Karadyi and Masada (1986) [23] use a linear spring and dashpot and included backlash in an early attempt to produce a computer simulation of an automotive damper. Duym [33] implements a model that has a cubic spring and tri-linear damper but reports that accuracy was lower when compared to other modelling methods such as a physical model or restoring force map.

Chapter 11

Rotary damper test rig design and experimental procedure

11.0 Test rig design and instrumentation

A test rig was built which could rotate the damper through ±0.4 radians at a maximum angular velocity of 4 rads/sec. The limiting factors being, maximum displacement and velocity of the hydraulic ram that provided the motive force. Driving motion was transmitted from the hydraulic ram to the rotary damper by a connecting rod and the apparatus mounted on a test bed. A schematic drawing of the arrangement is presented in Figure 11.0-1.

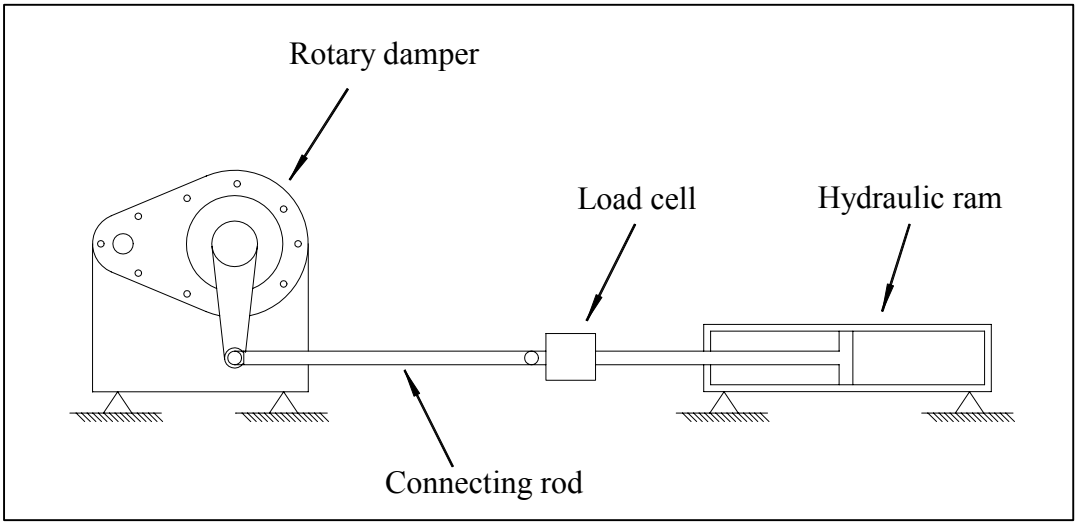

Fig. 11.0-1: Schematic drawing of the rotary damper test rig

Although the test rig arrangement allows a maximum displacement of ±0.4 radians and angular velocity of 4 rad/sec, due to flexibility of the test bed the limits were restricted to a maximum displacement of ±0.2 rads and maximum angular velocity of 1.0 rad/sec.

All tests where conducted by displacement controlled sinusoidal motion of the hydraulic ram. The hydraulic ram's position was measured by an internal Linear

Variable Displacement Transducer (LVDT) and the dampers angular displacement by a rotary potentiometer at its axis. A strain gauge load cell mounted on the hydraulic ram measured the force applied to the connecting rod. An accelerometer mounted on the hydraulic ram allowed for force correction due to the accelerating mass of the connecting rod. The four signals (linear ram displacement, angular rotary damper displacement, force and acceleration) were passed through a low pass filters and stored via an A-to-D interface board in computer memory. For drawings detailing test rig design, data acquisition and control see Appendix 7.

11.1 Data processing

11.1.1 Angular displacement measurement

A voltage proportional to angular displacement was produced by the rotary potentiometer mounted at the dampers axis. The voltage was multiplied by a calibration factor after storage in the computer.

11.1.2 Angular velocity measurement

To avoid differentiation of the potentiometer signal with respect to time, which would amplify noise, it was assumed that the angular displacement of the damper was sinusoidal. Angular displacement of the rotary damper is then described by:

$$\theta = \Theta.\sin(\phi) \qquad \textbf{Equation 11.1-1}$$

where θ is the dampers angular displacement, Θ is the dampers maximum angular displacement and φ is the angle of the drive signal (or angle of the hydraulic ram motion).

The angular velocity is then simply found from:

$$\dot{\theta} = \Theta.2\pi.f.\cos(\phi) \qquad \textbf{Equation 11.1-2}$$

The assumption that the dampers angular displacement is sinusoidal introduces a small error due to the connecting rod mechanism because it is the linear motion of the hydraulic ram that is displacement controlled, not the rotary motion of the damper. To demonstrate that this error is negligible the measured hydraulic ram and rotary damper displacements for the maximum amplitude (±0.2 rads) have been normalised and compared in Figure 11.1.2-1. Evidently the two motions are the same to a very small degree.

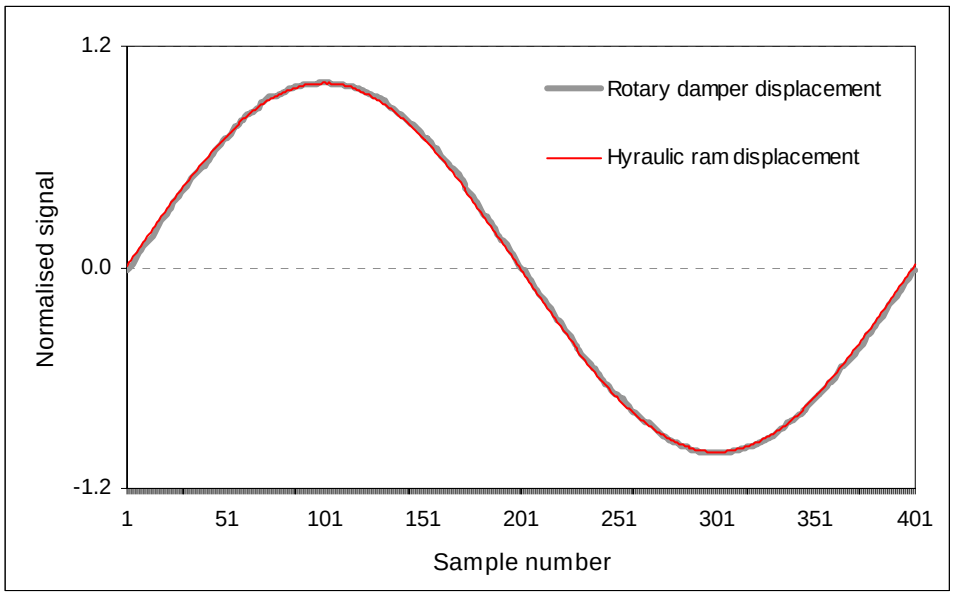

Fig. 11.1.2-1 *Comparison between normalised hydraulic ram and rotary damper motion*

11.1.3 Determining the torque at the damper

Torque applied to the damper is calculated by subtracting the force due to accelerating components from the measured load cell force then correcting for the angle between connecting rod and torque arm.

Referring to Figure 11.1.3-1: The mass of reciprocating components (load cell, pivot assembly and connecting rod) is 12 kg. Rotating inertia of the radius arm (which links connecting rod with damper) is 0.039 kg.m^2. Inertial force due to the rotation of the connecting rod is considered negligible because its angular displacement is small. Torque applied to the damper is then calculated as follows:

$$T = \left[F - \left(12.A.\omega^2.\sin(\omega.t)\right) - \left(\frac{I.\Theta}{r}.\omega^2.\sin(\omega.t) \right) \right] \times r \times \cos(\theta) \times \cos(\phi)$$

Equation 11.1.3-1

Where, 'T' is torque. 'F' is the force measured by the load cell. 'A' is the amplitude of the input linear displacement. $\omega = 2\pi f$ where 'f' is frequency of sinusoidal input. 'I' is the radius arm inertia; 'Θ' is amplitude of damper rotation. 'r' is radius arm length. 'θ' is radius arm angle and 'φ' is connecting rod angle.

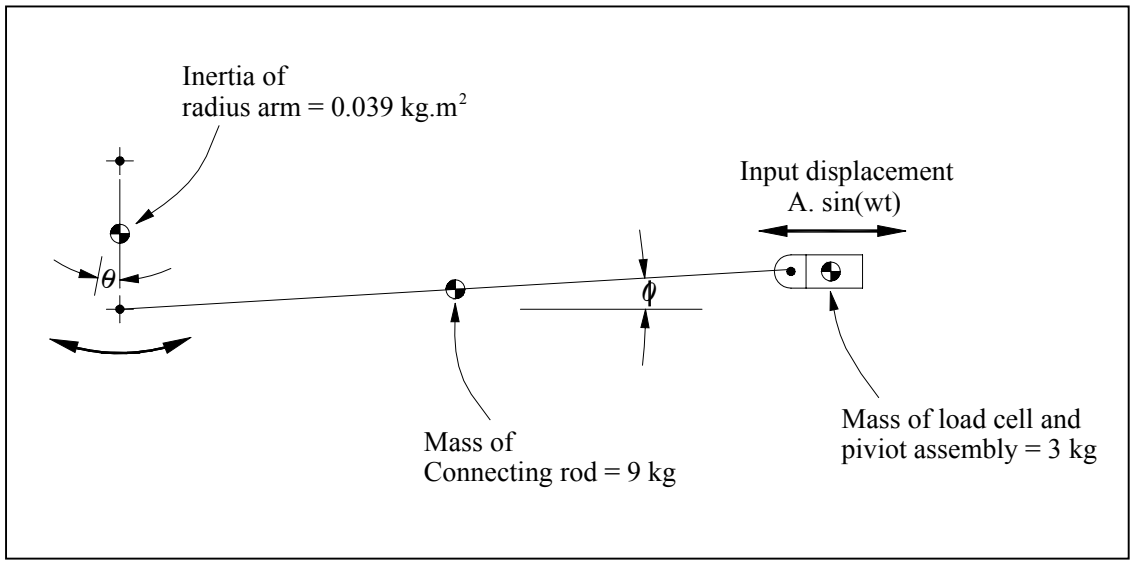

Fig. 11.1.3-1: *Schematic drawing of rotary damper test rig mechanism*

Because the connection rod is long, 'φ' is always small and cos 0 is 1, Equation 11.1.3-1 becomes:

$$T = \left[F - \left(12.A.\omega^2.\sin(\omega.t)\right) - \left(\frac{I.\Theta}{r}.\omega^2.\sin(\omega.t) \right) \right] \times r \times \cos(\theta)$$

Equation 11.1.3-2

The characteristic plot 'torque versus angular velocity' and the work diagram 'torque versus angular displacement' can then be produced.

11.2 Test settings

The following four test (A, B, C, & D) were carried out (Table 11.2-1). The amplitude of sinusoidal excitation remained constant; frequency was varied.

	Test A	Test B	Test C	Test D
Hydraulic ram amplitude (mm)	± 37.0	± 37.0	± 37.0	± 37.0
Rotary damper amplitude (radians)	± 0.21	± 0.21	± 0.21	± 0.21
Drive signal frequency (Hz)	0.75	0.5	0.25	0.1
Samples per cycle	400	400	400	400
Sample rate (Hz)	300	200	100	40
Low pass filter –3dB point (Hz)	100	50	25	10

Table 11.2-1: *Rotary damper test settings*

Chapter 12

Measured damper response and model development

12.0 Measured damper response

Figures 12.0-1 and 12.0-2 show the damper response to four sinusoidal displacement measurements of the same amplitude at 0.1Hz, 0.25Hz 0.5Hz and 0.75Hz. Higher frequency tests where not possible due to test rig structural limitations. Both Figure 12.0-1 and 12.0-2 show typical vehicle damper responses, however particular features are unique to this rotary damper.

Figure 12.0-1, referred to as the 'work diagram', shows energy dissipation increasing as frequency increases (as expected) but its asymmetric shape is evidence of non-linearity. A similar asymmetric work diagram shape is reported by Drum et. al. [36], who attribute this it to aeration where entrapped air in the oil chamber is compressed and expanded.

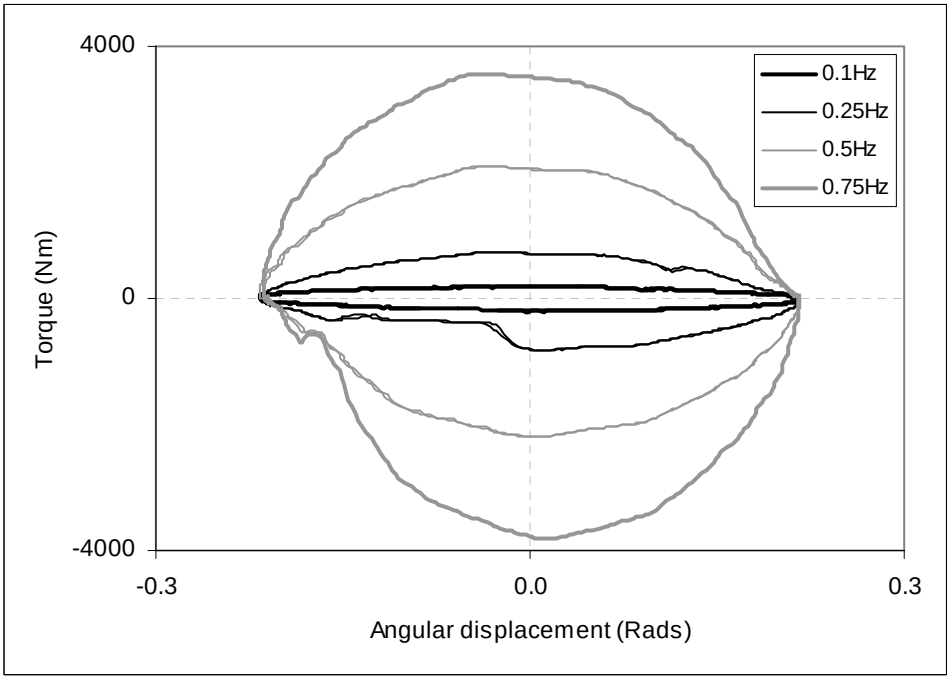

Fig. 12.0-1: *Torque versus angular displacement (Work diagram)*

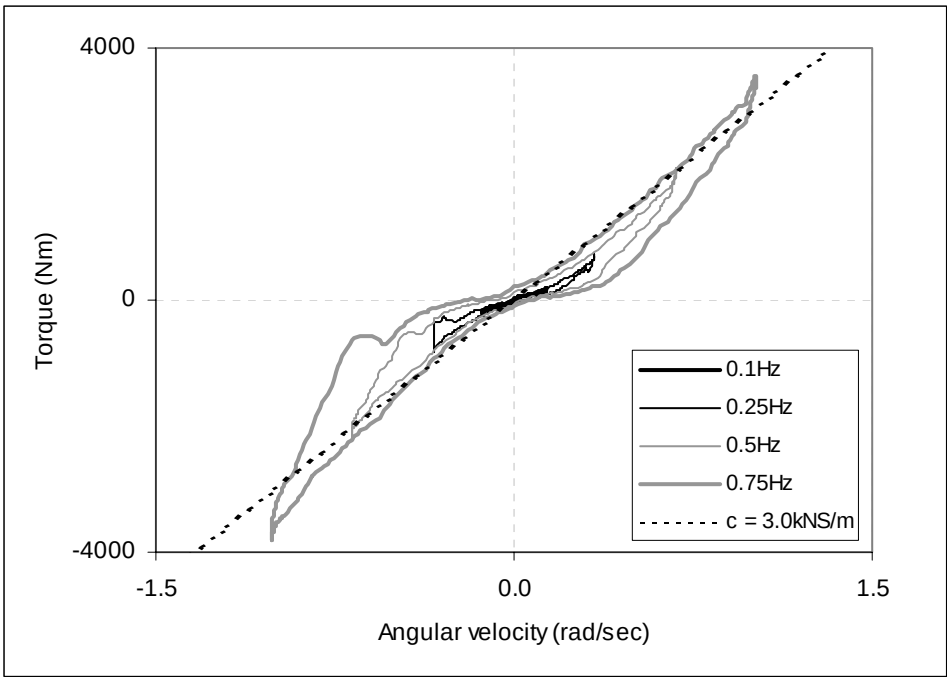

Fig. 12.0-2: *Torque versus angular velocity (Characteristic diagram)*

Figure 12.0-2, referred to as the 'characteristic diagram', is broadly typical of those reported for vehicle dampers showing hysteresis due to the compression of air, oil and compliance of the oil chamber (see Table 10.3-1). There is also a typical non-linear relationship between force and angular velocity, attributed to the turbulent flow relationship, $\Delta P \propto \dot{V}^{\alpha}$, where ΔP is pressure across the orifice, $\dot{V}$ is flow velocity and the power 'α' ranges from 1.7 to 2.0 [48]. Although these featured are common to all characteristic graphs, the degree to which the effect of each component is seen is unique to a given damper.

As a general observation it can said that except for a slight discrepancy in negative velocity where there is a discontinuity or 'step' at around 500 –1000Nm, damping force is the same in both forward and reverse velocity as expected for this design of damper. Also that the general slope of the torque versus angular velocity characteristic plot is approximately 3.0kNm/rad (indicated by the diagonal line in Fig. 12.0-2), laying within the specified design requirements shown in Figure 9.1-3.

The measurements presented in Figures 12.0-1 and 12.0-2 allows the examination of low velocity phenomena such as; friction, laminar to turbulent flow transition and the compression of entrapped gas. However, due to the test rigs structural limitations measurements presented here are taken at a relatively low torque (up to 4kNm). The designed pressure relief (blow-off) torque in compression is approximately 12kNm and in rebound 6kNm (see Fig. 9.1-3), so evidence of the relief valve beginning to open is not seen. The characteristics of the pressure relief value are therefore taken from Horstman Defence Systems Limited test data (Fig. 9.1-4).

12.1 Friction and laminar flow

Non-linearity due to friction and the laminar flow through orifice and passages is seen in the low frequency measurement (0.1Hz).

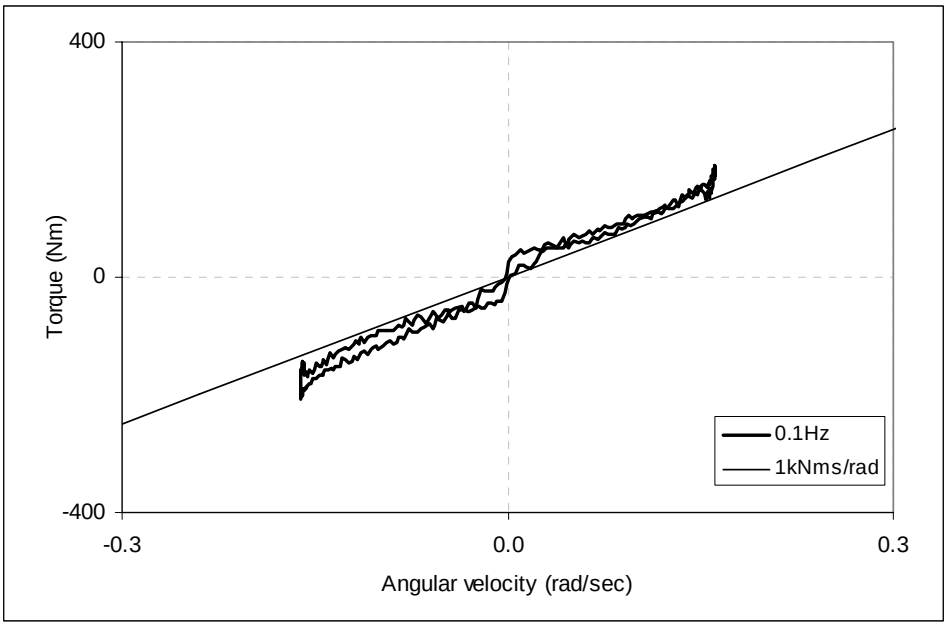

Fig. 12.1-1: *Torque versus angular velocity for the low frequency (0.1Hz) test*

Cole and Yung [32] demonstrated that the performance of a damper model at high frequencies (low amplitude) could be improved by changing the description of friction from a Coulombic model to one base on Berg's friction model [6]. This illustrates that the description of friction in a model improves its accuracy. However, the initial step at zero velocity in Figure 12.1-1 indicates that the friction force in this damper is less then 50Nm. This is small compared to the viscous force that the rotary damper generates, therefore for simplicity; a description of the friction force will be omitted from the dampers model.

This low value of friction is likely to be due to the dampers 'high quality' bearings, which also provide the main suspension support and are designed to withstand high off-axis loads.

We also see in Figure 12.1-1 that at low angular velocity the force-velocity relationship is linear. A straight line overlaying the plot shows that this relationship is approximately 1 kNms/rad. This laminar flow relationship at low velocity could explain the low energy dissipation at high frequency (low amplitude) reported by Holman [21].

12.2 Laminar to turbulent flow transition

The torque-velocity graph (Fig. 12.2-1) indicates three flow regimes: a low velocity region where flow is laminar, a transitional region and a region at high velocity where the flow is turbulent and the relationship non-linear.

We see in Figure 12.2-1 that laminar to turbulent flow transition occur at around 0.25 rad/sec where the response is unstable and begins to rise more steeply. However, laminar to turbulent transition is not modelled in any of the physical models listed in table 10.3-1. Yung & Cole [31] and Duym [34, 35] use the relationship $\Delta P \propto \dot{V}^{1.75}$ to

describe turbulence that is not ideal, other models describe turbulent flow simply using the squared relationship ($\Delta P \propto \dot{V}^2$) but in all cases this relationship begins at zero velocity.

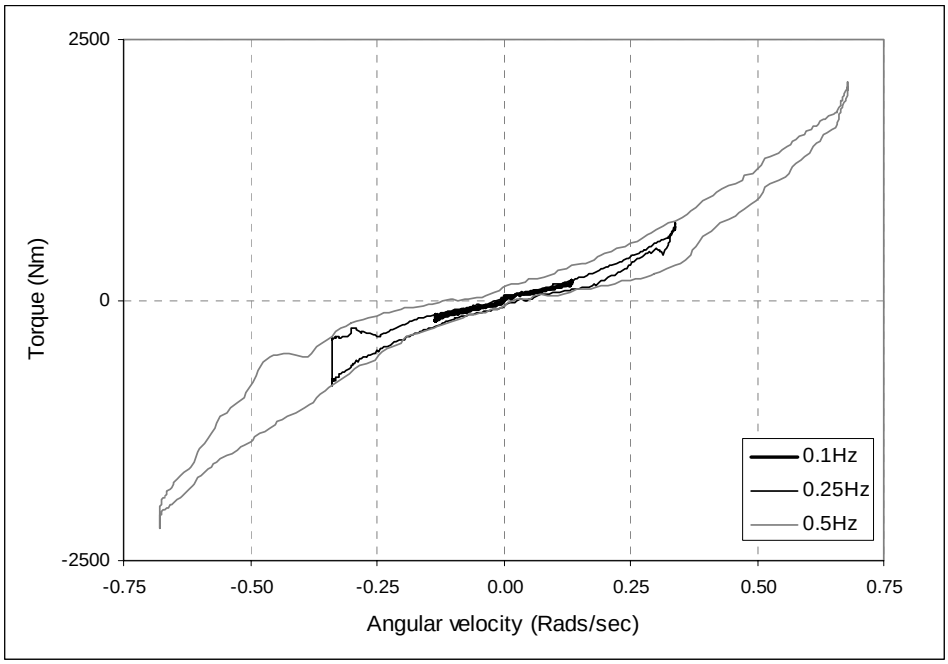

Fig. 12.2-1: Torque versus angular velocity (for frequencies up to 0.5Hz only)

It is proposed here that viscous force is modelled as laminar ($T = A.\omega$) up to 0.25 rad/sec, and above 0.25 rad/sec as turbulent ($T = B.\omega^{1.75} + C$), where '*T' is torque,* '*A*', B and 'C' are constants and 'ω' is angular velocity.

By fitting a straight line (Fig. 12.1-1) the constant '*A*' was found to be 1kNm and by fitting the equation for turbulence to the transition point (250Nm at 0.25 rad/sec) and the peak measured viscous force (3250Nm at 1rad/sec) The constants *B* and C are found. This is shown graphically in Figure 12.2-2.

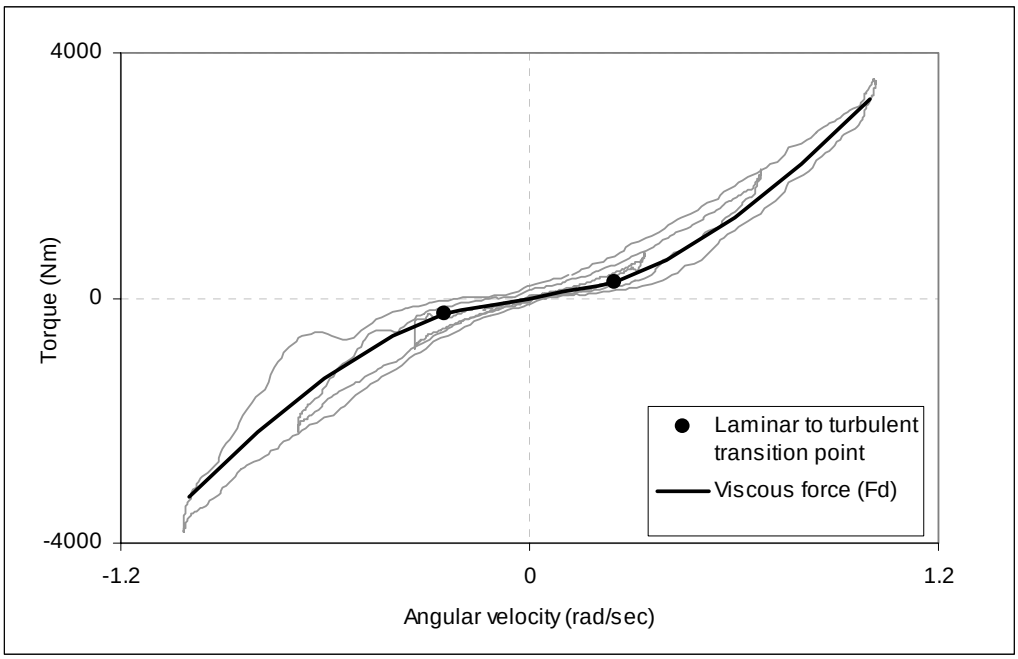

Fig. 12.2-2: *Laminar and turbulent flow regions of the viscous force*

12.3 Pressure relief valve characteristics (Blow-off)

Duym [34, 35] merges the transition between turbulent flow and opening of the pressure relief valve using a 'smoothing function'. Pressure relief valve blow-off is not seen in Figure 12.0-2 because the damper test rigs cannot generate the required torque. However, Horstman Defense Systems Limited has supplied test data showing the response of 49 damper units to constant velocity excitations. Figure 12.3-1 shows this Horstman data where curves have been drawn by hand through the upper and lower limits. The dampers viscous force is taken as the mean point through this plot, midway between the upper and lower limits. This line is merged with the measured viscous force (F_d) response (Fig. 12.2-2) assuming laminar flow up to 0.25 rad/sec and turbulent flow above this velocity up to where the turbulent response merges with the Hostman data.

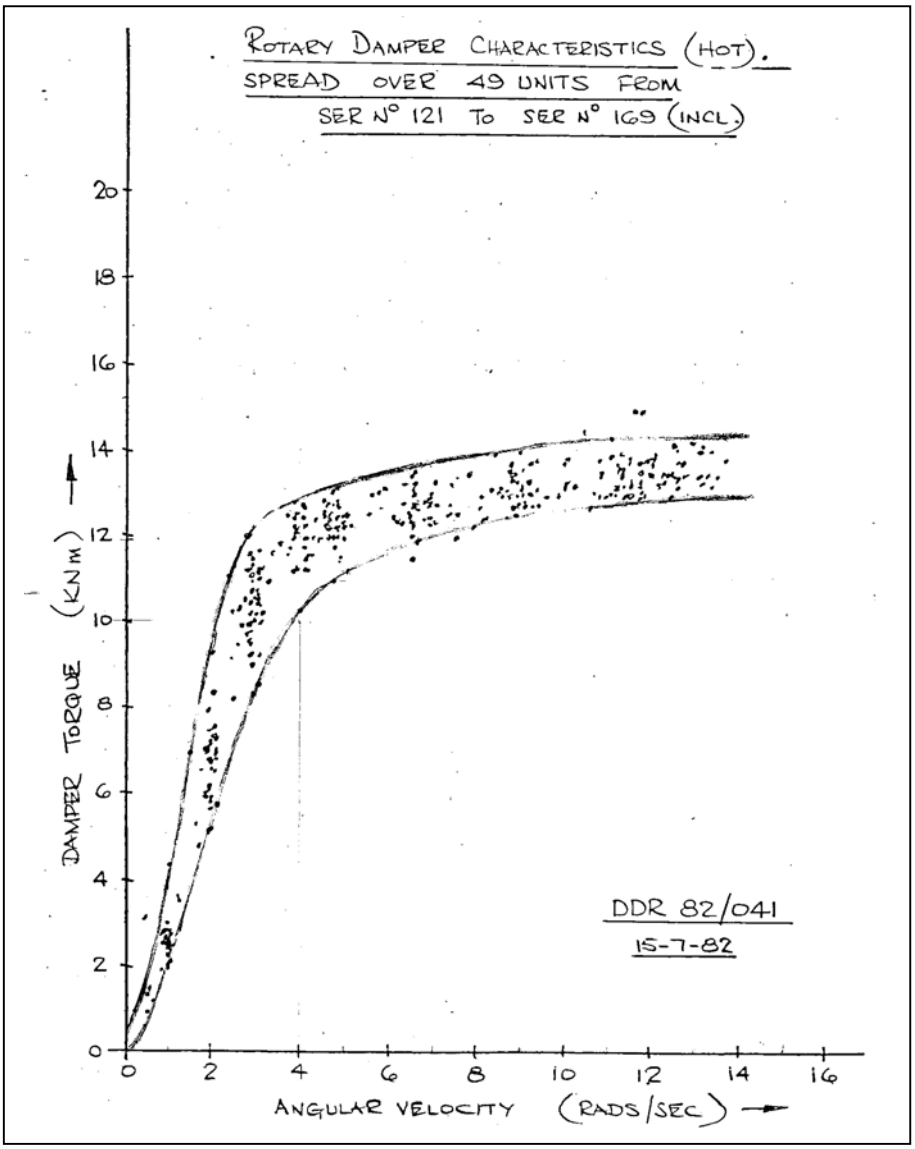

Fig. 12.3-*1 Data supplied by Horstman Defense Systems Ltd*

Equivalent data to Figure 12.3-1 for the pressure relief valve opening in rebound is not available from Horstman Defense Systems Limited. Therefore the data for compression is assumed to be representative and applied to rebound.

The complete force verses angular velocity viscous force showing, laminar, turbulent and pressure relief in both compression and rebound is presented in Figure 12.3-2. Also shown are the upper and lower design specification limits.

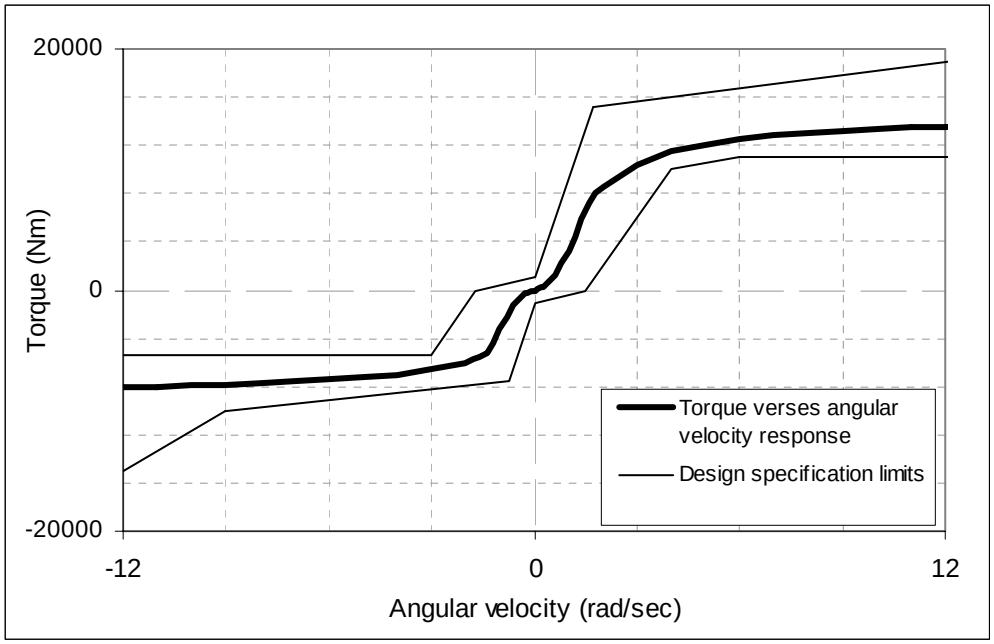

Fig. 12.3-2: *Rotary damper torque - angular velocity response without hysteresis*

12.4 Hysteresis due to entrapped air, oil compression and chamber compliance

The characteristic graph of torque versus velocity (fig. 12.0-2) shows significant hysteresis at 0.75Hz that could be caused by entrapped air, compression of oil or expansion of the oil chamber. However, the shape of the hysteresis loops indicates that it is predominantly due to the compression of air. The loop is 'broad' and 'rounded' at low velocity, becoming 'narrow' and 'pointed' at high velocity indicating non-linear compression; not the linearity expect for oil compression and chamber compliance. Oil compressibility and expansion of the chamber must make some contribution to this hysteresis but these effects will not be modelled independently a function is developed here which describes a range of compliance from isothermal compression of air to linear elastic compression of oil and chamber, depending on the value of its constants. Therefore these phenomena are 'lumped' together in the model, being described by a 'non-physical' function.

As described in Section 9.0, the Warriors rotary damper has a labyrinth of passageways connecting various chambers making the procedure for purging air from the system elaborate. We therefore might expect some entrapped air in the oil chamber. A model which includes the effect of entrapped air in the oil chamber, where Henry's law is applied, has been developed by Duym, et. al. [36]. Henry's law states that, '*The mass of gas that dissolves in a volume of liquid is directly proportional to the pressure'* and is described by the relationship:

$$P = \frac{H.m_{gs}}{V_{oil}} \qquad \textbf{Equation 12.4-1}$$

Where, 'P' is pressure, 'H' is Henry's constant, 'm_{gs}' is mass of gas dissolved in solution and 'V_{oil}' is volume of oil.

The application of Henry's law influences the understanding of the physical process active in the damper with the conclusion that compression and expansion of entrapped gas should be modelled as an isothermal process. This is illustrated in the schematic diagram, Fig. 12.4-1.

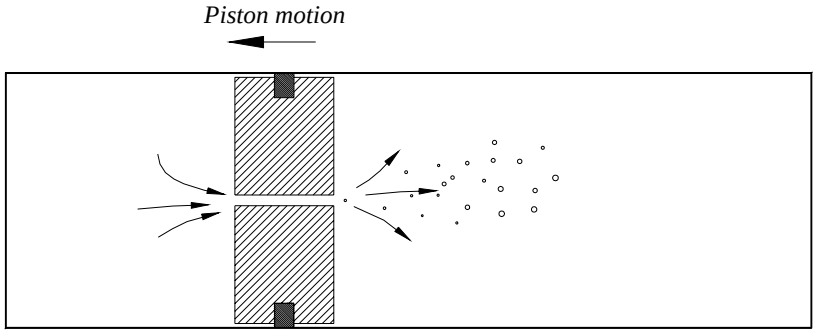

Fig. 12.4-1: *Schematic diagram illustrating the compression and expansion of entrapped gas*

Air on the compressed side of the piston dissolves in the oil under pressure and come out of solution on the low pressure side in the from of small bubbles. Duym, et. al. [36] showed that due to oil viscosity and low buoyancy the expected velocity that these bubbles rise due to gravity is approximately 0.001 m/s; Negligible relative to piston velocity. Because these bubbles are small and have insufficient time to collect and form a large volume of air, heat transfer to the oil is rapid and the process isothermal. Therefore from the ideal gas law ($P.V = mRT$) the following equation applies to the air bubbles either side of the piston:

$$\frac{P_0.V_0}{m_{gb0}} = \frac{P_1.V_1}{m_{gb1}} \qquad \textbf{Equation 12.4-2}$$

Where, P_0 is initial pressure, P_1 current pressure, V_0 initial volume, V_1 current volume, m_{gb0}, initial mass of gas bubble and m_{gb1}, current mass of gas bubble. It is shown in Appendix 5 that from Equations 12.4-1 and 12.4-2 force acting on the piston can be described by the following function:

$$F = C_1\left[\frac{1}{1+\frac{x_d}{C_2}} - \frac{1}{1-\frac{x_d}{C_2}}\right] \qquad \textbf{Equation 12.4-3}$$

Where, F is force acting on the piston, C_1 and C_2 are constants and x_d is change in gas volume.

It is possible to produce an almost linear relationship by setting the value of C_2 so that $C_2 >> x_d$. This would suit a model where the mass of entrapped air is small

12.5 Model implementation

The model has only two components. A non-linear viscous force described by laminar, turbulent and blow-off regions (Fig. 12.3-2) and compression of entrapped gas (described by Equation 12.4-3). Friction is negligible. The model is implemented as a non-linear spring and non-linear dashpot in ADAMS software as shown below in Figure 12.5-1

$$F_s = C_1\left[\frac{1}{1+\frac{x_d}{C_2}} - \frac{1}{1-\frac{x_d}{C_2}}\right]$$

F_d = *Splined response curve*

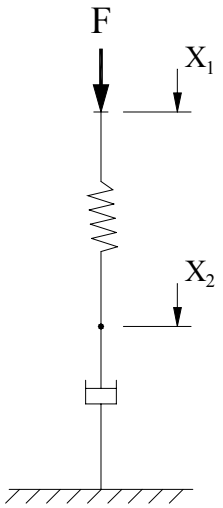

Where, F_s = Spring force, F_d = Dashpot force. C_1 and C_2 are constants and Gas compression, $x_d = X_1 - X_2$. The damper force-velocity response (F_d) is described by the splined curve presented in Appendix 6, Figure A6-1.

Fig. 12.5-1: *The rotary damper, modelled by a non-linear dashpot and non-linear spring in series*

Because the dampers torque-velocity characteristic (F_d) has three regions (laminar, turbulent and blow-off) it is convenient to describe the response using a 'splined' curve. The curve is fitted to data points rather then using three functions, one for each region. It is important for robust and trouble free implementation in Newton-Raphson Predictor-Corrector based simulation software that the curve is smooth at the transition between regions and this is more easily achieved using a splined curve.

Numerical values for the torque-velocity response are given in Appendix 6 and the smoothed splined response presented above in Figure A6-1.

12.6 Damper rotor inertia

The model requires a value of inertia for the dampers rotating mass. To find this value a damper was dismantled and the inertia of its rotating parts measured by means of 'bifilar suspension'. The damper rotor's inertia was found to be 0.118 $kg.m^2$.

Chapter 13

Comparison between measured and modelled rotary damper response

13.0 Introduction

The rotary damper model is presented in Figure 12.5-1.

$$F_s = C_1\left[\frac{1}{1+\frac{x_d}{C_2}} - \frac{1}{1-\frac{x_d}{C_2}}\right]$$

F_d = *Splined response curve*

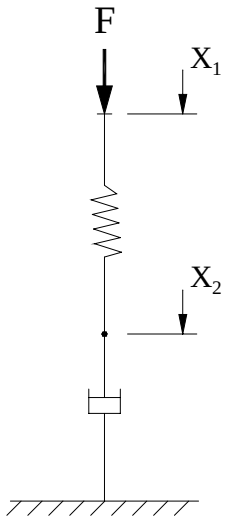

Where, F_s = Spring force, F_d = Dashpot force. C_1 and C_2 are constants and Gas compression, $x_d = X_1 - X_2$. The damper force-velocity response (F_d) is described by the splined curve presented in Appendix 6, Figure A6-1.

Fig. 12.5-1: *The rotary damper, modelled by a non-linear dashpot and non-linear spring in series*

The derivation of the viscous force (F_d) is described in Sections 12.1, 12.2, 12.3 and Appendix 6. Values for the constants C_1 and C_2 are found by trial and error, i.e. simulations are run repeatedly and the values adjusted manually to achieve 'best fit' by visual comparison. The values for C_1 and C_2 used for the results presented in Figures 13.1-1 and 13.1-2 are: $C_1 = 0.8 \times 10^6$ Nm, $C_2 = 0.03$ rads.

13.1 Measured and modelled results for the rotary damper

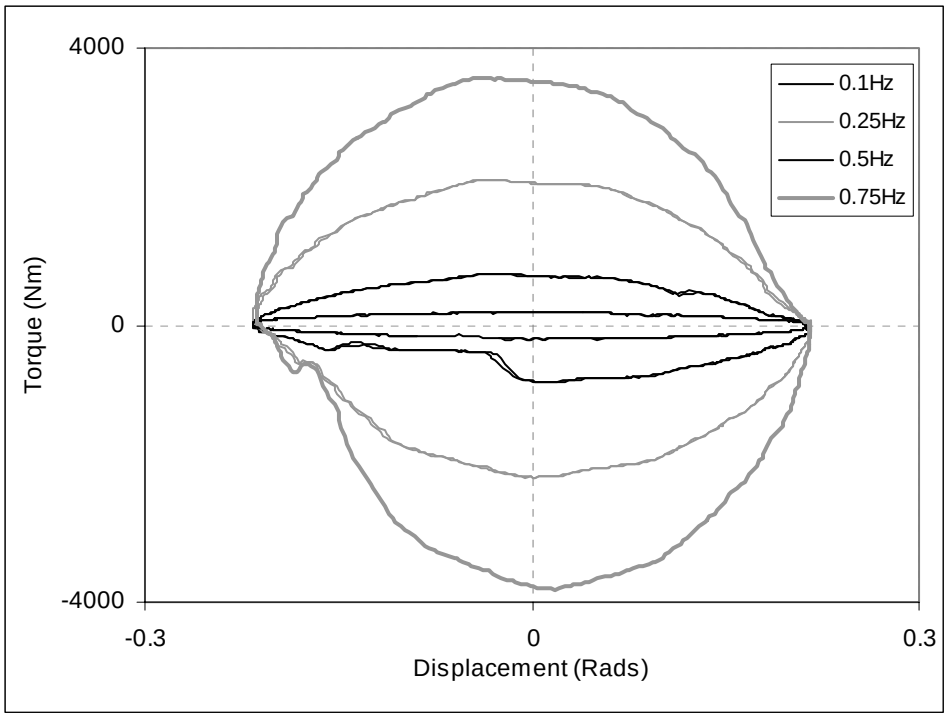

Fig. 12.0-1: *Measured torque versus angular displacement (Work diagram)*

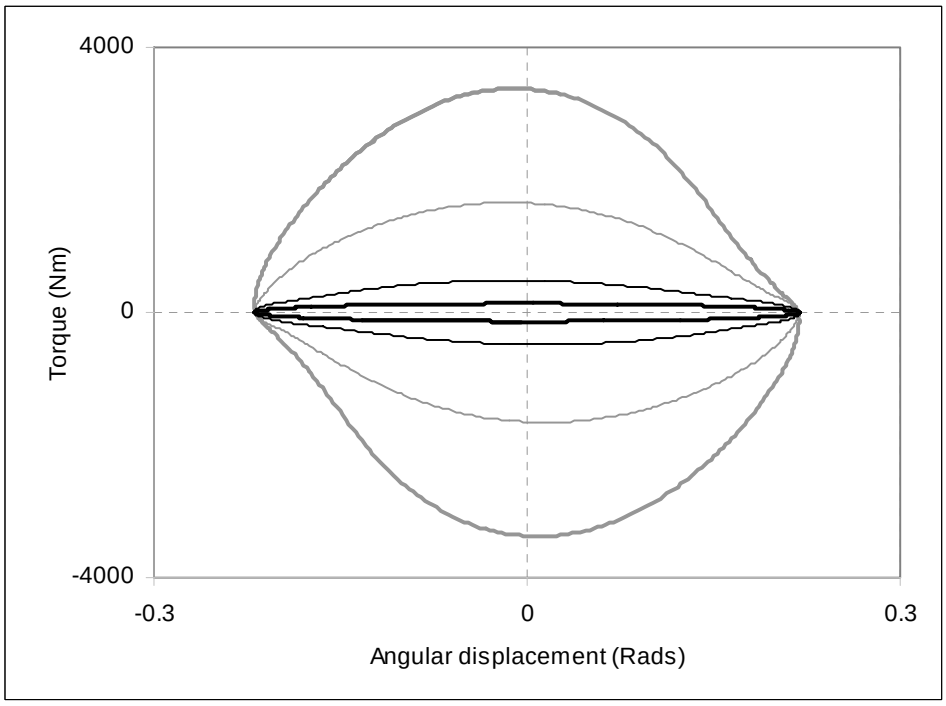

Fig. 13.1-1: *Modelled torque versus angular displacement (Work diagram)*

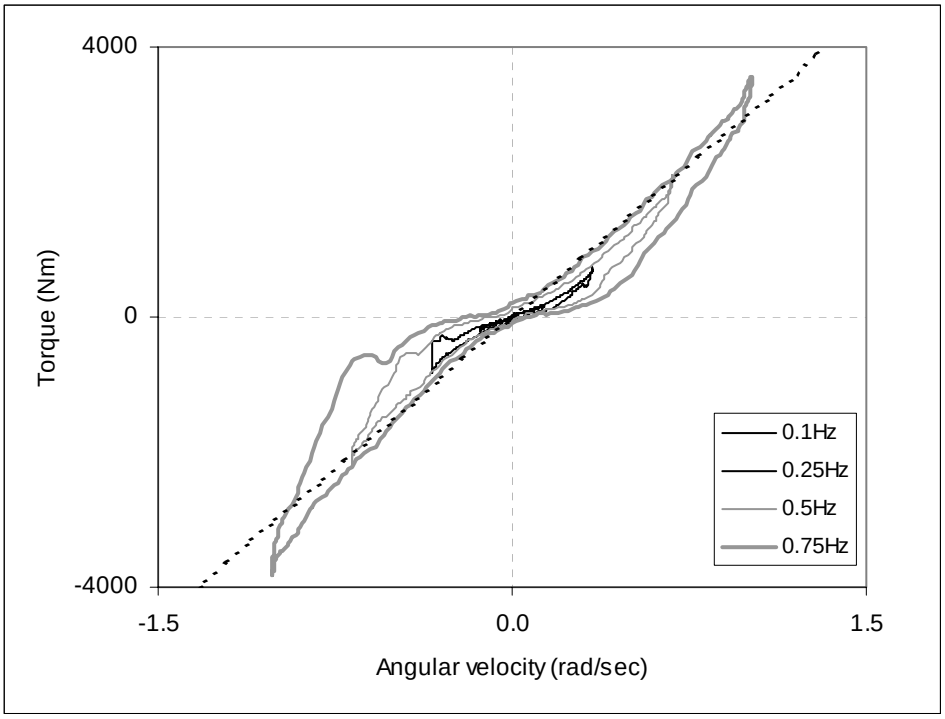

Fig. 12.0-2: *Measured torque versus angular velocity (Characteristic diagram)*

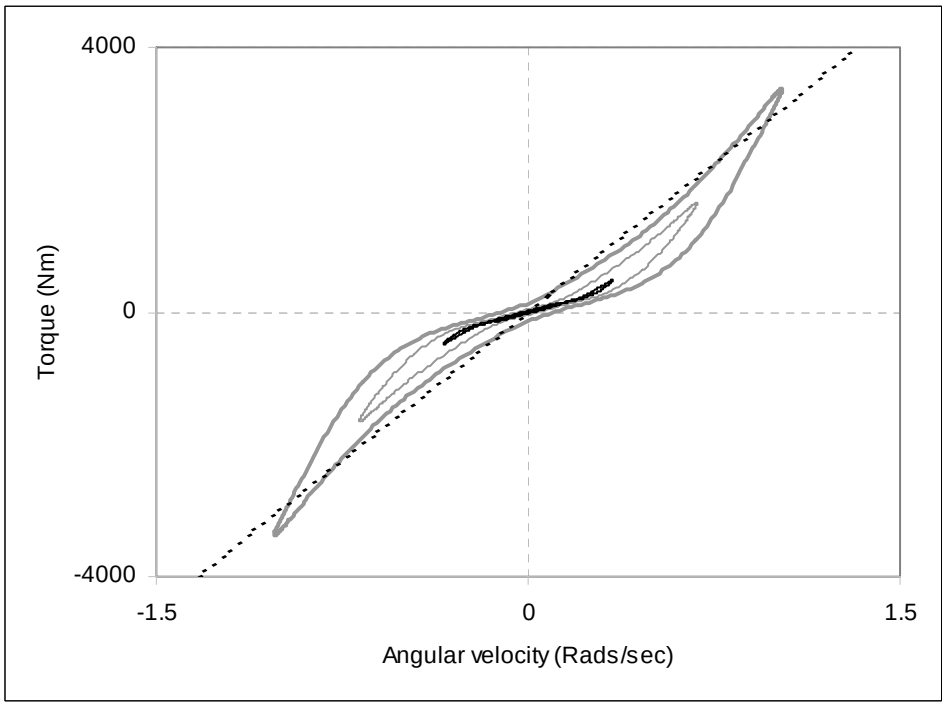

Fig. 13.1-2: *Modelled torque versus angular velocity (Characteristic diagram)*

13.2 Predicted response at high velocity

It is interesting to predict the dampers response to high frequency sinusoidal displacements that are beyond the limits of the test rig to measure. Also, the rapid changes in force and direction will test the models computational robustness for use in full vehicle simulations. The results are presented below in Figures 13.2-1 and 13.2-2.

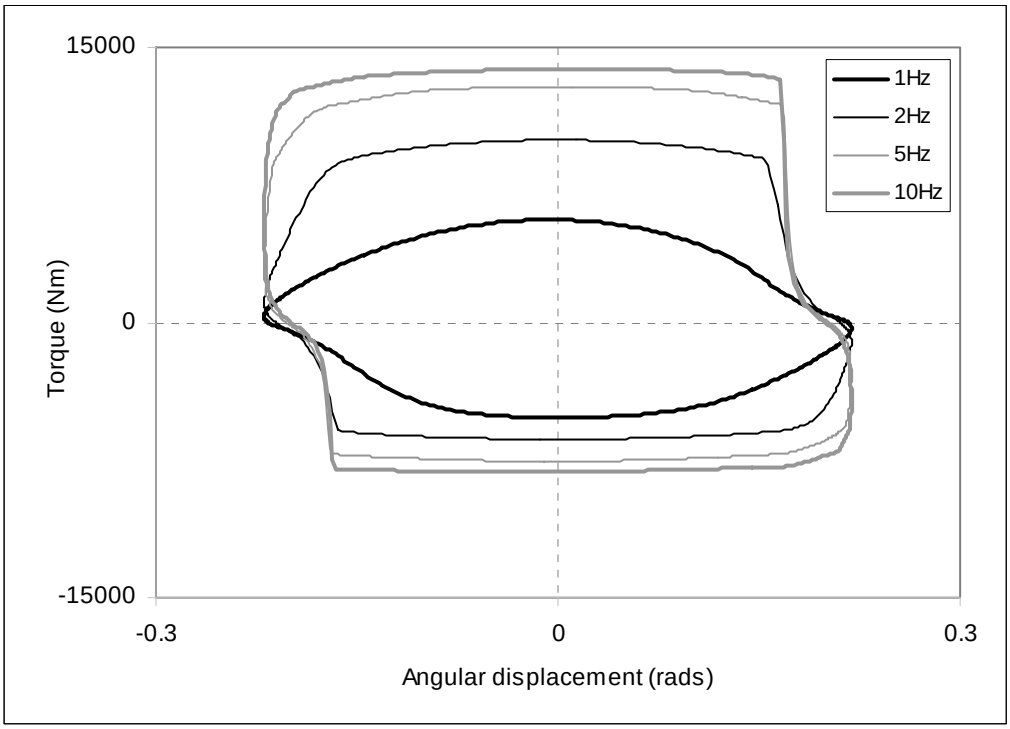

Fig. 13.2-1: *Modelled torque versus angular displacement in response to high frequency sinusoidal motion*

Figure 13.2-1 shows that the predicted response to high frequency sinusoidal motion is a rapid increase and decrease in torque to the limiting pressure relief valve settings. This would probably be found to be incorrect if the damper where tested at these high-frequency settings because flow through the pressure relief valve would become non-linear (turbulent) and damping force would increase. However, most importantly the simulation runs 'trouble free' without computational failure.

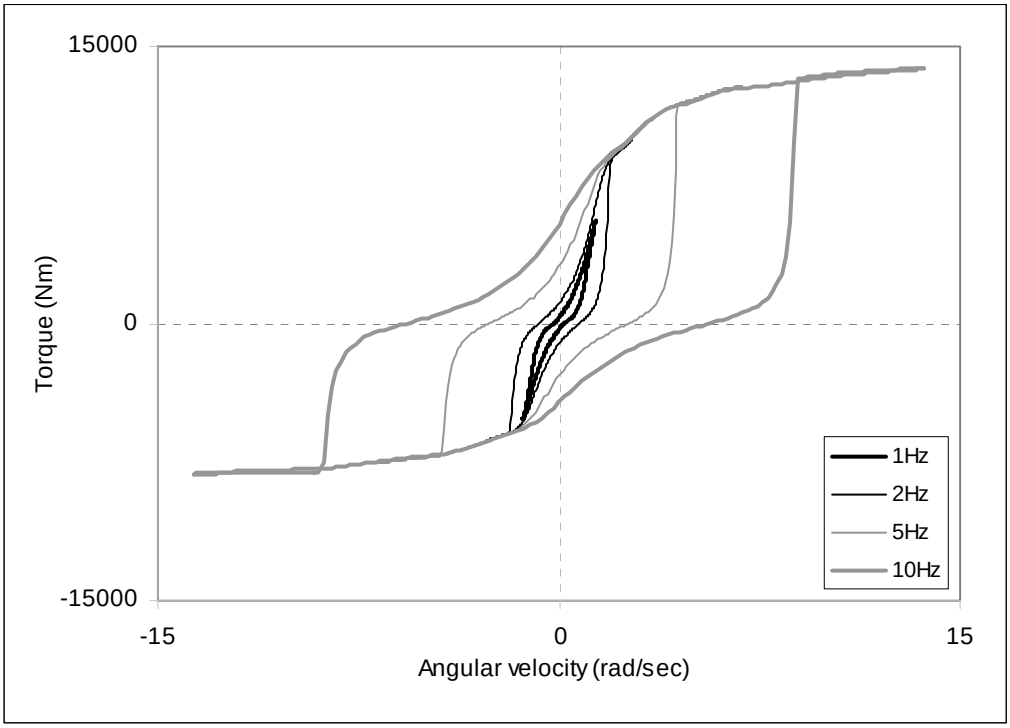

Fig. 13.2-2: *Modelled torque versus angular velocity in response to sinusoidal motion*

Figure 13.2-2 shows the predicted response to high frequency sinusoidal motion generating a high degree of hysteresis due to air compression.

Chapter 14

Rotary damper: Conclusion and Further work

14.0 Conclusion and further work

The modelled response presented above in Figure 13.1-1 and 13.1-2 shows that the main damper characteristics (non-linear force-velocity response and non-linear compliance) are described. The same trends are seen in both the modelled and measured data but in detail there are some differences between the plots. Possible causes of these differences are as follows:

1. For simplicity laminar to turbulent transition has been modelled as instantaneous and occurring at the same value when velocity is increasing and when decreasing. This is not 'realistic'. It is known that the transition from laminar to turbulent flow is not instantaneous and occurs at a higher velocity when moving from a laminar flow regime to a turbulent flow regime then in the reverse direction [37, 38] but modelling this behaviour would be complex and would introduce many more parameters for little improvement in the models accuracy.

2. Torque due to friction is less then 50Nm (see Section 12.1) and for simplicity has not been included in the model. If this effect where modelled correlation between measured and modelled response would improve.

3. It is possible that the restriction to flow presented by the pressure relief valve and the seals, is not constant with pressure. The 'step' we see in the measured response in one direction only between 500Nm and 1000Nm may be caused by

reverse flow through pressure relief valves and/or seals, which has a step change as chamber pressure increases.

In conclusion the model developed here represents the measured response to a close degree using only a simple splined curve and an isothermal description of entrapped air. An important objective was to produce a simple and robust model that could represent the rotary damper in a full vehicle simulation and includes nonlinearities, which reproduce the low damping at high frequency (low amplitude) reported by Holman [21]. These objectives have been achieved.

Further work

Areas for further work that would improve the damper model developed here are:

1. Strengthening the test rig for measurements at high force. It could then be determine whether the predicted response presented in Figs.13.2-1 and 13.2-2 is accurate.
2. It is known that damper model accuracy at high frequency and low amplitude can depend upon the description of friction [31, 32]. Further work in this area may be required for use in vehicle vibration models that operate up to 30Hz.
3. Investigate the effect of temperature on the dampers response and how the model developed here could describe this behaviour. For simplicity temperature effects were not studied in this work; all measurements were made at room temperature (approx. 20°C).
4. The damper model should be applied in a full vehicle simulation and the results assessed by comparison with measured data.

Chapter 15

Conclusion and further work

15.0 Overview

The objective set out at the beginning of this report was to develop models for Warrior Armoured Personnel Carrier running gear components for use in multibody dynamic simulations of the full vehicle. This objective has been achieved for three components. In Chapters 3-8 models for two Carbon Black Filled Natural Rubber (CBFNR) track components were developed. These were the Track Link Bush and the Road Wheel Tyre. In Chapters 9-14 a model for the Warrior's suspension rotary damper was developed. These models are shown to be computationally robust and compatible with software that uses the Newton-Raphson Predictor Corrector method.

For simplicity the models have been developed with a minimum number of parameters and it is shown that their response is adequate for vehicle simulations in the first instance where the development of a full vehicle model is at an early stage. The models have been implemented using ADAMS software and the results show good correlation with measured response but they are phenomenological in nature. That is: they reproduce the response that has been measured. They are not guaranteed to describe the response to force and displacement inputs at amplitudes and frequencies that have not been measured.

15.1 Rubber component models

The model developed for CBFNR in this work describes dynamic response at the component level. There has been no attempt to describe the materials microstructure, its micro-mechanical behaviour or develop constitutive equations. The measured

response is simply reproduced by combining three functions; an elastic force description, a viscoelastic force description and a geometric multiplier.

A novel method has been developed for measuring the CBFNR components elastic response and determining a geometric multiplier for its viscoelastic response where the component is exercised by small amplitude sinusoidal motion at varying preloads. The assumption being; that by applying a preload, then exercising the component first at large amplitude, then steadily reducing to a small amplitude; the hysteretic response becomes steady about its mean point and that this point lies on the elastic force line. The elastic force is then taken as a polynomial fit to successive measurements at varying preload and by subtracting the elastic force from the total response a viscoelastic multiplying function is determined from the change in amplitude of hysteresis loops at varying preloads.

The models viscoelastic description is based on a nonlinear Maxwell element used by Haupt and Sedlan [19]. This element is used primarily because values of force and displacement at turning points do not need to be stored (as in some other methods [6, 7, 8]) and is therefore suitable for use in dynamic simulation software that uses the Newton-Raphson Predictor Corrector method. But the element also naturally reproduces the fundamental features of CBFNR. These are an asymmetric hysteresis loop shape, a predominately frequency independent response and stress relaxation.

The model developed here for CBFNR components is a compromise though; it does not describe ‘strain history dependent viscosity’, which Haupt and Sedlan [19] and Haupt and Lion [20] include in their models. A ‘nested’ stiffening element has been added to better describe the materials response to dual-sine motion and stress relaxation but an attempt to describe strain history dependent viscosity has not been made for the sake of simplicity. The final CBFNR model has also been rationalised so

that many of the coefficient values and time constants are the same in both the Track Link Bush and Road Wheel Tyre models. This has reduced the number of parameter values required in each case to just four.

15.2 Suspension damper model

The Warrior APC rotary suspension damper model developed in this work shows good correlation with the measured response. The dampers main characteristics are a nonlinear torque-velocity response and nonlinear compliance that is predominately due to entrapped air in the oil chamber.

The viscous force developed by the flow of oil through orifices and past seals is described by a continuous torque-velocity curve that represents regions of, laminar flow, turbulent flow and pressure relief. Compliance due to entrapped air in the oil chamber is described by applying Henry's Law, the Ideal Gas Law and assuming isothermal compression and expansion. Coefficients for this description have been 'lumped' together where possible to produce a simple non-parametric function that has only two unknown constants and is therefore easily matched to measured data.

The damper model developed here is simple and computationally robust fulfilling its requirements as a component in full vehicle simulations.

15.3 Further work

Areas for further work on CBFNR component models are as follows:

1. Validate the novel measuring technique developed in this work, which determines the elastic force component, the viscoelastic force component and a geometric multiplier. Where the elastic force component is taken as a line drawn through the centre of small amplitude hysteresis loops at varying preloads.

2. Introduce ‘strain history dependent parameters’ such as strain-rate dependence similar to that used by Haupt and Sedlan [19] and Haupt and Lion [20].

3. Develop a three dimensional constitutive material model based on the elastic, viscoelastic and geometric descriptions presented in this work.

4. Determine whether a rolling Road Wheel model is required and if so develop one.

5. Investigate the effect of temperature on the dynamic response of CBFNR and how the model developed here could describe this behaviour. For simplicity temperature effects were not studied in this work, all measurements were made at room temperature (approx. 20°C).

6. Further work is required to determine whether the model developed here for describing CBFNR components in simulation software that uses the Newton-Raphson Predictor-Corrector algorithm has wider applications. Answering such questions as: Is the model suitable for use in other types of simulation software? And, does the model describe the internal damping of other materials?

7. An important area of study for further work is the CBFNR response to transient vibration. This has not been explored in depth in this study; only a few measurements of the rubber component’s response to a stepped displacement where made. This is an area where further work is required to developed the model and understand the materials behaviour.

8. The CBFNR component models developed here should be applied in a full vehicle simulation and the results assessed by comparison with measured data to determine whether the use of these models improves the accuracy of the full vehicle simulation.

Areas for further work on the Warrior suspension rotary damper are as follows:

1. The test rig should be strengthened so that measurements can be made at higher frequency and higher amplitude to further validate the damper model.

2. Friction is not described in the model because it is considered negligible but this is a possible area for further work if in the future the transmission of high-frequency low-amplitude force from ground to hull via the damper is considered significant for full vehicle simulations of the full Warrior APC. (see papers by Yung and Cole [31,32]).

3. Investigate the effect of temperature on the dampers response and how the model developed here could describe this behaviour. For simplicity temperature effects were not studied in this work, all measurements were made at room temperature (approx. 20°C).

4. As for the rubber model; the damper model should be applied in a full vehicle simulation and the results assessed by comparison with measured data.

References

[1] Robertson, B. 'Vibration of Tank Tracks' PhD Thesis, University of Newcastle upon Tyne, 1980

[2] Boast, D. and Fellows, S., Hale "Effects of temperature, frequency and amplitude on the dynamic properties of elastomers". AVON Automotive 24/09/2002 issue 03, Private communication.

[3] Lee, H. C., Choi, H. J. and Shabana, A.A., "Spatial Dynamics of Multibody Tracked Vehicles Part II: Contact Forces and Simulation Results". Vehicle Sys. Dynamics, 29 (1998), pp.113-137.

[4] Ma, Z. and Perkins, N. C., "Modeling of track-wheel-terrain interaction for dynamic simulation of tracked vehicles: Numerical implementation and further results" Proc. of DETC'01, ASME 2001 Design Eng. Tech. Conference. Pitts, PA, Sept. 9-12, 2001. DETC2001/VIB-21310

[5] Ryu, H. S, Huh, K. S., Bae, D. S., Choi, J. H. "Development of a Multibody Dynamic Simulation Tool for Tracked Vehicles (Part 1, Efficient Contact and Nonlinear Dynamic Modeling" JSME Int. J., Series C, Vol. 46, No.2, 2003.

[6] Berg, M., "A non-linear rubber spring model for rail vehicle dynamics analysis" Vehicle system dynamics, 30 (1998), pp.197-212

[7] Turner, D. M., "A triboelastic model for the mechanical behaviour of rubber" Plastics and rubber processing and applications 9, p197-201, 1988

[8] Coveney, V. A., Johnson, D. E., Turner, D. M., "A triboelastic model for the cyclic mechanical behaviour of filled vulcanizates" Rubber Chemistry and technology; 68, 1995, p660-670

[9] Coveney, V. A., Johnson, D. E., "Rate-dependent modelling of a highly filled vucanizate" Rubber Chemistry and technology; 73, 4; p565-577; Sep/Oct 2000

[10] Coveney, V. A., et. al. "Modelling the behaviour of an earthquake based-isolated building" Finite element analysis of elastomers, Ed. by D. Boast & VA Coveney, Prof. Eng. Pub.

[11] Coveney, V. A., "The role of natural rubber in seismic isolation – A perspective" Kautschuk und Gummi. Kunstsoffe 44. Jahrgang, Nr. 9/91.

[12] Coveney, V. A., Johnson, D. E., "Modeling of carbon black filled natural rubber vulcanizates by the standard triboelastic solid" Rubber Chemistry and technology; 72, 4; p673-583; Sep/Oct 1999

[13] Bergstrom, J. S., Boyce, M. C., "Large strain time-dependent behavior of filled elastomers" Mechanics of materials 32 (2000) 627-644

[14] Bergstrom, J. S., Boyce, M. C., “Constitutive modelling of ht large strain time-dependent behaviour of elastomers” J.Mech. Phys. Solids, Vol. 46, No.5, pp 931-954, 1998

[15] Arruda, E. M., Boyce, M. C., “A three dimensional constitutive model for the large stretch behaviour of rubber elastic materials.” J.Mech. Phys. Solids, 41 (2), 389-412.

[16] Miehe, C., Keck, J., “Superimposed finite elastic-viscoelastic-plastoelastic stress response with damage in filled rubbery polymers”. Experiments, modelling and algorithmic implementation” Journal of Mechanics and physics of solids, 48 (2000) 323-365

[17] Lion, A., “Phenomenological modelling of carbon black-filled rubber in continuum mechanics” KGK Kautschuk Gummi. Kunstoffe 57. Jahrgang, Nr. 4/2004

[18] Lion, A., “A constitutive model for carbon black filled rubber: Experimental investigation and mathematical representation” Continuum Mech. Thermodyn. 8 (1996) 153-169

[19] Haupt, P., Sedlan, K., “Viscoplasticity of elastomeric materials: experimental facts and constitutive modelling”
Archive of Applied Mechanics 71 (2001) 89-109

[20] Haupt, P. and Lion, A., “On the viscoelasticity of incompressible isotropic materials” Acta Mechanica 159, 87-124 (2002)

[21] Holman, T. J., “Rotary hydraulic suspension for high mobility off-road vehicles” Int. Soc. for Terrain Vehicle Systems 8th International Conference: The Performance of OFF-Road Vehicles and machines. p1065-1075, 1984.

[22] Hall, B. B., and Gill, K. F., “Performance of a telescopic duel-tube automotive damper and implications for ride prediction” Proc. Instn. Mech. Engrs. Vol 200 No.D2 (1986).

[23] Karadayi, R. and Masada, G. Y., “A nonlinear shock absorber model”
Proceedings of ASME Symposium on Simulation & Control of Ground Vehicles & transportation Systems, AMD-Vol. 80, DSC-Vol. 2, Dec 7-12, 1986.

[24] Hagedorn, P. & Wallaschek, J. “On equivilent harmonic and stochastic linearization for nonlinear shock-absorbers” Proceedings of Nonlinear stochastic Dynamic Engineering Systems IUTAM Symposium, Innsbruk/Igls, Austria, 21-26 June 1987.

[25] Wallaschek, J., “Dynamics of non-linear automobile shock-absorbers” Int. J. Non-linear Mechanics, Vol25, No. 2/3, pp. 299-308. 1990.

[26] Surace, C., Worden, K. and Tomlinson, G. R., “An improved nonlinear model for an automotive shock absorber” Nonlinear Dynamics 3: 413-429, 1992.

[27] Kwangjin Lee, “Numerical modelling for the hydraulic performance prediction of automotive momotube dampers” Vehicle System Dynamics Supplement 28 (1997), pp.25-39

[28] Mostofi, A., “The incorporation of damping in lumped-parameter modelling techniques” Proc. Inst. Mech. Engrs. Vol. 213, Part K, (1999), pp.11-17

[29] Rao, M. D., Gruenberg, S., Torab, H., Griffiths, D., “Vibration testing and dynamic modelling of automotive shock absorbers” (2000) Int. Soc. Optical Eng. Vol 3989, (2000), pp.423-429.

[30] Purdy, D. J., “Theoretical and experimental investigation into an adjustable automotive damper” Proc Instn Mech Engrs Vol 214 Part D (2000), pp.265-283.

[31] Yung, V. Y. B. and Cole, D. J., “Analysis of High Frequency Forces Generated by Hydraulic Automotive Dampers” Vehicle System Dynamics Supplement 37 (2002), pp.441-452

[32] Yung, V. Y. B. and Cole, D. J., “Mechanisms of high-frequency force generation in hydraulic automotive dampers” Vehicle System Dynamics Supplement 41 (2004), pp.617-626

[33] Duym, S., Stiens, R. and Reybrouck, K., “Evaluation of shock absorber models” Vehicle System Dynamics, 27 (1997) pp. 109-127.

[34] Duym, S., and Reybrouck, K., “Physical characterization of nonlinear shock absorber dymamics” European Journal Mech. Eng., Vol.43, No.4 (1998) pp 181-188.

[35] Duym, S., “Simulation tools, modelling and identification, for an automotuive absorber in the context of vehicle dynamics” Vehicle System Dynamics, 33 (2000), pp.261-285.

[36] Duym, S, Stiens, R. Baron, G. and Reyybrouck, K. “Physical modelling of the hysteretic behaviour of automotive shock absorbers” SAE Transactions – Journal of Passenger cars, SAE paper 970101, 1997.

[37] Eastop, T. D and McConkey, A., “Applied Thermodynamics for Engineering Technologists”, 4th Ed., ISBN 0-582-30535-7, Pub Longman Scentific & Technical.

[38] Scholar, C. and Perkins, N. C., “Longitudinal Vibration of Elastic Vehicle Track Systems”, SAE paper No. 971090, (1997).

[39] Assanis, D. N., Bryzik, W., et. al., " Modeling and Simulation of an M1 Abrams Tank with Advanced Track Dynamics and Integrated Virtual Diesel Engine", Mechanics of Structures and Machines, Vol.27, No.4, pp.453-505, (1999).

[40] RYU, H. S, Bae, D. S., Choi, J. H., and Shanana, A. A., "A compliant track link model for high-speed, high-mobility tracked vehicles", Int. J. Numer.

[41] Slattengren, J., "Utilization of ADAMS to Predict Tracked Vehicle Performance", SEA Paper 2000-01-0303.

[42] Negrut, D, Harris, B, " ADAMS Theory in a Nutshell for class ME543" Dept. of Mech. Eng., Univ. of Michigan, Ann Arbor, March 22, 2001.

[43] MSC.ADAMS 2003, "ADM 703 Training Guide, Advanced ADAMS/Solver, ADAMS Theory".

[44] Gear, C. W, "Simultaneous Numerical Solution of Differential – Algebraic Equations", IEEE transactions on circuit theory, Jan 1971.

[45] Ferry, J. D., "Viscoelastic Properties of Polymers" 3rd Ed. Pub: John wiley & Sons, ISBN 0-471-04894-1, Page430, Fig. 14-17.

[46] Ward, I. M. and Hadley, D. W., "An Introduction to the Mechanical Properties of Polymers", Pub: Wiley, ISBN:0-471-93887-4, Page 30.

[47] Ward, I. M. and Hadley, D. W., "An Introduction to the Mechanical Properties of Polymers", Pub: Wiley, ISBN:0-471-93887-4, Pages 27, 28, 309, 310 and 311.

[48] Massey, " Mechanics of Fluids" 2nd Ed. Page131, Fig 5.6, Pub Van Nostrand Reinhold, ISBN: 0 442 05176Meth. Engng 2000; **48**: 1481-1502

[49] Ewins, D. J. " Modal Testing, theory, practice and application", 2nd Ed., Pub. Research Studies Press, ISBN 0-86380-218-4

[50] Worden, K. and Tomlinson, G. R. " Nonlinearity in Structural Dynamics. Detection, Identification and Modelling" , Pub. Institute of Physics Publishing, ISBN 0-7503 –0356-5

[51] Cartwright, M. "Fourier methods for mathematicians, scientists and engineers", Pub. Ellis Horwood, 1990, ISBN 0-1332 –7016-5

Appendix 1: Time independent force-displacement relationship for the Haupt and Sedlan viscoelastic element

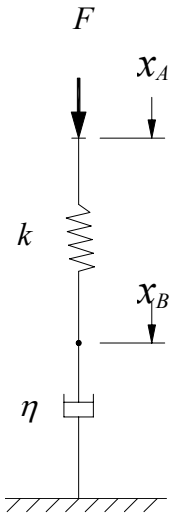

Fig. A1-1 *The viscoelastic Sedlan and Haupt element*

The Sedlan and Haupt viscoelastic element [19] is a modified Maxwell element where the dashpot viscosity coefficient 'η' is a function of x_A as follows:

$$\eta = \frac{c}{|\dot{x}_A| + \xi} \tag{A1.1}$$

Where; 'F' is force applied to the viscoelastic element, 'c' is maximum possible damping force, 'ξ' is a constant, x_A is displacement across the viscoelastic element (i.e. relative to ground) and x_B is displacement across the dashpot. So that:

$$F = \frac{c\dot{x}_B}{|\dot{x}_A| + \xi} \tag{A1.2}$$

$$F = kx_A - kx_B \tag{A1.3}$$

And $$\frac{dF}{dt} = k\dot{x}_A - k\dot{x}_B \tag{A1.4}$$

Rearranging (A1.4) $$\dot{x}_B = \dot{x}_A - \frac{1}{k}\frac{dF}{dt} \tag{A1.5}$$

Substituting (A1.5) into (A1.2)

$$F = \left(\frac{c.\dot{x}_A}{|\dot{x}_A| + \xi}\right) - \left(\frac{c}{k}\right)\left(\frac{1}{|\dot{x}_A| + \xi}\right)\frac{dF}{dt} \tag{A1.6}$$

Dividing the numerator and denominator of the right hand side by $\dot{x}_A$:

$$F = \left(\frac{c}{\text{sgn}(\dot{x}_A) + \frac{\xi}{\dot{x}_A}}\right) - \left(\frac{c}{k}\right)\left(\frac{1}{\text{sgn}(\dot{x}_A) + \frac{\xi}{\dot{x}_A}}\right)\frac{dF}{dx_A} \tag{A1.7}$$

Notice that the differential is now expressed in terms of dx_A not dt. Assuming that 'ξ' has a small value so that as the velocity '$\dot{x}_A$' increases; $\frac{\xi}{\dot{x}_A}$ tends to zero. Then we have:

$$F = c.\text{sgn}(\dot{x}_A) - \frac{c}{k}.\text{sgn}(\dot{x}_A).\frac{dF}{dx_A} \tag{A1.8}$$

Rearranging (A1.8):

$$-\int_{F_o}^{F_1} \frac{-1}{c.\text{sgn}(\dot{x}_A) - F}.dF = \int_{x_{A0}}^{x_{A1}} \frac{k}{c}.\text{sgn}(\dot{x}_A).dx_A \tag{A1.9}$$

Where, F_0 and x_{A0} are force and displacement at the previous turning point respectively; F_1 and x_{A1} are current force and displacement respectively.

Integrating (A1.9):

$$\left[-\ln\left|c.\mathrm{sgn}(\dot{x}_A)-F\right|\right]_{F_0}^{F_1}=\left[\frac{k.x_A}{c}.\mathrm{sgn}(\dot{x}_A)\right]_{x_{A0}}^{x_{A1}} \tag{A1.10}$$

Then:

$$F_1=C.\mathrm{sgn}(\dot{x}_A)-(C.\mathrm{sgn}(\dot{x}_A)-F_0).Exp\left(-\frac{k.\mathrm{sgn}(\dot{x}_A)}{c}.(x_{A1}-x_{A0})\right) \tag{A1.11}$$

Appendix 2: Response of the Haupt and Sedlan viscoelastic element to a stepped input

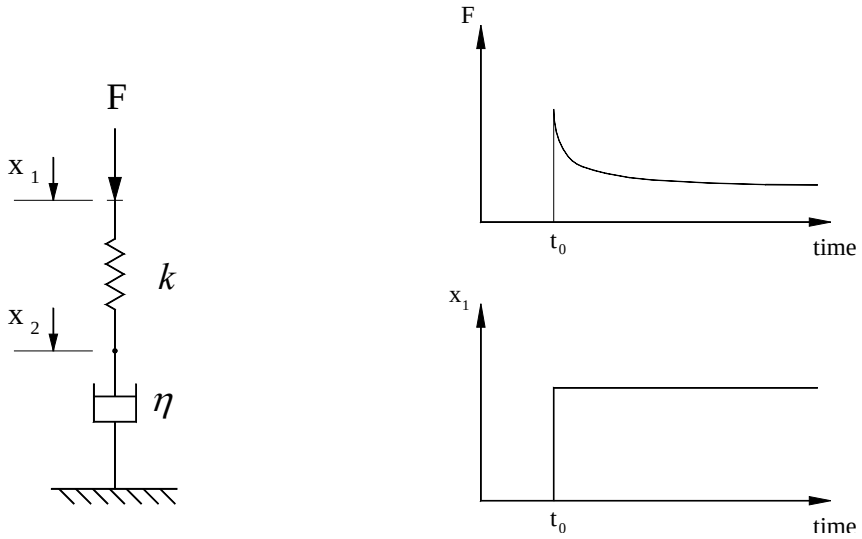

Fig. A2-1: Response to stepped displacement

The Sedlan and Haupt viscoelastic element [19] is a modified Maxwell element where the dashpot coeffiecient 'η' is a function of $\dot{x}_1$ as follows:

$$\eta = \frac{c}{\dot{x}_1 + \xi} \tag{A2.1}$$

So that:

$$F = \frac{c.\dot{x}_2}{\dot{x}_1 + \xi} = k(x_1 - x_2) \tag{A2.2}$$

Where, 'F' is applied force, 'c' is the maximum possible damping force, 'ξ' is a constant, x_1 is total displacement of the element and x_2 is displacement across the dashpot. So that:

From (A2.2), when $\dot{x}_1 = 0$, $$\dot{x}_2 = \frac{\xi.F}{c} \tag{A2.3}$$

Also from (A2.2),

$$\frac{dF}{dt} = k.\dot{x}_1 - k.\dot{x}_2 \qquad \text{(A2.4)}$$

Substituting (A2.3) into (A2.4) we have:

$$\frac{dF}{dt} = k.\dot{x}_1 - k.\frac{\xi.F}{c} \qquad \text{(A2.5)}$$

For the stepped input at, $t > t_0$, $\dot{x}_1 = 0$. Therefore:

$$-\frac{1}{k}.\frac{dF}{dt} = \frac{\xi.}{c}F \qquad \text{(A2.6)}$$

$$\int_{F_0}^{F_1} \frac{1}{F}.dF = \int_{t_0}^{t_1} -\frac{\xi.k.}{c}.dt \qquad \text{(A2.7)}$$

Therefore the response to a stepped input is an exponential function dependent upon, *ξ, k, and c*, as follows:

$$F_1 = F_0.Exp\left[-\frac{\xi.k.t}{c}\right] \qquad \text{(A2.8)}$$

Where, F_0 is force at t_0 and F_1 is force at time '*t*'.

Appendix 3: Test rig frequency response for rubber component measurement

The ‘dynamic compliance frequency response’ for each rubber component test rig was determined before time domain measurements were taken and the lowest test rig resonant frequency determined. The track running gear component time domain measurements where then taken less then 50% of this value to avoid the effect of test rig resonance.

Dynamic compliance is also known as, receptance, admittance or dynamic flexibility [49]; it is the inverse of ‘dynamic stiffness’ and defined as:

$$H(\omega) = \frac{X(\omega)}{F(\omega)} \tag{A3.1}$$

Where, $H(\omega)$ is dynamic compliance, $X(\omega)$ is complex displacement and $F(\omega)$ complex force. Dynamic compliance and phase angle are plotted against frequency in Figures, A3-1b, A3-2b and A3-3b. These response plots have been produced by random excitation. The frequency response is then found as follows:

$$H(\omega) = \frac{S_{dx}(\omega)}{S_{df}(\omega)} \tag{A3.2}$$

Where, $S_{dx}(\omega)$ is ‘cross spectral density’ (CSD) of the random drive signal and displacement, and $S_{df}(\omega)$ is CSD of the random drive signal and force and $H(\omega)$ the frequency response function (FRF).

CSD is the Fourier transforms of the cross correlation (or product) in the time domain of two signals, averaged for many sections (or lengths) of data. Details of this method can be found in Ewins [49], Worden and Tomlinson [50] and Cartwright [51]. Essentially, the random drive signal is used as a ‘reference’ and by averaging a

number of frequency response plots (more then 100), the effect of noise and spurious signals is reduced. The random drive signal component is cancelled in the division of Equation A3.2 and the plot of dynamic compliance and phase angle determined in the frequency domain. Software supplied by ‘Prosig Limited’ was used to record and process the test data. In this software, the algorithm for determining Cross Spectral Density is pre-programmed and is simply applied to the time domain measurements.

The broadband random excitation method used here has the advantage that it quickly produces an FRF over a wide frequency range but the method has limitations regarding the analysis of nonlinear systems. These limitations are discussed in detail both by Ewins [49], and Worden and Tomlinson [50]. However for the purpose of identifying the test rigs resonant frequency the method is adequate.

The graphs (A3-1b, A3-2b and A3-3b) show large spikes at zero frequency, which should be ignored as they are due to the DC components of the signal. But we also see that compliance below the first resonant frequency tends to increase as zero hertz is approached (Fig A3-2b) and does not stay level as would be expected for a linear system. This is likely to be due to the rubbers amplitude dependant stiffness, as discussed in Section 3.3, which reduces as amplitude increases. The ‘random drive signal’ results in higher amplitude displacements across the rubber component at low frequency then at high frequency due to the acceleration of test rig masses and so lower frequencies show higher compliance.

Fig. A3-1a: Road wheel tyre test rig

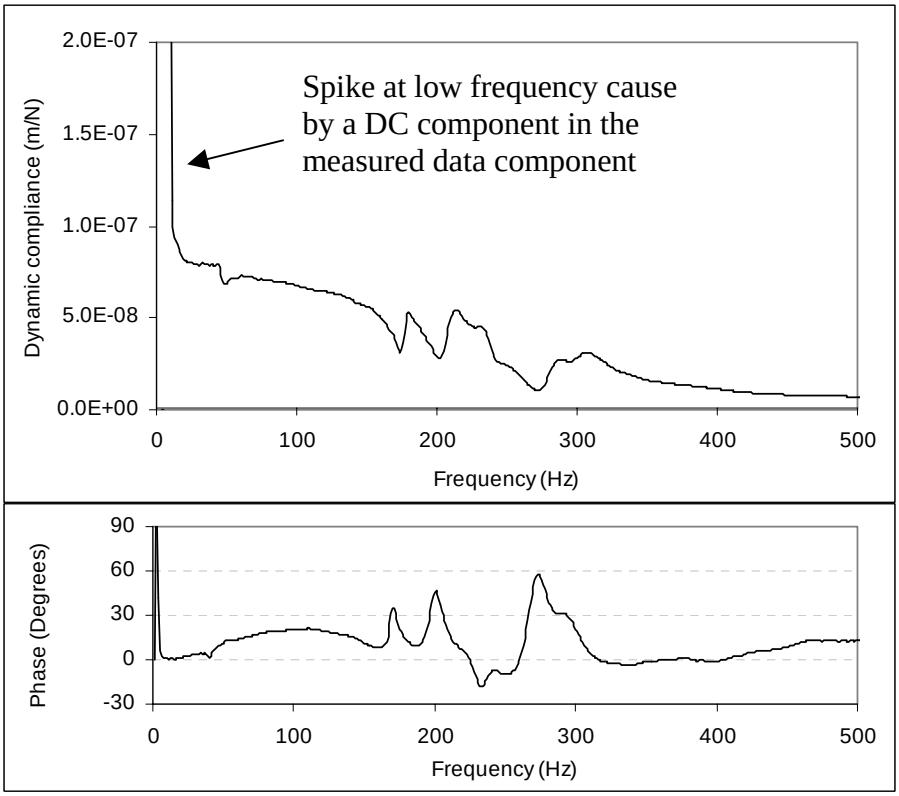

Fig. A3-1b: *Road wheel tyre test rig FRF*

The tyre test rig shows the first significant resonance occurring at approximately 40Hz. Therefore measurements of the road wheel response in the time domain will not be taken at frequencies above 20Hz .

Fig. A3-2a: *Track bush radial force test rig*

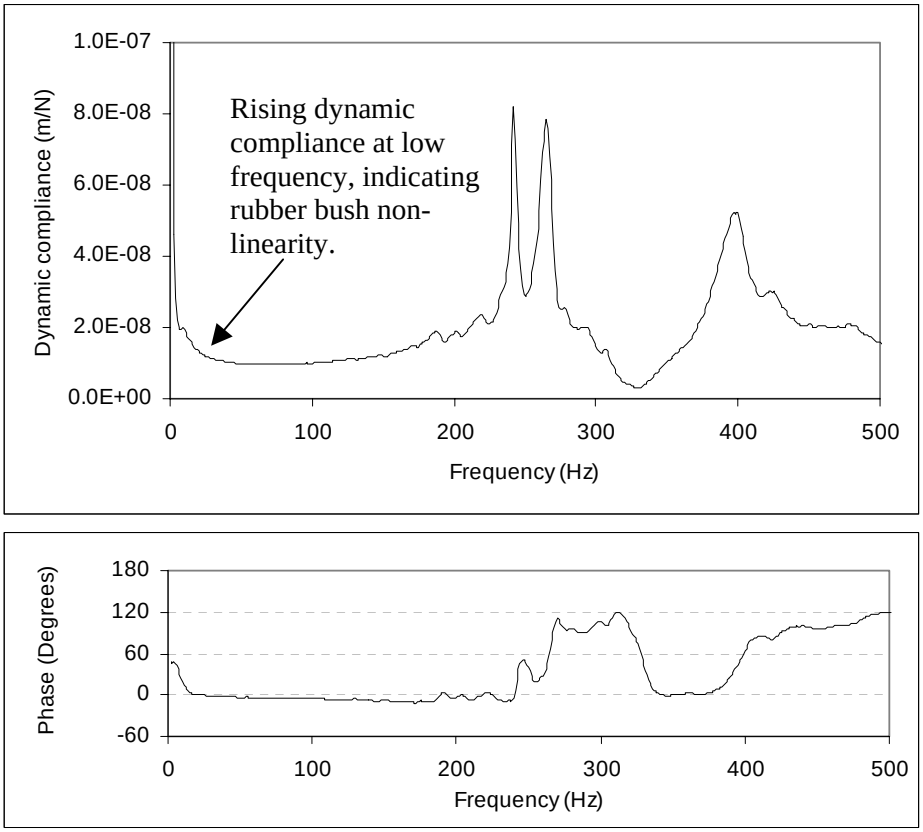

Fig. A3-2b: *Track bush radial force test rig FRF*

The track bush radial force test rig does not show significant resonant effects below 150Hz.

Fig. A3-3a: *Track bush torsional response test rig*

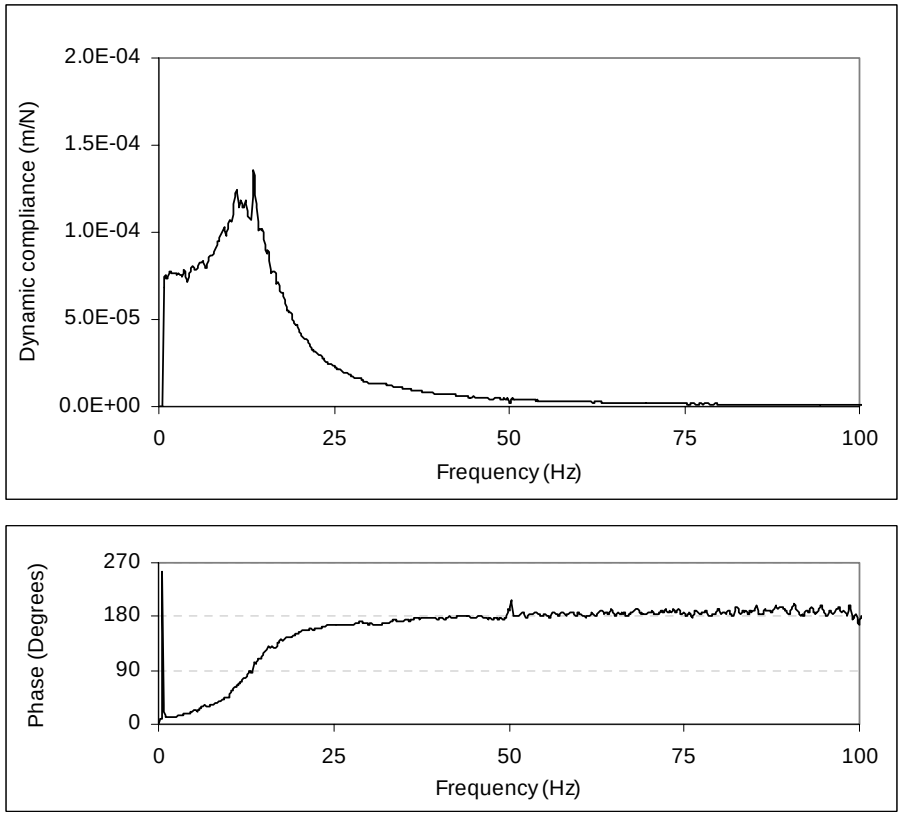

Fig. A3-3b: *Track bush torsional response test rig FRF*

The track bush torsional force test rig shows significant resonance at approximately 12Hz.

Appendix 4a: The 'Four viscoelastic element' model

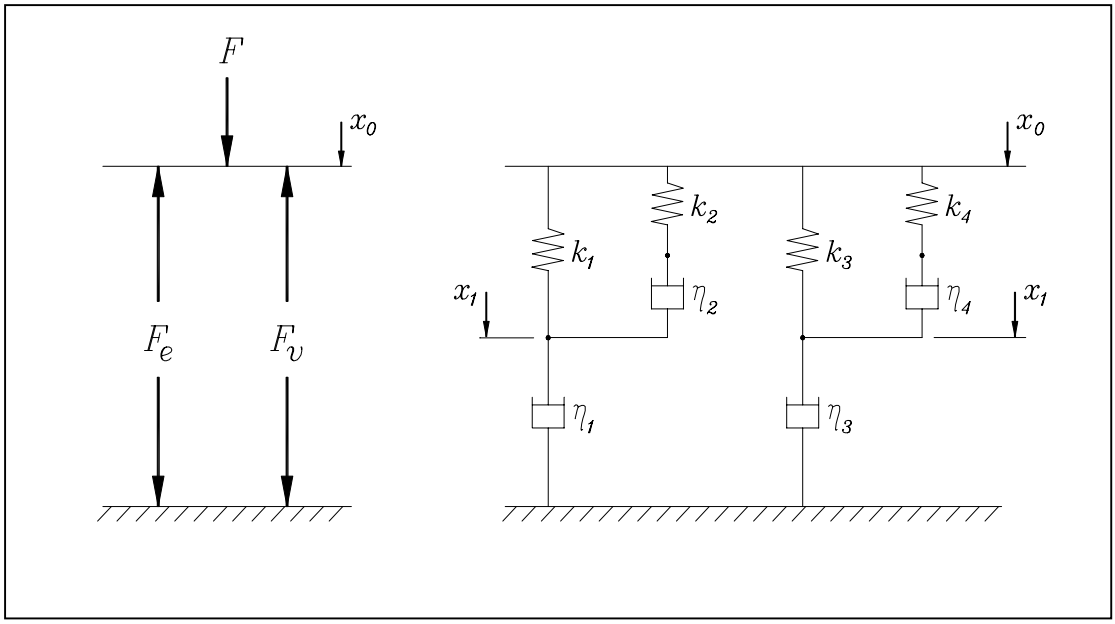

Fig. A4a-1: *Four viscoelastic element model*

Values for the track bush torsional model

Nm/Degree	*Nm*	*Degrees/sec*	$\tau = \frac{c}{k.\xi}$
$k_1 = 10$	$c_1 = 20$	$\xi_1 = 0.02$	$\tau_1 = 100$
$k_2 = 20$	$c_2 = 20$	$\xi_2 = 20$	$\tau_2 = 0.05$
$k_3 = 3$	$c_3 = 40$	$\xi_3 = 13.3$	$\tau_3 = 1.0$
$k_4 = 40$	$c_4 = 40$	$\xi_4 = 20$	$\tau_4 = 0.05$

Elastic force: $F_e = 12.4\,\theta + 130.4$ *Nm/Degree* **Equation 5.3.1-1**

Geometric multiplier: $f(x_0) = 0.033\,|x_0 - 10| + 1$ **Equation 5.3.2-1**

Appendix 4b: The final 'three viscoelastic-element' model

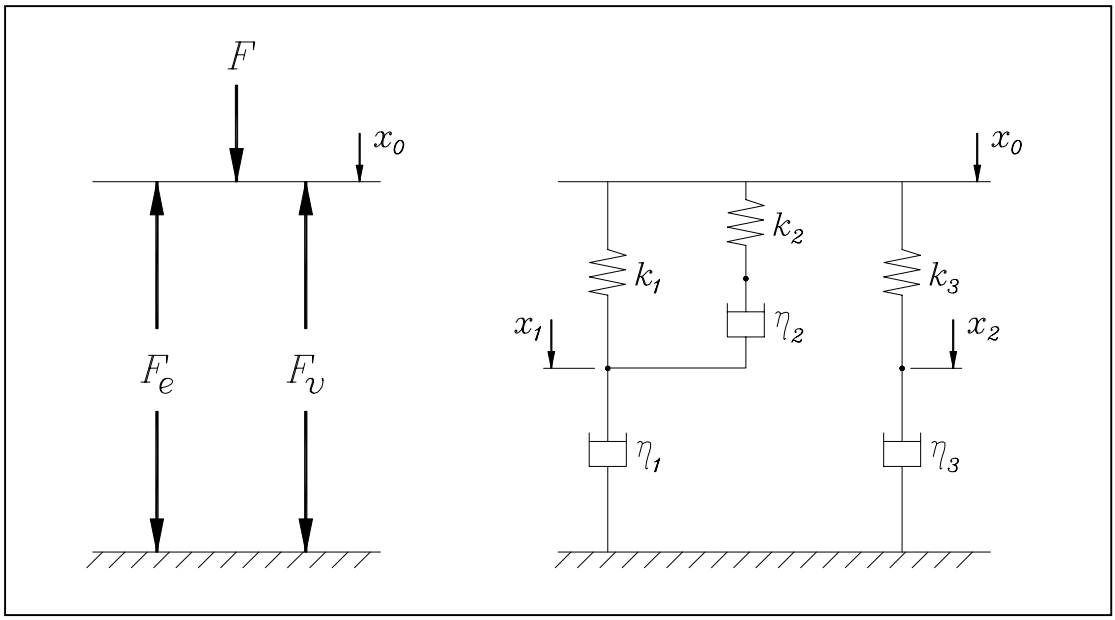

Fig. A4b-1: *Three viscoelastic element model*

Values for the road wheel tyre model

N/m	*N*	*m/sec*	$\tau = \frac{c}{k.\xi}$
k_1 = 1500	**c_1 = 1000**	ξ_1 = 0.0067	τ_1 = 100
k_2 = 1500	c_2 = 1000	ξ_2 = 6.67	τ_2 = 0.1
k_3 = 150	**c_3 = 500**	ξ_3 = 3.33	τ_3 = 1.0

Note: The four variable parameters (k_1, k_3, c_1 and c_3) are highlighted in bold.

Elastic force: $F_e = 1.82 \times 10^{11}.x^3 - 2.14 \times 10^8.x^2 + 2.17 \times 10^6.x \quad N/m$

Equation 5.3.1-3

Geometric multiplier: $f(x_0) = 543.x_0 + 1$ **Equation 5.3.2-2**

Values for the track bush torsional model

N/m	*N*	*m/sec*	$\tau = \frac{c}{k.\xi}$
k_1 = 10	**c_1 = 20**	ξ_1 = 0.02	τ_1 = 100
k_2 = 10	c_2 = 20	ξ_2 = 20	τ_2 = 0.1
k_3 = 3	**c_3 = 40**	ξ_3 = 13.3	τ_3 = 1.0

Note: The four variable parameters (k_1, k_3, c_1 and c_3) are highlighted in bold.

Elastic force: $F_e = 12.4\theta + 130.4 \quad Nm/Degree$ **Equation 5.3.1-1**

Geometric multiplier: $f(x_0) = 0.033|x_0 - 10| + 1$ **Equation 5.3.2-1**

Values for the track bush radial model.

N/m	*N*	*m/sec*	$\tau = \frac{c}{k.\xi}$
k_1 = 60,000	**c_1 = 3,800**	ξ_1 = 0.00063	τ_1 = 100
k_2 = 60,000	c_2 = 3,800	ξ_2 = 0.63	τ_2 = 0.1
k_3 = 17,000	**c_3 = 100,000**	ξ_3 = 5.9	τ_3 = 1.0

Note: The four variable parameters (k_1, k_3, c_1 and c_3) are highlighted in bold.

Elastic force: $F_e = 81.8 \times 10^6.x \quad N/m$ **Equation 5.3.1-2**

Geometric multiplier: $f(x_0) = 1$

Appendix 5: Compression of damper oil, entrapped air and compliance of oil the chamber

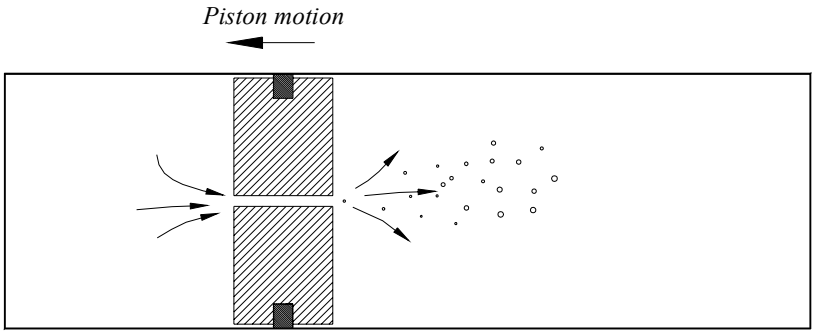

Fig. A5-1: *Schematic representation of the damper showing how entapped air is compressed and expanded as oil flows from one chamber into the other*

Figure A5-1 illustrates a possible physical mechanism where entrapped air is dissolved in oil on the high pressure side of the piston and comes out of solution as small bubbles on the low pressure side according to Henry's law which states: *'The mass of gas that dissolves in a volume of liquid is directly proportional to the pressure'*. Henry's law is described by the following relationship:

$$P = \frac{H.m_{gs}}{V_{oil}} \quad (\mathrm{N/m^2}) \tag{A5-1}$$

Where, 'P' is pressure, 'H' is Henry's constant (m^2/s^2), 'm_{gs}' is mass of gas dissolved in solution and 'V_{oil}' is volume of oil.

The mass of gas in solution (m_{gs}) and mass of gas in bubble (m_{gb}) are related by:

$$m_{gt} = m_{gs} + m_{gb} \tag{A5-2}$$

Where m_{gt} is the total mass of gas in the chamber.

Combining equation A5-1 and A5-2 we have:

$$m_{gb} = m_{gt} - \frac{P.V_{oil}}{H} \tag{A5-3}$$

Since, m_{gt}, V_{oil} and H are all constants equation A5-3 can be rewritten as:

$$m_{gb} = c_1 - c_2.P \tag{A5-4}$$

Because the gas bubbles are small we can assume rapid heat transfer between air and oil and therefore constant temperature. Applying the ideal gas law, $P.V = mRT$, to the entrapped air on one side of the piston we have:

$$\frac{P_0.V_0}{m_{gb0}} = \frac{P_1.V_1}{m_{gb1}} \tag{A5-5}$$

Where, P_0 is initial pressure (atmospheric), P_1 instantaneous pressure, V_0 initial volume, V_1 instantaneous volume, m_{gb0}, initial mass of gas bubble and m_{gb1}, instantaneous mass of gas bubble.

Equation A5-5 applies up to the point where all entrapped air is dissolved in oil after which we have compression of the oil and compliance of the chamber only. Substituting Equation A5-4 in to Equation A5-5 we have:

$$\frac{P_0.V_0}{c_1 - c_2.P_0} = \frac{P_1.V_1}{c_1 - c_2.P_1} \tag{A5-6}$$

Rearranging Equation A5-6:

$$P_1 = \frac{c_1.P_o.V_0}{c_1.V_1 - c_2.P_0.V_1 + c_2.P_0.V_0} \tag{A5-7}$$

Because piston and cylinder areas are constant we can substitute ‘volume of entrapped air’ for ‘piston displacement’ and ‘chamber pressure’ for ‘force acting on the piston’ so that:

$$V_0 \rightarrow x_0 \tag{A5-8}$$

$$V_1 \rightarrow x_0 - x_d \tag{A5-9}$$

$$P_0 \rightarrow F_0 \tag{A5-10}$$

and $$P_1 \rightarrow F_1 \tag{A5-11}$$

Where, x_0 represents the initial volume of entrapped gas, x_d is change in gas volume, F_0 is force on piston at x_0 and F_1 is the dampers reaction force. The units of c_1 remain as (kg) the units for c_2 become (s^2/m). This substitution gives:

$$F_1 = \frac{F_o.x_0.c_1}{c_1.x_0 - c_1x_d - c_2.F_0.x_0 + c_2.F_0.x_0 + c_2.F_0.x_0} \tag{A5-12}$$

dividing through by $x_0.c_1$ Equation A5-12 reduces to:

$$F_1 = \frac{F_o}{1 - \frac{x_d}{x_0} + \frac{c_2}{c_1}.F_0.\frac{x_d}{x_0}} \tag{A5-13}$$

Letting $\frac{c_2}{c_1}F_0 = c$, where c and rearranging equation A5-13 we have:

$$F_1 = \frac{F_o}{1 - \frac{x_d}{x_0}(1+c)} \tag{A5-14}$$

Since both F_0 and x_0 are constants Equation A5-14 reduces to:

$$F_1 = \frac{C_1}{1 - \frac{x_d}{C_2}} \qquad \text{(A5-15)}$$

Where the unit for C_1 are Newtons (N) and C_2 meters (m).

It is worth noting the following points regarding equation A5-15.

1. The following condition applies: $0 < \frac{x_d}{C_2} < 1$

2. It is possible to produce an almost linear relationship by setting the value of C_2 so that $C_2 >> x_d$. This would suit a model where the mass of entrapped air is small and compressibility primarily due to oil bulk modulus and chamber compliance.

3. Equation A5-15 relates piston force to displacement (x_d) with only two 'tuneable' parameters, C_1 and C_2, but we have lost the physical meaning of these constants. The model has become 'non-physical' or 'non-parametric'. Henry's constant, initial volume of oil, initial volume of gas, initial mass of gas and initial pressure are 'lumped' together because all these values are unknown constants.

Equation A5-15 relates the force exerted on the piston by gas pressure in one chamber only. But the damper has chambers either side of the piston. Therefore the dampers reaction force (F_1) is described by the following equation (A5-16).

$$F_1 = C_1 \left[\frac{1}{1 + \frac{x_d}{C_2}} - \frac{1}{1 - \frac{x_d}{C_2}} \right] \qquad \text{(A5-16)}$$

Figure A5-2 illustrates how Equation A5-16 behaves, summing the force on either side of the piston.

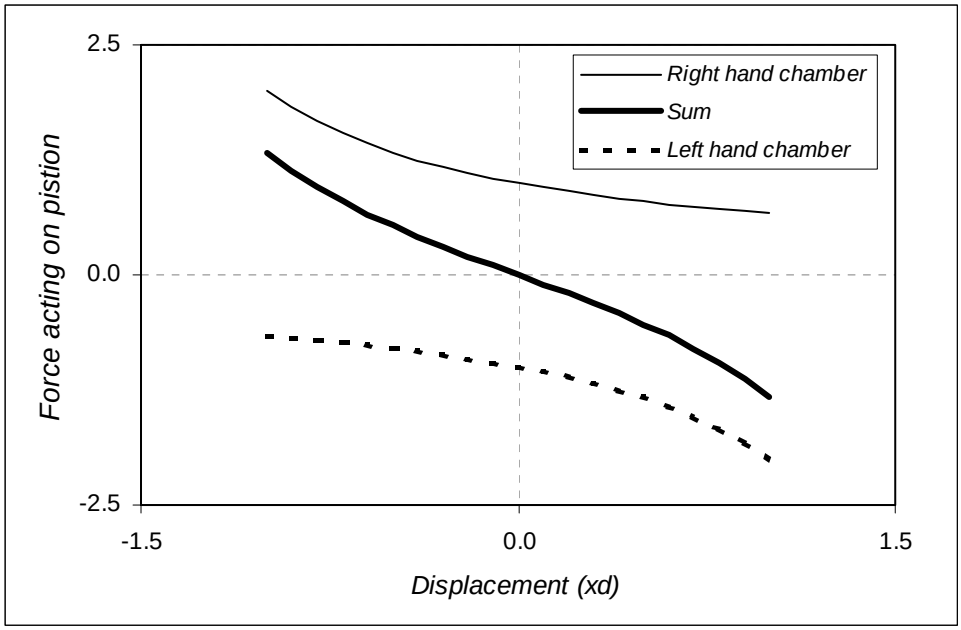

Fig. A5-2: *Response described by Equation A5-15 for C_1 =1 and C_2 =2*

In figure A5-2: for the purpose of demonstration, C_1 and C_2 have been given the values '1' and '2' respectively, but in the damper model, C_1 and C_2 are set to match experimental data. This was achieved by repeatedly running simulations and visually comparing the measured and modelled characteristic force-velocity graphs.

Appendix 6: Torque-Angular velocity relationship for the Warrior APC rotary damper model (excluding hysteresis)

In chapter 12, points on the dampers characteristic response plot where found which represented three viscous flow regimes, laminar, turbulent and pressure relief (Blow-off). These values are presented in the first and second columns of Table A6-1. The table shows ‘smoothed’ values in the third column (highlighted by a heavy boarder) that have been corrected manually to produce a smooth transition between the turbulent flow region and the pressure relief valve opening.

Figure A6-1 shows this ‘smoothed’ curve implemented in ADAMS software as a ‘splined curve’ for uses in the damper model.

		Angular velocity (rad/sec)	Measured response (Nm)	Smoothed curve (Nm)
Rebound	Blow-off	-14.0	-8050	-8050
		-13.0	-8050	-8050
		-12.0	-8050	-8050
		-11.0	-8050	-8050
		-10.0	-7950	-7950
		-9.0	-7950	-7950
		-8.0	-7800	-7800
		-7.0	-7600	-7600
		-6.0	-7400	-7400
		-5.0	-7250	-7250
		-4.0	-7000	-7000
		-3.0	-6500	-6500
		-2.0	-6000	-6000
	Turbulent flow	-1.8	-9091	-5800
		-1.6	-7398	-5550
		-1.4	-5856	-5200
		-1.2	-4471	-4471
		-1.0	-3250	-3250
		-0.8	-2186	-2186
		-0.6	-1306	-1306
	Laminar flow	-0.4	-622	-622
		-0.2	-194	-194
		-0.1	-100	-100
		0.0	0	0
		0.1	100	100
		0.2	194	194
	Turbulent flow	0.4	622	622
		0.6	1306	1306
		0.8	2186	2186
		1.0	3250	3250
		1.2	4471	4471
		1.4	5856	5856
		1.6	7398	7200
		1.8	9091	8000
		2.0	10932	8500
Compression	Blow-off	3.0	10300	10300
		4.0	11600	11600
		5.0	12100	12100
		6.0	12600	12600
		7.0	12850	12850
		8.0	13000	13000
		9.0	13200	13200
		10.0	13400	13400
		11.0	13550	13550
		12.0	13550	13550
		13.0	13650	13650
		14.0	13650	13650

Table A6-1: *Numeric data for the damper torque verses angular velocity response*

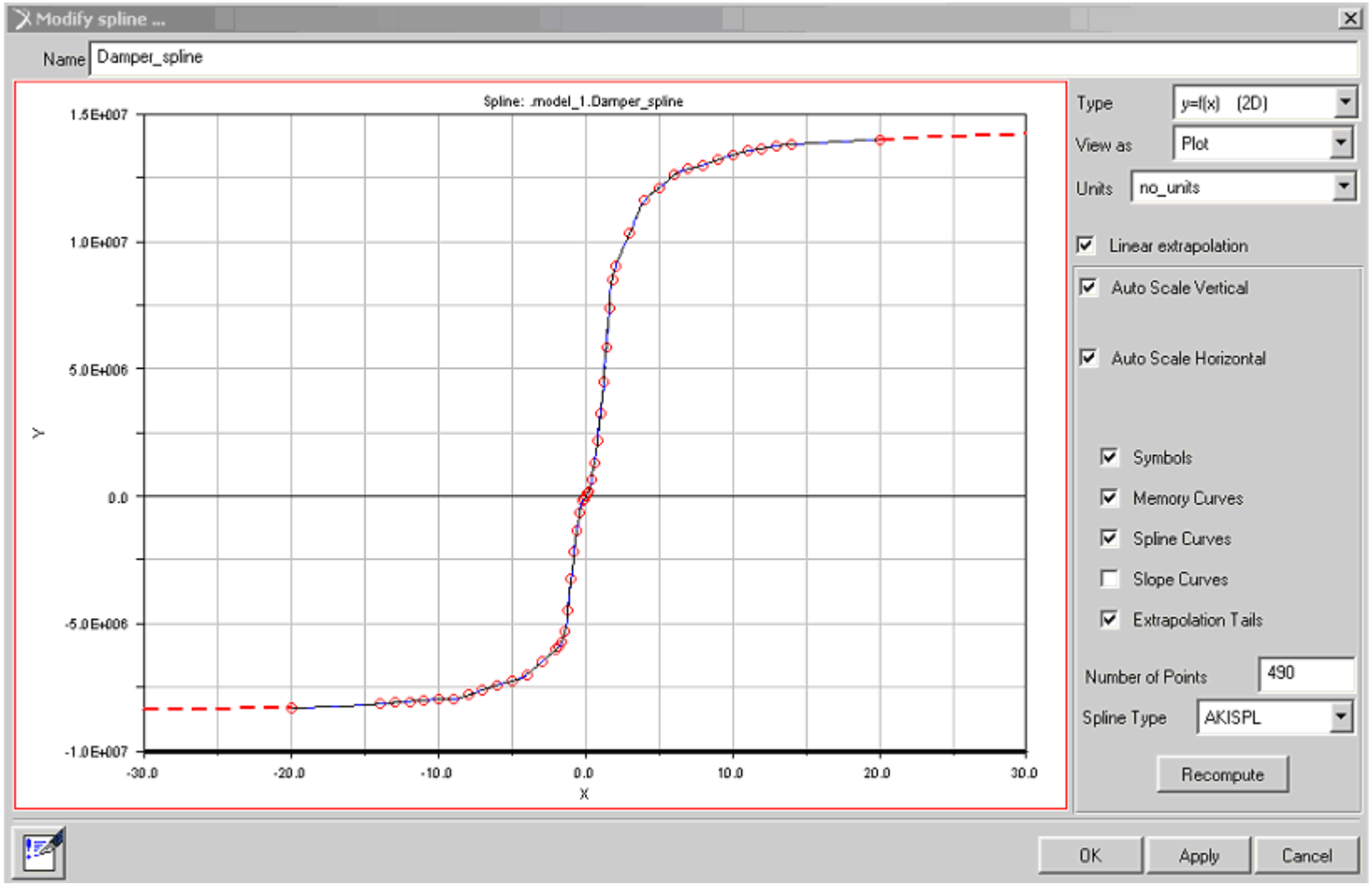

Fig A6-1: The rotary damper viscous force-velocity response implemented in ADAMS software as a splined curve.

Appendix 7: Test rig design and instrumentation

Test rigs were built to measure the dynamic response of each rubber track components. These were; track bush radial response, track bush torsional response and road wheel tyre radial response. A test rig was also built to measure the rotary damper's response. Drawings depicting each of these test rigs are presented in Figures, A7-2, A7-3, A7-4 and A7-5 respectively.

Figure A7-1 is a schematic drawing of the data acquisition and control system setup for a measurement of Track Link Radial response to random excitation. This is shown as an example since the main features of this setup remained the same in all tests. Two types of test were conducted on each component; sinusoidal excitation and random excitation. The instrumentation and channel allocations for each case are listed in Table A7-1.

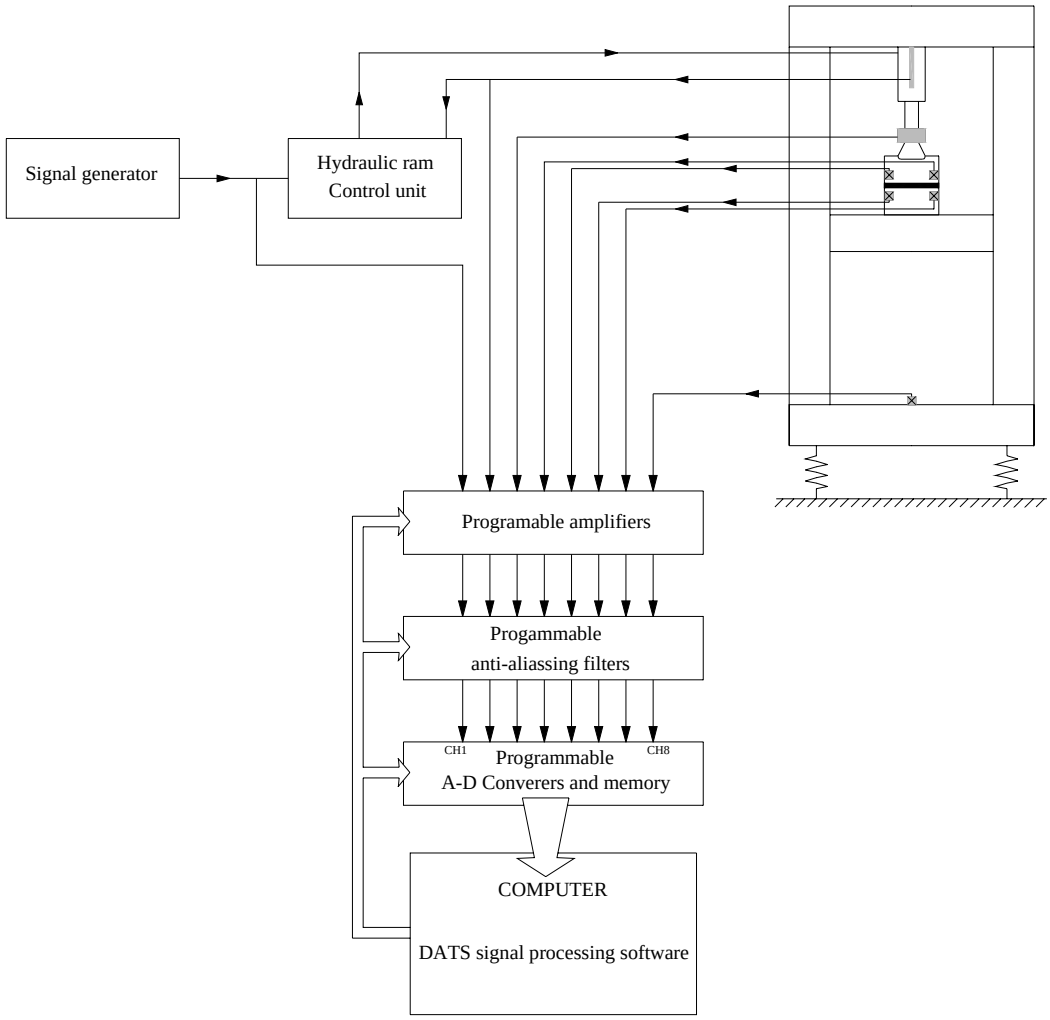

Fig. A7-1: *Test rig control and instrumentation set up for random drive signal (Transducer power supplies and amplifiers have not been shown for clarity)*

Data Channel	Measurement 1	Measurement 2
1	Random drive signal	Sinusoidal drive signal
2	Hydraulic ram LVDT	Hydraulic ram LVDT
3	Load cell	Load cell
4	Accelerometer	LVDT
5	Accelerometer	
6	Accelerometer	
7	Accelerometer	
8	Test rig base motion accelerometer	

Table A7-1: *Data acquisition channel assignment for both random and sinusoidal drive signals*

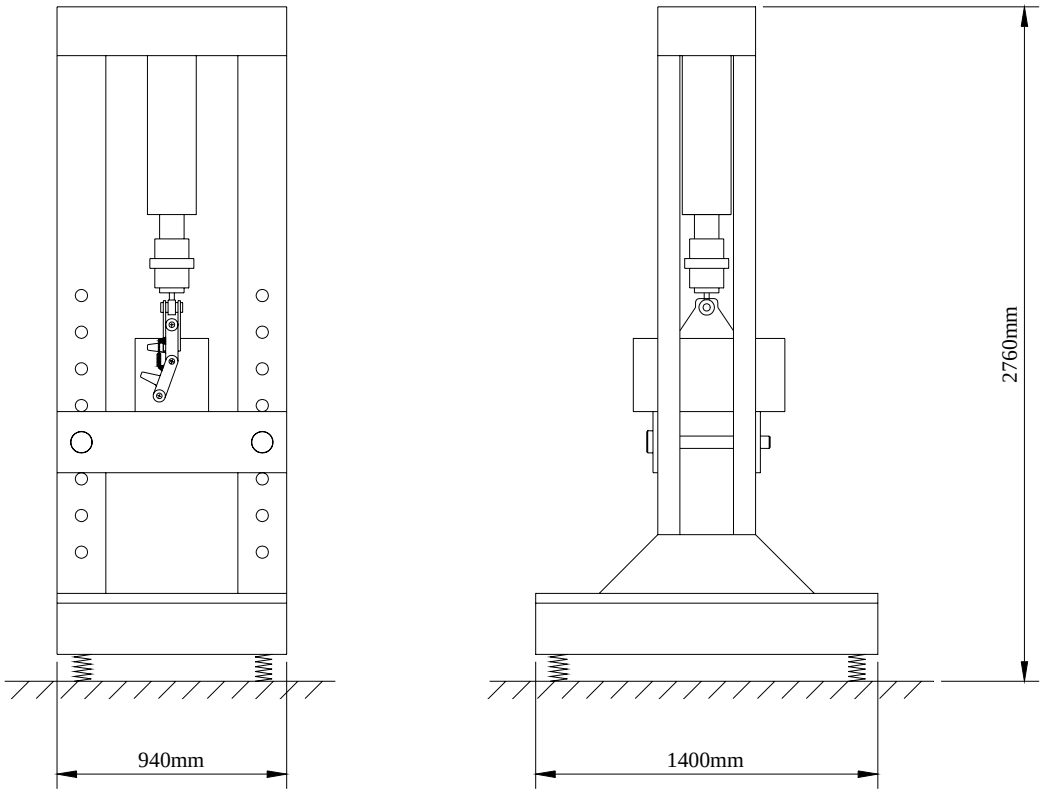

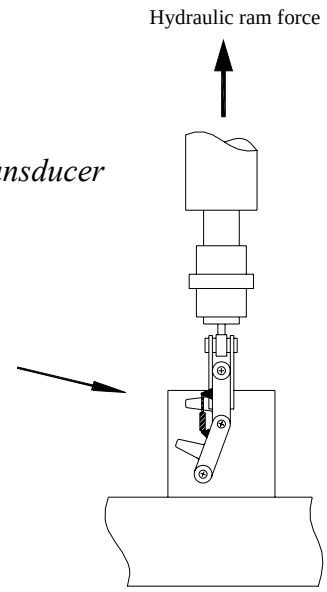

The Linear Variable Displacement Transducer is positioned across the Track Links to measure relative displacement

Fig. A7-2: *Test rig for the measurement of Track Bush Radial Response*

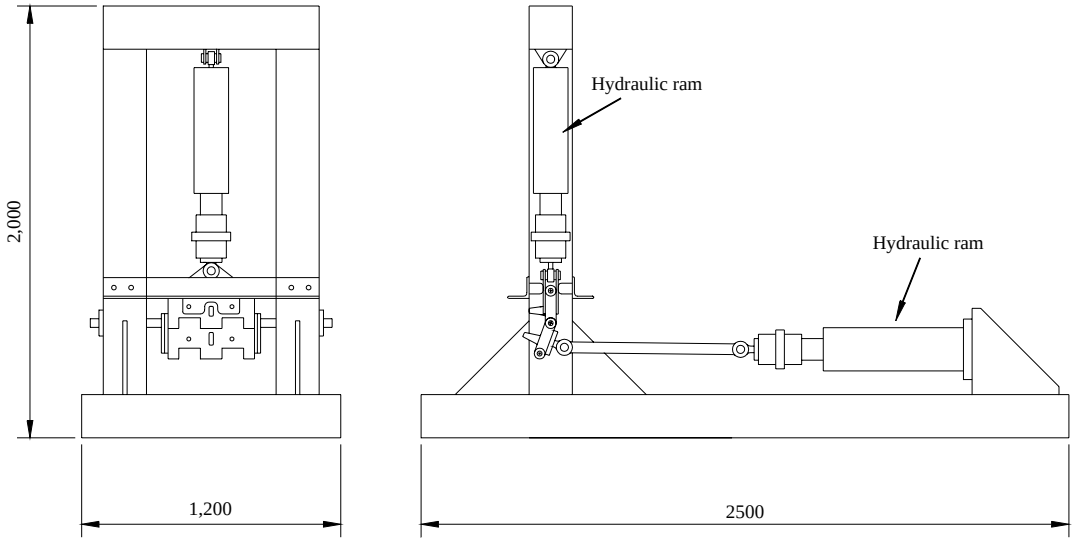

Fig. A7-3: *Test rig for the measurement of the Track Bush Torsional Response*

Figure A4-3 shows the two hydraulic rams required to measure Track Bush Torsional response. The vertical hydraulic ram applies a constant radial load; simulating track tension. The horizontal hydraulic ram rotates the lower link about the track bush axis.

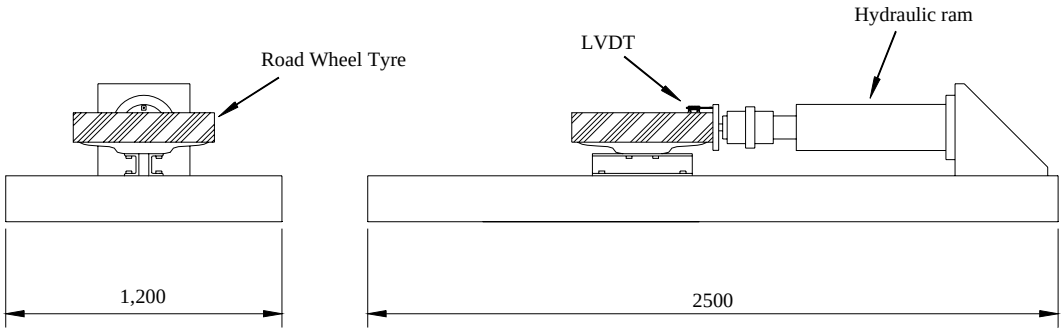

Fig. A4-4: *Test rig for the measurement of the Road Wheel Tyre Response*

Figure A7-4 shows the Linear Variable Displacement Transducer positioned to measure distance across the Tyre only. Flexing of the wheels aluminium hub or the test rig does not effect the measurement.

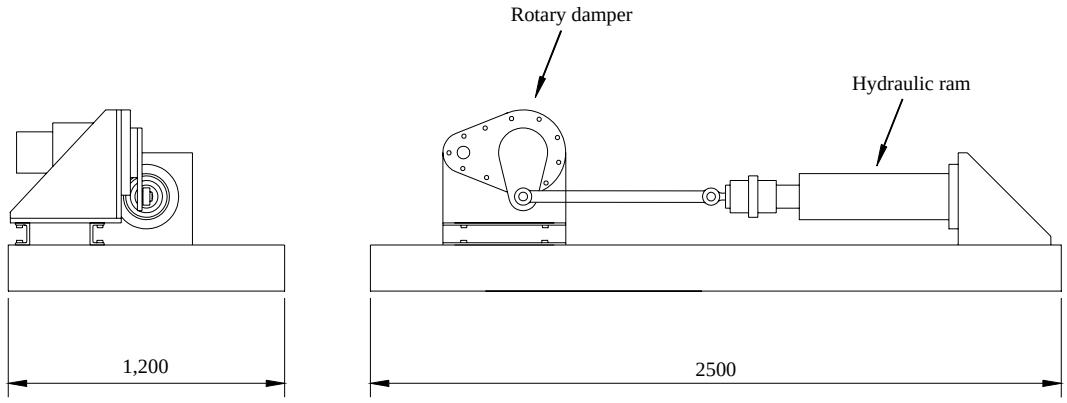

Fig. A4-5: *Test rig for the measurement of the rotary damper's Response*